# Fast Adaptive Observers for Battery Management Systems

by

Benjamin Michael Jenkins

B.S., University of New Hampshire (2009)
M.S., University of New Hampshire (2011)



Submitted to the Department of Mechanical Engineering
in partial fulfillment of the requirements for the degree of

Doctor of Philosophy

at the

MASSACHUSETTS INSTITUTE OF TECHNOLOGY

June 2017



Signature redacted

Author.... .....
Department of Mechanical Engineering
March 31, 2017

Signature redacted

Certified by..... .....
Anuradha M. Annaswamy
Senior Research Scientist
Thesis Supervisor

Signature redacted

Accepted by ..... .....
Rohan Abeyaratne
Chairman, Department Committee on Graduate Theses

# Fast Adaptive Observers for Battery Management Systems

by

Benjamin Michael Jenkins

Submitted to the Department of Mechanical Engineering
on March 31, 2017, in partial fulfillment of the
requirements for the degree of
Doctor of Philosophy

## Abstract

With the proliferation of batteries in transportation, mobile devices and, more recently, large scale energy storage, the demand for new efficient and safe algorithms for battery management has surged. More complex chemistry cells, such as lithium-ion batteries, with their sensitivity to mishandling, misuse and defects as is evident with recent device recalls due to fires, have historically been treated more conservatively. Maximizing performance of these cells safely requires knowledge of internal variables of interest which are not directly measurable. Therefore, accurate models which estimate these variables are needed. The focus of this thesis will be on a modified Single Particle Model (SPM), specifically its internal state estimates. Unfortunately, while the model structure is known, internal parameters which specify it are not, hence, state estimation alone is not enough. This motivates simultaneous state estimation and parameter identification of the electrochemical model. Existing solutions to this task are minimal in the literature. Hence this thesis.

This thesis enumerates multiple developments in electrochemical modeling and adaptive observers in general. The first and fundamental component is a modification of the SPM with attractive features such as the encapsulation of lithium diffusion as a linear dynamical system independent of nonlinearities and decoupling of the nonlinear relationships defining the kinetic properties of lithium ion transfer and open circuit potential respectively. A second development defines a set of guidelines reducing the design parameters for adaptive observers to a single tuning parameter, enabling rapid implementation and prototyping. Third, a new variant of adaptive observer, using multiple simultaneous equivalent system representations, is derived for fast parameter convergence. A novel selection of observer design variables and augmentation of the underlying equivalent system with nonlinear basis functions constitutes a fourth development extensively validated through numerical simulation and theory. This adaptive observer combined with an independent offline algorithm

to update effective electrode capacity and available lithium adapts every parameter of the modified SP model to account for aging or manufacturing differences. Validation of this observer in hardware using commercially available Panasonic 18650 cells completes the goals originally set forth for this research.

The developments presented pave the way for fast, computationally efficient, advanced battery management systems with the potential to increase the effective capacity of a battery or alternatively reduce the size, and therefore cost, of batteries in various applications.

Thesis Supervisor: Anuradha M. Annaswamy
Title: Senior Research Scientist

# Acknowledgments

First and foremost, I would like to thank my advisor Dr. Anuradha Annaswamy for her guidance and immense support over the past few years. From the beginning, she was an incredible source of inspiration and knowledge. Working with her in the AACL has been a privilege.

Both Eugene Lavretsky and Dieter Schwarzmann were great sources of insight and advice. I can pinpoint a significant fork in my research where the path chosen was guided by conversations with each of you. I also need to thank Dieter, not only for being instrumental in forming this project, funded by Bosch, but also for being a great friend.

While at Bosch there are a number of employees who, without, this research would not be what it is. Thank you, Ashish Krupadanam, Nikhil Ravi, Sungbae Park, Anahita MirTabatebaei, Aleksandar Kojic and Reinhardt Klein for your support and knowledge.

I am incredibly grateful for my lab-mates and office-mates who I have had countless conversations in support of my research. I had the privilege of working with two extraordinary Masters students over the years, Pierre Bi and Damas Limoge, who I cannot thank enough for their collaboration and friendship. My fellow lab-mate and PhD candidate Heather Hussain has become an invaluable friend and coworker.

This journey would not have been possible without the great support of my Family. Their encouragement from the very beginning was inspirational and their assistance through tough times was integral to my success throughout the years.

And countless others, there is an enormous network of friends and coworkers for whom I am tremendously grateful for their friendship and support.

THIS PAGE INTENTIONALLY LEFT BLANK

# Contents

# List of Figures

# List of Tables

THIS PAGE INTENTIONALLY LEFT BLANK

# Chapter 1

# Introduction

With the proliferation of batteries in transportation, mobile devices and energy storage, research for the safe and efficient use of various chemistry based cells has erupted. There are two major fronts to this eruption, the first approaching from a material science perspective, and the second from control engineers. Material science research is continuously investigating and producing new cell designs using alternative chemistry electrodes or electrolytes. While control engineers have the task of enabling safe and efficient use of batteries with these advanced chemistries, such as those based on lithium ion transfer. To accomplish this task both the State of Charge (SoC) and the State of Health (SoH) within a battery pack must be known. SoC is the equivalent of a fuel gauge for the battery pack in electric devices. It is a relative measurement ranging from 0% at 'empty' to 100% when 'fully' charged. However, 'empty' and 'full' are dependent on the battery's total capacity, a metric of the State of Health (SoH) which also must be known to guarantee safety, durability and performance. SoH encapsulates a number of metrics, usually providing a measure of the battery's condition relative to its designed specifications. Historically, the knowledge of these variables of interest has been only moderately accurate, which allows only moderate

performance and requires conservative use. To obtain the most out of more advanced chemistry cells, such as lithium ion, more accurate battery SoC estimation algorithms are of extreme importance. [14, 62]

Together, algorithms for determining SoC and SoH and their associated hardware are part of the battery management system (BMS). Throughout the past decade there have been a multitude of applications inspiring research using various mathematical models and algorithms. In relation to this work it is helpful to break down the existing literature on BMS development into categories based on the mathematical battery model used. There are three main categories which we will define. The first are equivalent circuit models (ECM), these were the first to be widely used and offer a model which is simple in structure, modular and expandable for higher accuracy. These are built upon linear dynamics. Notable work using these models are [1, 23, 45, 62]. Although ECMs offer simple and linear structure, to obtain a high level of accuracy a large number of states is required which yields a system which is not relatively complex, but cumbersome and unattractive computationally.

The second category of models are electrochemical models, including that of Doyle, Fuller and Newman (DFN) [14]. Not only are these more accurate than ECM but also have physically relevant parameters. This makes the SoH task with a BMS more natural. Although the most accurate, these electrochemical models are also the most unwieldily, relying on chemical properties and phenomena most accurately described by partial differential equations, in addition to algebraic relationships and static nonlinearities. For this reason, these models are rarely if ever considered for use in actual applications.

Models from a third category, which is a subset of electrochemical models are gaining popularity. This third category includes simplified electrochemical models such as the Single Particle Model (SP model) [10] and recent extensions including electrolyte dynamics [35] and thermal dynamics [20] have been explored as of late.

The reduced electrochemical models of the third category offer a balance of model simplicity and accuracy while retaining physical significance of parameters. This makes them attractive for BMS applications. To attain the accuracy desired in both SoC and SoH determination, we not only need access to models which are accurate in form, we need algorithms that can track the states, and update the parameters within these models to account for upfront manufacturer deviations, and aging and abuse over time. Although reduced electrochemical models such as the SP model are not as complex as DFN, these models are still composed of dynamics best described by partial differential equations and algebraic constraints. For this reason, the full SP model does not lend itself well to many robust linear observation and system identification tools. For this reason, the focus of this paper is specifically on a modification of the SP model, notably with diffusion processes described by linear ordinary differential equations. If the model is assumed to be fully known, the internal states such as the SoC could be adequately determined using a state observer, however, this assumption is not valid. The model form is assumed to be known, but the parameters which specify it cannot be, hence, an adaptive observer is desired to simultaneously identify the model parameters and estimate the internal states. To account for modeling errors and ensure parameter estimates are as current as possible a type of *fast* adaptive observer is implemented to ensure the safety of the cell during rapidly changing operating conditions or abusive operating conditions.

Previous approaches to the BMS task can generally be broken into three categories. Methods which attempt to estimate SoC alone, methods which attempt to estimate SoH alone and the third group of algorithms which attempts to perform these SoC and SoH estimations simultaneously. This third category is where, adaptive observers, the algorithms of this thesis fall.

SoC estimation has been approached a number of different ways both in laboratory settings and in applications. Estimating SoC without destruction of the battery

or disconnecting from a load/source is quite challenging. The most reliable method of determining SoC is a discharge test, however, this results in a fully discharged cell and capacity is only determined after the fact. [30] Thus, this is not a reasonable method for on-line estimation. The most general and simple method is integrating the input current to the cell, or the so-called coulomb counting method. This results in $\text{SoC} = \text{SoC}_0 - \frac{1}{\text{Capacity}} \int_{t_0}^{t} I(\tau)d\tau$, where $\text{SoC}_0$ is the state of charge at $t_0$. Two critical issues arise with this approach. First, the initial $\text{SoC}_0$ must be known precisely, and this is not easily achieved. Secondly, sensor bias can quickly result in drift of the SoC estimate. A third method does not require any past history of signals, but relies on adequate resting after which there is a $1-1$ correspondence between the cell voltage and SoC. This long resting time makes this method poor in application but could be combined with coulomb counting to provide an accurate $\text{SoC}_0$ if at $t_0$ the cell has been resting for a sufficient length of time. Unfortunately, this rest can take upwards of several hours [58] for certain chemistry lithium ion cells. Inversion of the 1-1 relationship between the open circuit potential and the state of charge is a fundamental component of nearly all SoC estimation algorithms. The resting requirement for open circuit inversion can be eliminated if a battery model can provide the open circuit voltage estimate regardless of the operating condition. This is the category of SoC estimation which this thesis falls. This method works well for on-line SoC estimation, but the estimate precision is only as good as the model and OCP-SOC mapping precision. Other black box approaches have been proposed [8, 11, 52] but rely on experimentally training using physical cells. These algorithms are not transparent in their estimation process, and may exhibit questionable performance outside of the trained operating region. Fusion of multiple algorithms previously mentioned is common, often using algorithms such as the Kalman Filter or Sliding mode observers.

Estimation of the SoH is determined using one of two overarching methods.

Either model-based open loop estimation or closed-loop parameter identification. Open-loop directly predicts SoH metrics such as loss of lithium, loss of active electrode material or internal resistance using the age of the cell, the number of cycles the cell has been used and the depth of discharges, among other quantities. [6, 16, 17, 30, 34, 48, 53, 59] These are highly dependent of the accuracy of the aging models and can not account for unforeseen side reactions or operating conditions, as well as environmental situations encountered while the battery management system was not active. Closed-loop methods are much more powerful and are either performed on-line or off-line. The most common of which involve augmentation of a SoC estimator's state with the parameters expected to change. [18, 19, 30, 44, 47, 57] Although this augmentation approach has been shown to work in numerous other applications, it violates the assumptions of the original estimators. Less ad-hoc methods such as recursive least squares and adaptive observers have also been attempted. However, often unmeasurable signals are assumed to be known or signals are differentiated resulting in algorithms which are not realistically implementable. [12, 13]

We take a distinct approach from others which have appeared in the literature and break apart the complex differential equations of the SP model into manageable blocks of both linear dynamics and static nonlinearities. By doing so tools such as fast Matrix Regressor Adaptive Observers (MR-AOs) [22] and other well known system identification techniques [28] can be combined to accurately estimate both the state of charge of the cell as well as internal parameters representative of the SoH of the cell.

The adaptive observer proposed is an algorithm which simultaneously identifies the parameters and estimates the states of a system. In the late 1960's and early 1970's considerable work was done to develop adaptive observers that guaranteed global stability [7,26,28,31,32] for linear systems. These observers were also shown to be uniformly asymptotically stable under conditions of persistent excitation (PE) on

the underlying regressor vector. This in turn was shown to be feasible if the external input into the observer contained sufficient frequency content [3, 40, 50]. Later a number of authors introduced modifications to these original algorithms to provide 'arbitrarily fast' convergence of the errors under the same PE conditions [24, 25, 42, 43]. These methods introduced a matrix of regressors or past regressor information, rather than simply a single regressor vector. This eliminated the hyperplane within the error state space on which slow convergence can occur, a characteristic exhibited by vector regressor based adaptive observers. A strict limitation still existed, in that these Matrix regressor adaptive observers still could only be used on linear time invariant systems with measured output and input. This thesis will attempt to overcome this limitation.

## 1.1 Thesis Overview

The first contribution of this thesis is the modified SP model presented in Chapter 2. This chapter begins with an overview of existing battery models and a description of the underlying partial differential equation based cell model whose coarse discretization results in a single particle model. The key contribution here are two alterations to existing SP models justified by experimental results, existing literature and an observability analysis. These alterations decouple the nonlinearities in the SP model and enable the use of a modified adaptive observer, whose use was previously restricted to linear systems.

Chapter 3 begins with the introduction of an adaptive observer, referred to here as a vector regressor based adaptive observer (VR-AO). Following the description of the AO algorithm, a set of guidelines for designing adaptive observers is presented, a contribution of this research. Notably, these guidelines reduce the number of design parameters for a $n'th$ order system from $4n^2 + n$ to a pair of tuning parameters. Ex-

ceptionally slow convergence of VR-AOs are greatly improved using these guidelines. To increase the performance further, two matrix regressor adaptive observers (MR-AOs) are presented, the first of which appeared in literature previously, the second of which is the third contribution of this research resulting in a fundamentally new type of MR-AO for fast parameter convergence.

A fourth contribution of this thesis is the modification of MR-AOs for use with the SP model derived in Chapter 2. The modifications involve a new methodology of creating additional regressors which make up the full matrix of regressors. This effectively generates regressors which contain predominantly high frequency content, these can then be used to estimate feedthrough parameters nearly independent of any unknown lower frequency dynamics. This ability to identify parameters associated with strictly high frequency signal content allows the synthesis of an internal signal otherwise unavailable for use in generating nonminimal system states.

In Chapter 5, a fifth contribution is presented, this algorithm estimates the parameters associated with the equilibrium open circuit potential. This can be accomplished using a large class of inputs which are likely to occur during normal use of many electrical products such as electric vehicles or power tools. This procedure involves the generation of a feature set providing conservative estimates of unavailable signals which are required to effectively determine these parameters of interest. The key parameters estimated by this algorithm are the effective volume of each electrode and the total available lithium within the system, which correspond to two SoH metrics, loss of active electrode and loss of lithium respectively. Following this OCP parameter estimation, the final contribution of this research is validation of the modified MR-AO on a physical cell. Using a specifically formulated excitation signal, with high signal strength and the ability to identify nonlinearities, 18650 cells are cycled generating rich datasets for testing of BMS algorithms. The OCP calibration algorithm also provides accurate state of charge signals for every experiment, which

are used to validate the MR-AO.

# Chapter 2

# Electrochemical Battery Modeling for Observer Design

## Contents



There are many compelling reasons to use an electrochemical model for representing Lithium-Ion cells. Perhaps most importantly, using a electrochemical model inherently results in a clear correlation between the model parameters and key physically representative parameters of the actual cell. These physical parameters are

often used as metrics of the State of Health (SOH). Secondly, the states which are to be monitored and controlled for fast charging and deep discharging are internal states of the electrochemical model. When black or grey box representations are used we may loose the ability to observe these specific internal states of the system. Lastly, for parameter adaptation, with only input current and output voltage measurements available for such a complex system, we would like to leverage all the physically and chemically relevant information possible about the cell. This is accomplished by using a model structure which uses a minimal number of parameters for the system description.

Primarily, models are developed and derived with a goal of cell optimization or simulation. Due to this, complexity is usually not the largest concern when these models are developed. However, for observation and control a compromise between model accuracy and model complexity must be made. The model developed here is designed to be simple but also modular in order to allow the use of more complex blocks to replace the modeling of particular chemical phenomena. This may be desired when more demanding applications are encountered or new chemistries are developed. Trade-off between model accuracy and model complexity is not only to achieve a model which can be numerically evaluated in at least real-time, but also, of particular importance in context of adaptive observers is a model with a number of parameters which is low enough to be uniquely determined with the excitation experienced under normal operation.

In the development of the model within this chapter we begin with the Doyle-Fuller-Newman (DFN) model [14,55] which is the most accessible to the public and widely accepted as an accurate mathematical representation of lithium ion batteries over a wide range of operating conditions. When used in applications the underlying partial differential equations (PDEs) of this model are discretized to achieve varying levels of fidelity for the purpose of analysis or within an observer. Within this chapter

we will describe the full DFN model and its most coarse discretization commonly referred to as the Single Particle Model (SPM or SP model). We take this model one step further, similar to [51, 54] arriving at a model composed of diffusion described by ordinary differential equations (ODEs) and static nonlinearities representing the Butler Volmer kinetics and the open-circuit potential. The Butler Volmer kinetics describe the equilibrium current from a specific load, it can be thought of as a combination of Kirkoffs voltage law and Ohm's law. The open-circuit potential represents the equilibrium electrochemical potential between the cell's electrodes as a function of the lithium concentration within each electrode's solid matrix.

Batteries are a store of chemical energy providing electrical energy to a load or storing electrical energy from a source via a redox reaction. A battery can consist of a number of electrochemical cells. For example, a standard AA battery is one cell, a 9-volt battery is made up of 6 small cells within an outer metal canister, and a typical electric car battery consists of between a dozen and thousands of individual cells. Each cell is composed of two half-cells connected internally by a flow of ions through an electrically insulating separator. Each half cell includes electrolyte and either the positive or negative electrodes. During charging, cations are reduced (addition of electrons) at the cathode and anions are oxidized (removal of electrons) at the anode. During discharge the process is reversed and the half cells switch processes. We define the negative and positive electrodes to remain consistent but their alternative designations as anode and cathode switch depending on if the cell is being discharged or charged.

Each of these half-cells can be modeled as a continuum of material with interstitial sites for lithium to bond. Physically cells are composed of a sandwich of current collector, electrode and electrolyte, separator, electrode and electrolyte and another current collector (Figure 2-1). The sheets of this sandwich are very thin compared to their other dimensions motivating the reduction of the underlying dynamics to

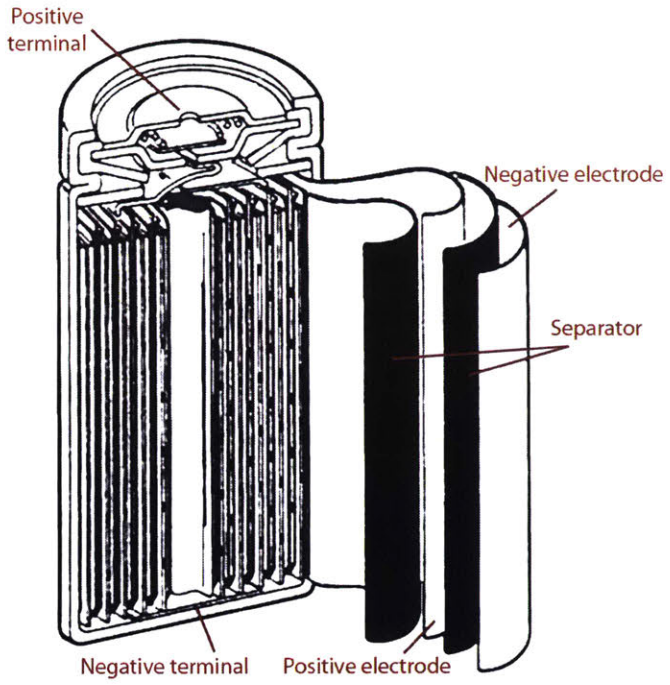


Figure 2-1: A typical 18650 lithium ion cell is constructed as a 'jellyroll' with sheets of each electrode's material and separator rolled inside a metal canister. These cells are commonly used in laptop and power-tool batteries as well as Tesla vehicle batteries.

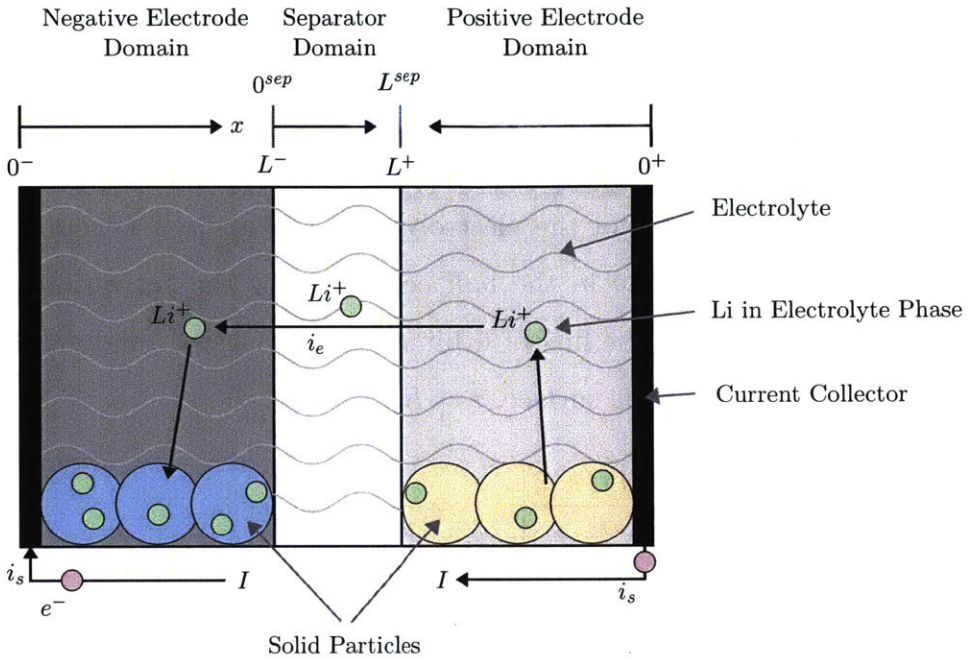


Figure 2-2: A discretized DFN model results in each electrode's solid material modeled as a number of spheres. When charging $Li^+$ migrates from the positive electrode solid through the electrolyte to the negative electrode solid

a single dimension, $x$, and small particles which spread along the $x$ dimension with their own single dimension, $r$. The movement of lithium ions can be represented by a diffusion process in both the solid and electrolyte. The ideally continuous media is modeled as many spheres into which the lithium can intercalate. A schematic of this is shown in Figure 2-2. This diffusion into the solid spheres can be mathematically represented by a PDE,

$$\frac{\partial c_s(x,r,t)}{\partial t} = \frac{1}{r^2}\frac{\partial}{\partial r}\left(D_s r^2 \frac{\partial c_s(x,r,t)}{\partial r}\right) \tag{2.1}$$

where $D_s$ is the diffusion coefficient in the solid. Empty space between these spheres

is filled with an electrolyte through which movement of ions is represented by,

$$\frac{\partial c_e(x,t)}{\partial t} = \frac{\partial}{\partial x}\left(D_e \frac{\partial c_e(x,t)}{\partial x}\right) + \frac{1}{F\varepsilon_e}\frac{\partial (t^0 i_e(x,t))}{\partial x} \tag{2.2}$$

with $D_e$ the diffusion coefficient of the electrolyte, $F$ is Faraday's constant, $\epsilon_e$ is the volume fraction of electrolyte in the half cell and $t^0$ is the activation energy coefficient. Continuity between the flux of lithium ions leaving the solid defines the boundary condition of (2.1) at the surface, $r = R_p$, as

$$\left.\frac{\partial c_s(x,r,t)}{\partial r}\right|_{r=R_p} = \frac{-1}{D_s} j_n \tag{2.3}$$

and due to symmetry of each sphere,

$$\left.\frac{\partial c_s(x,r,t)}{\partial r}\right|_{r=0} = 0 \tag{2.4}$$

A net electromotive force results in ions migrating from the cathode to the anode during discharge. Once a circuit is completed the flux of ions out of the solid particles, $j_n$, is determined by the Butler-Volmer Kinetics

$$j_n(x,t) = \frac{i_0}{F}\left[\exp\left(\frac{\alpha_a F}{RT}\eta_s(x,t)\right) - \exp\left(\frac{-\alpha_c F}{RT}\eta_s(x,t)\right)\right] \tag{2.5}$$

where $\alpha_a$ and $\alpha_c$ are the anodic and cathodic charge transfer coefficients respectively, $T$ is the temperature, $R$ is the universal gas constant. $i_0$ is the exchange current density and $\eta_s$ is the difference between the open-circuit potential and the half cell potential respectively,

$$\eta_s(x,t) = \phi_s(x,t) - \phi_e(x,t) - U(c_{ss}(x,t)) - FR_f j_n(x,t) \tag{2.6}$$

where $\phi_s$ is the solid potential, $\phi_e$ is the electrolyte potential, $U$ is the half-cell open-circuit potential, $c_{ss}(x,t)$ is the surface concentration of the sphere at $x$ and $R_f$ is a film resistance. The solid potential along the spatial dimension $x$ is determined by Ohm's law,

$$\frac{\partial \phi_s(x,t)}{\partial x} = \frac{i_e(x,t) - I(t)}{\sigma} \tag{2.7}$$

where $\sigma$ is the conductivity of the solid and the electrolyte current governed by

$$\frac{\partial i_e(x,t)}{\partial x} = aFj_n(x,t) \tag{2.8}$$

where $a$ is the interfacial area

$$a = \frac{3}{R_p}\epsilon_s \tag{2.9}$$

with $R_p$ being the particle radius and $\epsilon_s$ is the volume fraction of the solid electrode material in the half-cell. The electrolyte potential is described in the $x$ dimension as a PDE dependent on the electrolyte current $i_e$ and the electrolyte concentration $c_e$ as

$$\frac{\partial \phi_e(x,t)}{\partial x} = \frac{-i_e(x,t)}{\kappa} + \frac{2RT}{F}(1-t^0)\left(1 + \frac{d\ln f_{\pm}}{d\ln c_e}(x,t)\right)\frac{\partial \ln c_e(x,t)}{\partial x} \tag{2.10}$$

the net voltage of the cell is determined by the boundary conditions of (2.7) as

$$V(t) = \phi_s(0^+,t) - \phi_s(0^-,t) \tag{2.11}$$

where $0^+, 0^-$ are the locations of the current collectors in positive and negative half cells respectively. Continuity of current between the solid, electrolyte and through

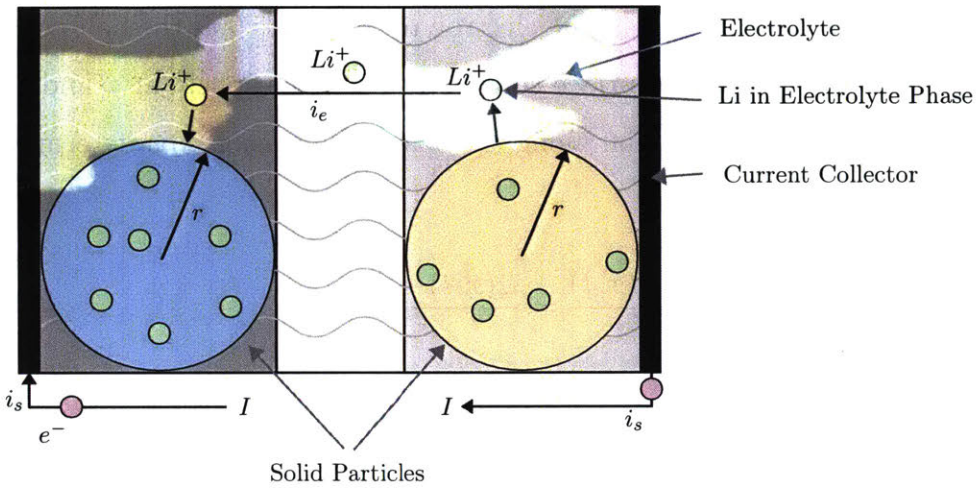


Figure 2-3: The most coarse discretization of the DFM model results in the single particle model. Each electrode is represented as a single particle in electrolyte. This coarse discretization is most accurate at low currents.

the cell obeys Kirkoff's current law,

$$i_s(x,t) + i_e(x,t) = I(t) \tag{2.12}$$

Equations (2.1)-(2.12) outline the DFN model for each half-cell with more detailed descriptions found in [9, 10, 14, 55]. Whereas the DFN is defined by a PDE in the $x$-dimension and a continuity of additional PDEs in the radial direction representing an infinite number of solid particles, numerical evaluation is accomplished by considering a finite number of these spherical particles. The most coarse discretization results from consideration of a single particle in each half-cell, and is commonly referred to as the Single Particle Model (SPM). In this model the electrolyte concentration, and therefore potential as well, are assumed constant across the cell. Additionally due to conservation of lithium within the cell we obtain the constraint,

$$n_{tot} = \frac{\epsilon_s^+ L^+}{4/3\pi(R_p^+)^3}\int_0^{R_p^+} 4\pi r^2 c_s^+(r,t)dr + \frac{\epsilon_s^- L^-}{4/3\pi(R_p^-)^3}\int_0^{R_p^-} 4\pi r^2 c_s^-(r,t)dr \tag{2.13}$$

with $c_s^+$ and $c_s^-$ the lithium concentration within the solid governed by (2.1) for the positive and negative half-cells respectively. With only two particles present (2.7) and (2.8) reduce to

$$\begin{aligned} j_n^+(t) &= \frac{-I(t)}{Fa^+L^+} \\ j_n^-(t) &= \frac{I(t)}{Fa^-L^-} \end{aligned} \tag{2.14}$$

Here we reduce the model one step further and describe an ordinary differential equation (ODE) simplification of the single particle model which will be used to simulate the lithium ion cell within this paper. The reduction to an ODE based model is attractive since in addition to state estimation, simultaneous online parameter identification is being performed.

## 2.1 Modified Single Particle (SP) Model

The SP model in [10] is a commonly used reduced electrochemical model of the DFN. In essence, the electrolyte dynamics are assumed to be constant in time and space in the SP model , which has been shown to be a valid approximation for current rates under 1C[1] [10, 20]. Unfortunately, although this assumption eliminates some of the complex dynamics involved, PDEs remain, as well as nonlinear relationships. A full exposition of the SP model can be found in [10].

The SP model can be reduced further using polynomial approximations [49] or eigenfunction approximations [20] resulting in diffusion processes described by linear ordinary differential equations. Each electrode of the resulting modified SP model is described by two linear differential equations, the first of which describes the mean

[1]It is common to define charging and discharging currents normalized by the battery capacity. For a 3AH (amp-hour) battery 1C current is 3A.

concentration in each electrode. Using the superscript $^{\pm}$ to compactly represent each electrode,

$$\begin{aligned} \frac{d\overline{c}_s^{\pm}}{dt} &= \alpha^{\pm} I \\ \alpha^{\pm} &= \frac{\pm 3}{R_p^{\pm}} \frac{1}{Fa^{\pm} L^{\pm} c_{s,max}^{\pm}} \end{aligned} \tag{2.15}$$

where $\overline{c}_s^+, \overline{c}_s^-$ are the normalized bulk lithium ion concentrations of the positive and negative electrodes, respectively, with the actual cell concentrations

$$c_s^{\pm} = c_{s,max}^{\pm} \overline{c}_s^{\pm}. \tag{2.16}$$

Notice that the differential equation (2.15) is simply an integrator. Therefore there is a linear dependence between $\overline{c}_s^+$ and $\overline{c}_s^-$ resulting in an algebraic constraint equivalent to the reduction of (2.13)

$$\frac{1}{\alpha^+} \overline{c}_s^+ + \frac{1}{\alpha^-} \overline{c}_s^- = n_{tot} \tag{2.17}$$

where $n_{tot}$ is the total moles of available lithium in the cell and $\alpha^{\pm}$ were defined in (2.15). The remaining states of the SP model are the normalized lithium ion fluxes of the positive and negative electrodes, $\overline{q}_s^{\pm}$, and are described as

$$\frac{d\overline{q}_s^{\pm}}{dt} = -30 \frac{D_s^{\pm}}{(R_p^{\pm})^2} \overline{q}_s^{\pm} + \alpha^{\pm} \frac{12}{7} I \tag{2.18}$$

Defining an intermediate output $\overline{c}_{ss}^{\pm}(t)$, which corresponds to the normalized surface concentration of each electrode one can derive the relation,

$$\overline{c}_{ss}^{\pm} = \overline{c}_s^{\pm} + \overline{q}_s^{\pm} \tag{2.19}$$

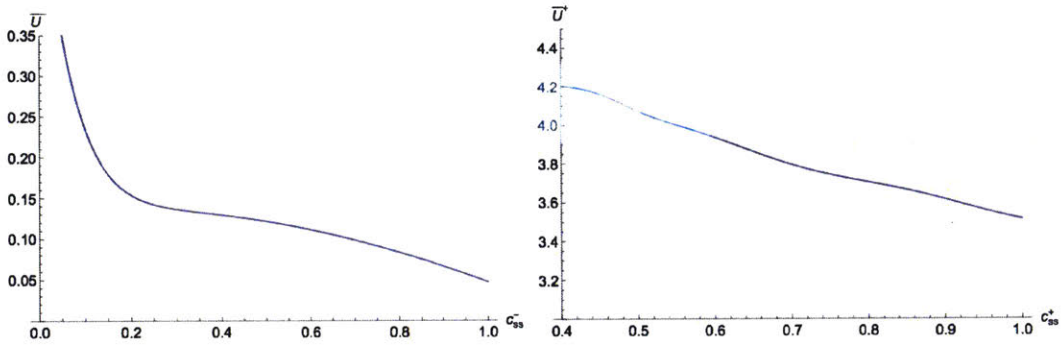


Figure 2-4: Half cell potentials of a Lonza $KS_6$ graphite negative electrode and a $NiO_2$ positive electrode. These cell potentials are used for simulated cells of Chapter 4

The open circuit potential is composed of the two half-cell electrochemical potentials which are functions of the particle surface concentrations,

$$V_{ocp} = f_{ocp}(\overline{c}_{ss}^+, \overline{c}_{ss}^-) = \overline{U}^+(\overline{c}_{ss}^+) - \overline{U}^-(\overline{c}_{ss}^-) \tag{2.20}$$

The half-cell potentials $\overline{U}^{\pm}(\overline{c}_{ss}^{\pm})$ used for simulation were originally defined within the Dualfoil cell simulator [41] and are shown in 2-4. $\overline{U}^{\pm}(\overline{c}_{ss}^{\pm})$ are usually empirically determined and will be different for each electrode chemistry. The full $\mathbb{R} \times \mathbb{R} \to \mathbb{R}$ mapping is shown in 2-5, with the equilibrium open circuit potential marked in green on the surface. Equation (2.5) can be inverted assuming the common approximation $\alpha^+ = \alpha^- = 0.5$ [14, 15, 49, 55] yielding

$$V_{over} = f_{over}(I, i_0^+, i_0^-) = \frac{2RT}{F}\sinh^{-1}\left(\frac{I}{i_0^+}\right) + \frac{R_f^+}{a^+L^+}I - \frac{2RT}{F}\sinh^{-1}\left(\frac{-I}{i_0^-}\right) + \frac{R_f^-}{a^-L^-}I \tag{2.21}$$

with the exchange current density

$$i_0^{\pm} = a^{\pm}L^{\pm}k_{eff}^{\pm}\sqrt{c_e^{0\pm}c_{s,max}^{\pm}\overline{c}_{ss}^{\pm}(1-\overline{c}_{ss}^{\pm})} \tag{2.22}$$

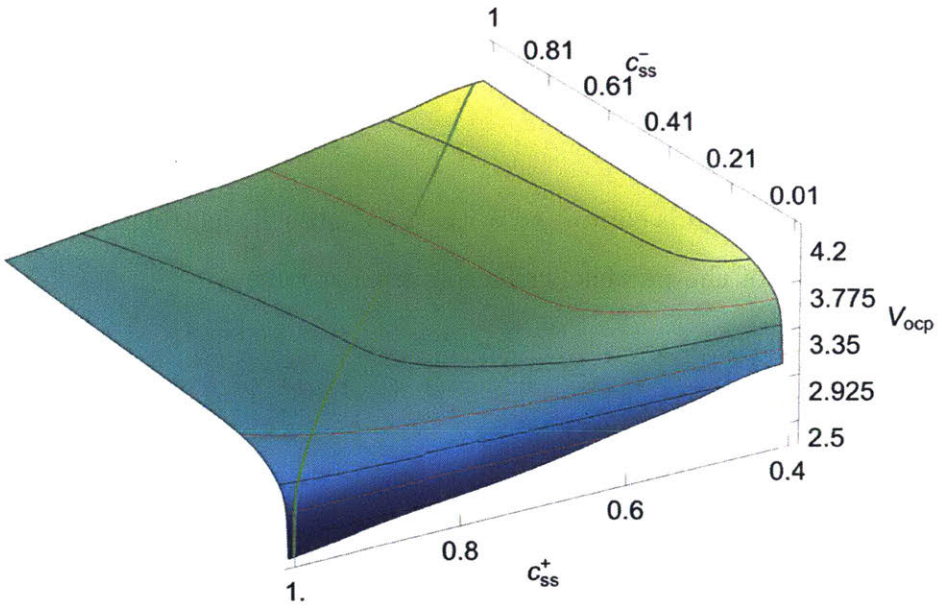


Figure 2-5: Open circuit potential mapping of (2.20) for a Panasonic NCR18650B cell. When in a relaxed state the cell voltage will lie on the green line, deviating from this line during transients. The location of this line is determined by the total available lithium within the system and the ratio of the effective electrode volumes. It is these parameters and hence this line which is calibrated in Section 5.1

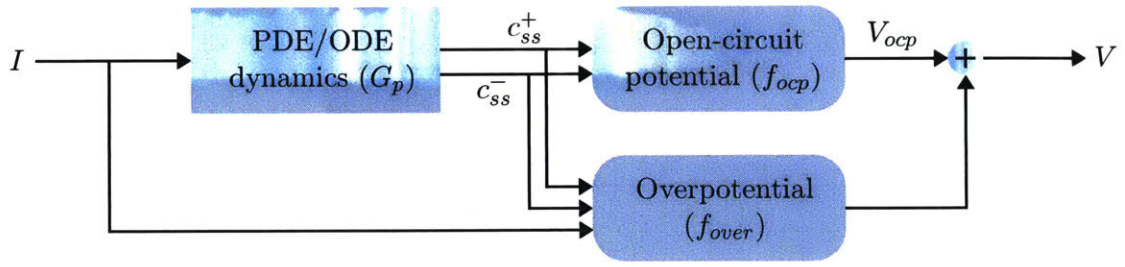


Figure 2-6: Modular system representation of the single particle model of (2.15)-(2.23)

The resulting output of the system is the cell voltage

$$V = V_{ocp} + V_{over} \tag{2.23}$$

yielding an ODE based SP model completely defined by (2.15)-(2.23) and is shown in Figure 2-6.

The $\mathbb{R} \times \mathbb{R} \to \mathbb{R}$ mapping of $f_{ocp}$ and the dependence of $f_{over}$ on $c_{ss}^{\pm}$ both prevent the direct use of adaptive observers on the previously formulated model. For the purposes of this work two modifications are made which reduce the complexity while maintaining accuracy and hold for the majority of the operating window. This results in the decoupling of the two nonlinearities. As pointed out in [55], the reaction mechanisms at the solid electrolyte interphase are not understood in great detail. And furthermore, the rapid kinetics in lithium batteries reduce the importance of the exact mechanism. This leads to the common first order approximation within the Butler-Volmer equation and $\alpha^+ = \alpha^- = 0.5$. This first order approximation of (2.22) yields a nonlinearity dependent on the solid surface concentrations within (2.21) of the form

$$\frac{1}{\sqrt{\overline{c}_{ss}^{\pm}(1 - \overline{c}_{ss}^{\pm})}} \tag{2.24}$$

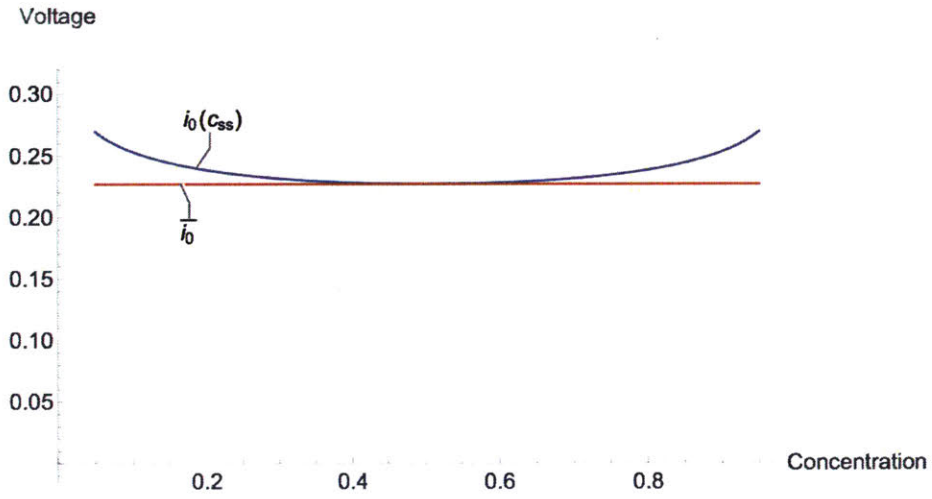


Figure 2-7: The effect of lithium concentration on the overpotential according to (2.21) is minimal except at extreme high/low concentrations. $\overline{i_0}$ of (2.25) is used as an approximation which is independent of the lithium concentration. This is assumption is justified by examination of the overpotential from experimental results as well as [55] who points out that the reaction mechanisms at the solid electrolyte interphase are not well understood and [4] who shows experimentally that the exchange current is indeed nearly flat across the full range of concentrations

The sensitivity of $V_{over}$ according to (2.21) to a change in the surface concentration $c_{ss}^{\pm}$ is shown in Figure 2-7. Noting that this function was already an approximation of the true kinetics and the relative flatness of this function between 0.1 and 0.9 motivates further investigation into the true sensitivity of the exchange current density $i_0^{\pm}$ to lithium concentration. Through analysis of experimental results collected as well as the results presented by [4] in which calculations of the exchange current density $i_0^{\pm}$ are nearly flat across the full range of concentrations tested justifies an approximation of

$$\overline{i_0^{\pm}} = a^{\pm} L^{\pm} k_{eff}^{\pm} \sqrt{c_e^{0\pm} c_{s,max}^{\pm} 0.5^2} \tag{2.25}$$

This decouples the nonlinearity $f_{over}$ from the surface concentration states of the

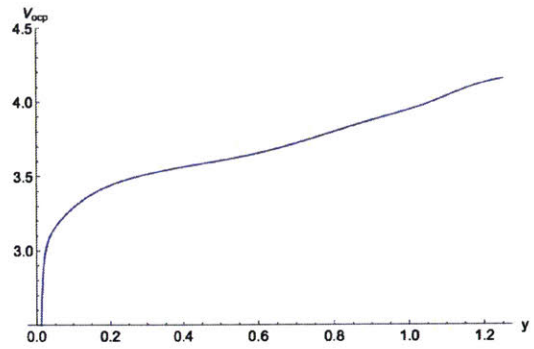


Figure 2-8: Full equilibrium open circuit potential for a cell with electrode half cell potentials of Figure 2-4. This function is $f^1_{ocp}(y)$ of (2.26) used for the OCP in simulation

dynamical system, $G_p$. The importance of this for modeling may be trivial, however, for state observers, particularly observers with simultaneous system identification, this results in $f_{over}$ which is purely a function of the measurable input $I$.

Additionally, we make two distinct approximations to $V_{ocp}$ of (2.20) with the primary purpose of reducing the $\mathbb{R} \times \mathbb{R} \to \mathbb{R}$ mapping to a $\mathbb{R} \to \mathbb{R}$ invertible non-linearity. Due to differences in the half-cell potentials of the simulated cell and the cell used for experiments individual approximations are made for each. For simulation we assume that the open circuit potential in (2.20) is dependent on a linear combination of the electrode surface concentrations, $\gamma_{ocp}\overline{c}^-_{ss} - \overline{c}^+_{ss}$, resulting in,

$$f^1_{ocp}(y = \gamma_{ocp}\overline{c}^-_{ss} - \overline{c}^+_{ss}) = \overline{U}(\gamma_{ocp}\overline{c}^-_{ss} - \overline{c}^+_{ss}) \tag{2.26}$$

This simplification is most accurate at low charge/discharge rates for the electrode chemistries used in simulation. The validity of this assumption is derived from the fact that the sensitivity of each half-cell are relatively constant and related by the gain $\gamma_{ocp}$. Unlike an approximation in which the surface concentrations maintain the algebraic constraint (2.17) as has been made in [38] this system approximation retains observability. A different chemistry cell used for experimental results motivates a

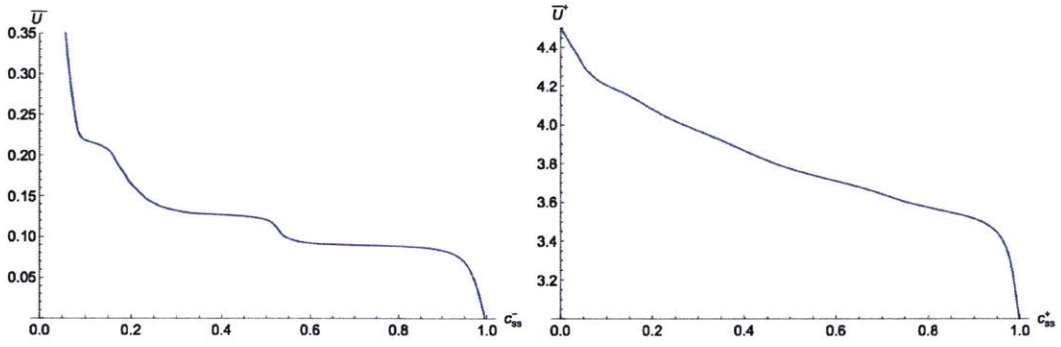


Figure 2-9: Half cell potentials of a Panasonic NCR18650B cell. The negative electrode is $C$ and the positive electrode is $LiCoNiAlO_2$. The flat sections $0.3 \leq c_{ss}^- \leq 0.5$ and $0.6 \leq c_{ss}^- \leq 0.9$ motivate approximation of the total opencircuit potential by (2.28).

different approximation of $V_{ocp}$ for Chapter 5.2. We observe in Figure 2-9 that the negative electrode half-cell potential is not sensitive to the lithium concentration for over 50% of its domain. While in these concentration ranges the negative electrode surface concentration becomes unobservable from the output voltage. Due to this, an assumption similar to [38] is made that

$$\overline{c}_{ss}^- = -\frac{\alpha^-}{\alpha^+}\overline{c}_{ss}^+ + \alpha^- n_{tot} \tag{2.27}$$

The result is that the negative electrode diffusion dynamics are no longer observable and the resulting open circuit potential is

$$f_{ocp}^2(y = c_s s^+) = \overline{U}(\overline{c}_{ss}^+) - \overline{U}(-\frac{\alpha^-}{\alpha^+}\overline{c}_{ss}^+ + \alpha^- n_{tot}) \tag{2.28}$$

With the negative electrode diffusion no longer observable, the corresponding state of the diffusion dynamics $\overline{q}^-$ is removed from the observer's system representation.

With the resulting modular structure shown in Figure 5-1, either of the nonlinear blocks or the linear dynamic block can be changed for higher fidelity models without

effecting the remaining two. Additionally, the basic structure is consistent between simulation and experimental results.

With a control theory audience in mind, the system can be represented in a more familiar state space representation with nonlinear outputs. Denoting the current, $I$, as the input one can compactly represent this reduced modified SP model for simulation using

$$\begin{aligned} x &= \begin{bmatrix} \overline{c}_s^- & \overline{q}_s^+ & \overline{q}_s^- \end{bmatrix}^\top \\ \dot{x} &= Ax + BI \\ y &= Cx \\ V &= f_{ocp}^i(y) + f_{over}^i(I) \end{aligned} \tag{2.29}$$

where $A, B$ contain the coefficients of (2.15) and (2.18), and are not assumed to be known, with (2.19) and (2.17), $C$ contains the coefficients resulting in

$$y = \gamma_{ocp}\overline{c}_{ss}^- - \overline{c}_{ss}^+ \tag{2.30}$$

The overall modified SP model is therefore a combination of a linear dynamic system $G_p(s)$ and nonlinearities $f_{ocp}^i$ and $f_{over}^i$ (see Figure 5-1), where

$$G_p(s) = C(sI - A)^{-1}B. \tag{2.31}$$

### 2.1.1 Approximation of the Cell Overpotential using sigmoidal basis functions

In anticipation of considering parametric uncertainty within $V_{over}$ of (2.21) we seek a formulation of the nonlinearity which is linearly parameterized. This will allow the

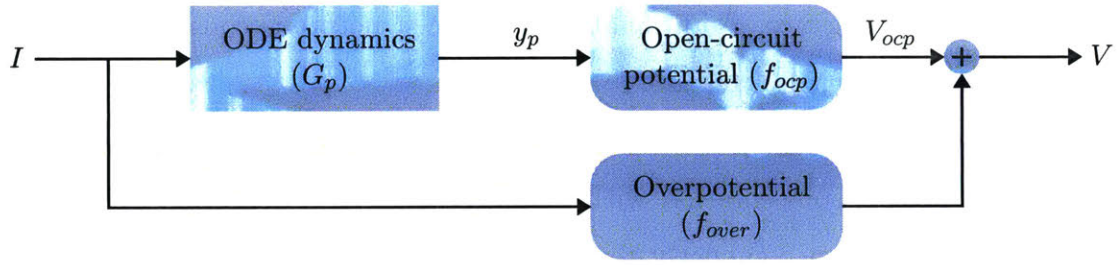


Figure 2-10: Block diagram of the electrochemical model used to represent a Lithium-Ion battery cell after simplifications are made for the observer.

use of linear system identification tools. Noting that the initial form is sigmoidal in nature, a sigmoidal basis function will be used to approximate $V_{over}$ as

$$f^b_{over}(I) = \alpha_1 I + \sum_{i=2}^{N} \alpha_i f_i(I) \tag{2.32}$$

$\alpha_i$ are unknown constant coefficients of the current, $I$ and known basis functions $f_i(I)$. Here we use a basis function derived from the cumulative distribution function of a Beta distribution [5] with $\alpha = 1$ and $\beta = 2$. The original function only defined from $0 \leq x \leq 1$ as $1 - (1 - x)^2$ is mirrored about the origin, stretched by swapping $\frac{x}{\beta_i}$ for $x$ and extrapolated for $x < \frac{-1}{\beta_i}$ and $x > \frac{1}{\beta_i}$ resulting in

$$f_i(x) = \begin{cases} 1 - (1 - \frac{x}{\beta_i})^2 & 0 < x < \beta_i \\ -1 + (1 + \frac{x}{\beta_i})^2 & -\beta_i < x < 0 \\ 1 & x \geq \beta_i \\ -1 & x \leq -\beta_i \\ 0 & otherwise \end{cases} \tag{2.33}$$

The desirable properties which resulted in the use of this basis function over other sigmoidal functions are that it saturates at $x = \pm\beta_i$, is continuous and differentiable and requires only one parameter, $\beta_i$, with a clear correlation to its impact of stretch-

ing $f_i$ over its domain. Since $V_{over}$ of (2.22) is a strictly monotonically increasing function we can expect all coefficients $\alpha_i$ to be positive. An accurate fit can be accomplished using three basis functions with $\beta_i \in \{\frac{1}{2}\ 1\ 2\}$. The agreement of $f^1_{over}$ of (2.32) with (2.21) is seen in Figure 2-11. Symmetry of the function allows fitting to be performed and displayed for positive currents, using points in red, a fit for $0 < I_k < 2$ is performed using the method of least squares. The fitting extrapolates well past the domain used for fitting matching the nonlinearity up to $3A$.

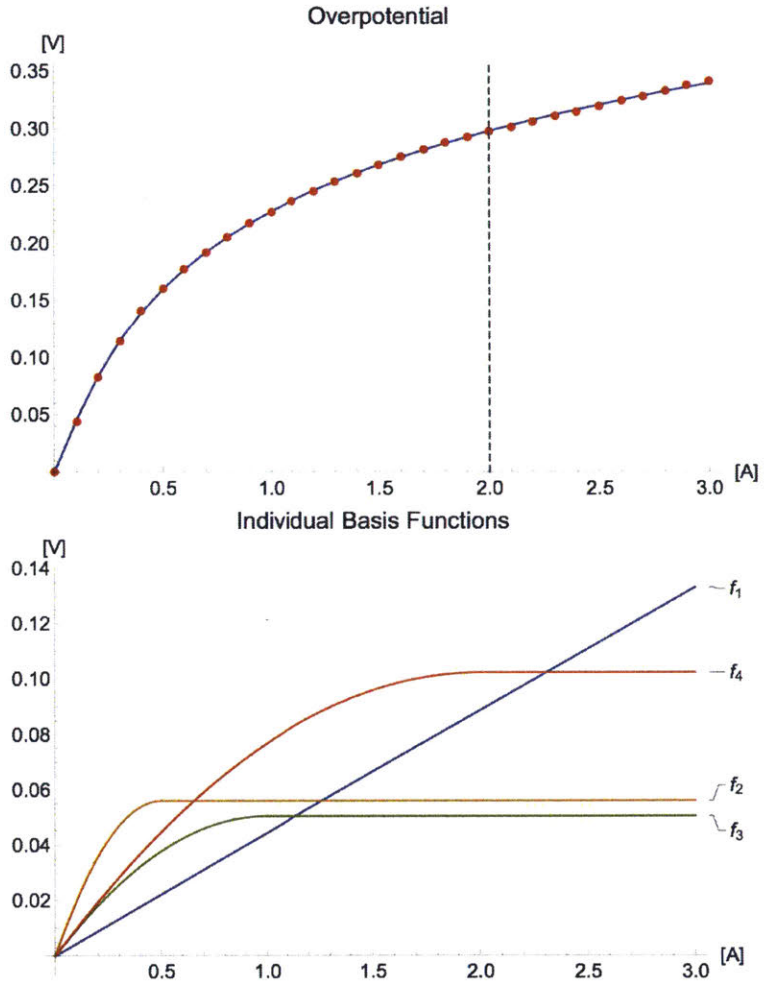


Figure 2-11: Approximation of the overpotential function $f^1_{over}$ using sigmoidal basis functions. The resulting coefficients are $\alpha = \begin{bmatrix} 0.0443 & 0.0559 & 0.0504 & 0.102 \end{bmatrix}^\top$

## 2.2 Sensitivity to parametric uncertainties in the modified SP model

The focus of this thesis is simultaneous estimation of parameters and states. In this section we briefly explore the effect of parametric uncertainty on the plant response in comparison to the resulting error from modeling simplifications. Due to manufacturing processes, aging or abuse, many of the physical variables will not be consistent cell to cell or remain constant over time. This in turn implies that the parameters of $A, B$ and the nonlinearities $f_{ocp}$ and $f_{over}$ of (2.29) as well as the algebraic constraint (2.17) may not be known initially and can change over time. One approach to solve this issue would be to calibrate each cell post production and model the slow aging process explicitly, but this would be a time consuming process, add to the already complex model, and assume that we fully understand every possible aging mechanism. We propose a different approach which consists of real-time parameter estimation in the battery model specified by (2.15)-(2.23) using real-time measurements of the input $I$ and output $V$.

One of the questions that arises is the accuracy and relevance of parameter estimation using the nonlinear, yet ODE-model as in (2.15)-(2.23), which is based on a reduced SP model, given that the underlying battery dynamics is spatio-temporal in nature. As shown previously in the literature [10, 37, 61] we maintain that for a significant class of operating conditions, the ODE model does indeed accurately capture the variations of a higher fidelity PDE model, which is also based on the SP model. This is justified by the following simulation studies. Table 1 lists all of the parameters used in the all simulation studies reported in this paper.

Denoting the modified SP model with nominal parameters as ODE* and the SP model with nominal parameters as PDE*, we compare the error between the two

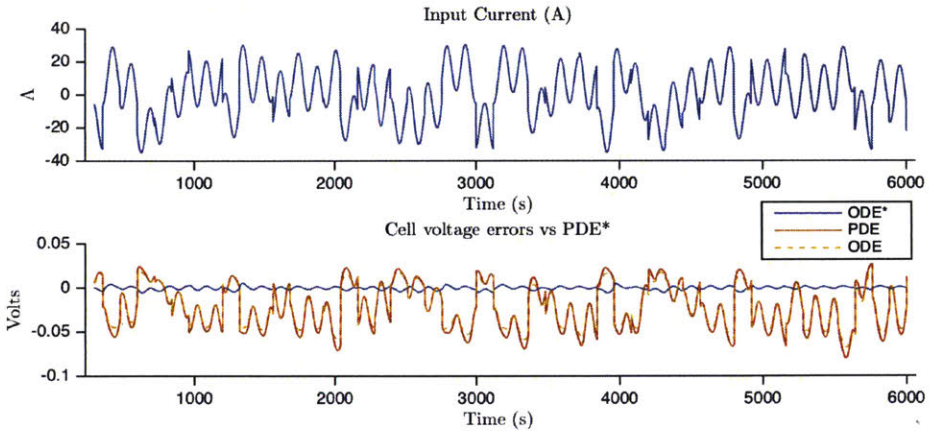


Figure 2-12: Output voltage errors due to model reduction and/or parametric uncertainty with maximum input current of less than 1C. The baseline model is the SPM with PDE dynamics (PDE*). Error due to ODE reduction is in blue (ODE*). Error due to introduction of parametric uncertianty to the PDE SP model is in red (PDE). Error due to parameter error in the ODE SP model is in dotted yellow (ODE).

model outputs for charge-discharge rates of up to 1C, and present the results in Figure 2-12. We then introduce parametric uncertainties of $\underline{D_s^{\pm}} = 0.5D_s^{\pm}, \underline{k_{eff}^{\pm}} = 0.5k_{eff}^{\pm}, \underline{L}^{+} = 1.2L^{+}, \underline{L}^{-} = 0.9L^{-}$ into both models, denoting the corresponding models as ODE and PDE respectively, and evaluate their output error responses relative to PDE* in Figure 2-12 as well.

We do not focus on a comparison of ODE to PDE-model or ODE* to PDE*-model, as that has been discussed extensively in existing literature [10, 37, 61]. Instead, we compare the responses of ODE* with PDE* as well as ODE with PDE, where the former will only reflect the error due to ODE discretization while the later will show both the errors due to discretization and parametric uncertainties. The effect of parametric uncertianty alone is captured by the comparison of PDE and PDE*-model error. We see in Figure 2-12 that modest parametric uncertainties of the models can yield more than a 10-fold increase in model output error compared to ODE discretization alone.

The complexity as well as combined presence of linear dynamics together with the two nonlinearities $f_{ocp}$ and $f_{over}$ introduces a number of challenges for simultaneous state estimation and parameter identification. In order to overcome this, we separate the identification of each, but do so in a way which is guaranteed to result in bounded errors. For ease of exposition we first assume that the nonlinearities are known and therefore can be isolated and removed or inverted. This allows us to consider unknown linear dynamics only, and propose an adaptive observer that is capable of fast parameter estimation. As a second step, we extend this adaptive observer to accommodate the estimation of the overpotential nonlinearity $f^1_{over}$ of (2.32) with an approximation using sigmoidal basis functions while assuming only $f_{ocp}$ is known.

## 2.3 Summary of the modified SP models

Table 2.1: The nominal Li-Ion Battery parameters used for all simulation results reported in this paper.

| | | | |
|---|---|---|---|
| $R_p^+$ | $10^-5$ | $R_p^-$ | $10^-5$ |
| $L^+$ | $10^-4$ | $L^-$ | $10^-4$ |
| $R_f^+$ | 0 | $R_f^-$ | $10^-3$ |
| $k_{eff}^+$ | $4.5 \times 10^-6$ | $k_{eff}^-$ | $4.5 \times 10^-6$ |
| $\sigma^+$ | 3.53 | $\sigma^-$ | 46.47 |
| $\epsilon_e^+$ | 0.3 | $\epsilon_e^-$ | 0.3 |
| $a^+$ | $1.5 \times 10^5$ | $a^-$ | $1.8 \times 10^5$ |
| $t_a^0$ | 0.6 | $c_{e0}$ | 1000 |
| $c_{s,max}^+$ | 51217 | $c_{s,max}^-$ | 24983 |
| $D_e^+$ | $4.58 \times 10^-11$ | $D_e^-$ | $2.79 \times 10^-11$ |
| $D_s^+$ | $1 \times 10^-13$ | $D_s^-$ | $4 \times 10^-14$ |

### 2.3.1 Summary of modified SP model for simulation

We now present a summary of the modified SP model used for simulations. The diffusion of lithium in the solid particles is modeled as,

$$x = \begin{bmatrix} \overline{c}_s^- \\ \overline{q}_s^+ \\ \overline{q}_s^- \end{bmatrix}$$
$$\dot{x} = Ax + BI = \begin{bmatrix} 0 & 0 & 0 \\ 0 & -30\frac{D_s^+}{(R_p^+)^2} & 0 \\ 0 & 0 & -30\frac{D_s^-}{(R_p^-)^2} \end{bmatrix} x + \begin{bmatrix} \alpha^- \\ \frac{12}{7}\alpha^+ \\ \frac{12}{7}\alpha^- \end{bmatrix} I \tag{2.34}$$

with dynamical system output,

$$y = Cx = \begin{bmatrix} \left(\gamma_{ocp} + \frac{\alpha^+}{\alpha^-}\right) & -1 & \gamma_{ocp} \end{bmatrix} x \tag{2.35}$$

which is related to the measurable cell voltage as,

$$V = f_{ocp}^1(y - \alpha^+ n_{tot}) + f_{over}^b(I) \tag{2.36}$$

where $f_{ocp}^1$ is the open circuit potential function used for simulation,

$$f_{ocp}^1(y = \gamma_{ocp}\overline{c}_{ss}^- - \overline{c}_{ss}^+) = \overline{U}(\gamma_{ocp}\overline{c}_{ss}^- - \overline{c}_{ss}^+) \tag{2.37}$$

and $f_{over}^1$ is the overpotential function used for simulation,

$$f_{over}^1(I) = \alpha_1 I + \sum_{i=2}^{4} \alpha_i f_i(I) \tag{2.38}$$

using the basis functions $f_i$,

$$f_i(x) = \begin{cases} 1-(1-\frac{x}{\beta_i})^2 & 0 < x < \beta_i \\ -1+(1+\frac{x}{\beta_i})^2 & -\beta_i < x < 0 \\ 1 & x \geq \beta_i \\ -1 & x \leq -\beta_i \\ 0 & otherwise \end{cases} \tag{2.39}$$

$$\beta_i \in \{\frac{1}{2}\ 1\ 2\} \tag{2.40}$$

### 2.3.2 Summary of modified SP model for experimental results

We now summarize the modified SP model structure used for experiments. The diffusion of lithium in the solid particles is modeled as,

$$\begin{aligned} x &= \begin{bmatrix} \overline{c}_s^- \\ \overline{q}_s^+ \end{bmatrix} \\ \dot{x} = Ax + BI &= \begin{bmatrix} 0 & 0 \\ 0 & -30\frac{D_s^+}{(R_p^+)^2} \end{bmatrix} x + \begin{bmatrix} \alpha^- \\ \frac{12}{7}\alpha^+ \end{bmatrix} I \end{aligned} \tag{2.41}$$

where due to unobservability of the negative electrode for the majority of operating conditions the dynamical system is reduced by one order relative to (2.34). The dynamical system output is,

$$y = Cx = \begin{bmatrix} \left(\frac{\alpha^+}{\alpha^-}\right) & -1 \end{bmatrix} x \tag{2.42}$$

which is related to the measurable cell voltage as,

$$V = f_{ocp}^2(y) + f_{over}^2(I) \tag{2.43}$$

where $f^2_{ocp}$ is the open circuit potential function used for experiments,

$$f^2_{ocp}(y = c_s s^+) = \overline{U}(\overline{c}^+_{ss}) - \overline{U}(-\frac{\alpha^-}{\alpha^+}\overline{c}^+_{ss} + \alpha^- n_{tot}) \tag{2.44}$$

using the approximation of the negative electrode surface concentration

$$\overline{c}^-_{ss} = -\frac{\alpha^-}{\alpha^+}\overline{c}^+_{ss} + \alpha^- n_{tot} \tag{2.45}$$

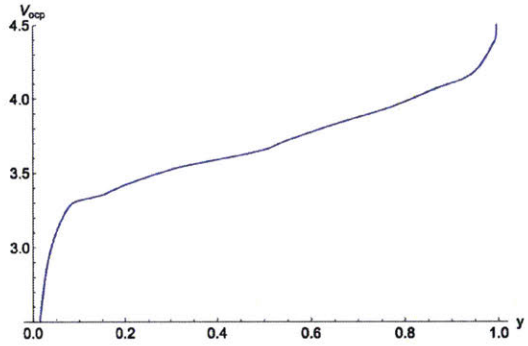


Figure 2-13: Although this looks quite similar to 2-8 when one looks at the underlying half-cell potentials in 2-4 and 2-9 you see that the flat sections which make up 50% of the operating region of the negative electrode prevent observability of the corresponding electrodes concentration

and $f^2_{over}$ is the overpotential function used for experiments,

$$f^2_{over}(I) = \alpha_1 I \tag{2.46}$$

# Chapter 3

# Adaptive Observers for Linear SP Models

## Contents

Chapter 3 begins with the assumption that both $f_{ocp}$ and $f_{over}$ are known allowing them to be inverted and removed respectively. Next, in Chapter 4, we allow $f_{over}$ to be unknown, and it is replaced by an approximation using basis functions. The unknown coefficients of the basis functions are added to the adaptive observer parameter vector. This resulting observer estimates the equivalent dynamic system as well as the nonlinear overpotential simultaneously. This chapter focuses on the generation and analysis of adaptive observers for linear system observation and identification. Section 3.1 reviews the basic adaptive observer which has appeared in [7,31,39]. The stability of the vector regressor based adaptive observer (VR-AO) is analyzed and the notion of persistence of excitation (PE), which is required for convergence of the parameter errors to 0, is explored. Design guidelines, a primary contribution of this thesis are explored and a set of tools is suggested to generate the adaptive observer with a significantly reduced number of tuning parameters. The topic of parameter constraints is addressed by utilizing a projection algorithm. Lastly the procedure for state transformations is formally laid out, with an example relevant to our battery model of transforming back to a Jordan-canonical form.

In section 3.2 two matrix regressor adaptive observers (MR-AO) are explored and the notion of strong persistent excitation (SPE) is introduced. The first of which, designated MR-AO-I was previously proposed by [24,25,39] as an adaptive observer capable of arbitrarily fast parameter convergence. This claim is explored using the notion of Strong-PE (SPE) and a stability analysis will show that there exists a limiting factor of the speed of convergence. Next we propose a new form of MR-AO previously reported in [22]. There is a fundamental difference to in the generation of regressors which offers multiple advantages over MR-AO-I. The chapter is concluded with a comparison of the three adaptive observers and a summary of their algorithms.

Since the underlying battery model is in the form of the block diagram in Figure

5-1 and defined by (2.34)-(2.39), from observations of $V$, one can accurately estimate the parameters of $G_p(s)$ from input-output measurements of $I(t), y(t)$ using an adaptive observer [40], with $y = f_{ocp}^{-1}(V - f_{over}(I))$.

## 3.1 Vector-regressor (VR) Adaptive Observers (AOs)

Consider a stable linear, time-invariant system which is both controllable and observable, and of known order $n$. This system can be represented in state space form as

$$\begin{aligned} \dot{x}(t) &= A_p x(t) + b_p u(t) \\ y(t) &= c_p^\top x(t) \end{aligned} \tag{3.1}$$

The system matrices $A_p \in \mathbb{R}^{n\times n}, b_p, c_p \in \mathbb{R}^n$ as well as the initial state $x(t_0) \in \mathbb{R}^n$ are unknown. The problem we wish to solve is to use the input $u(t)$ and output $y(t)$ and estimate the states $x(t)$ as well as the dynamics described by $A_p, b_p, c_p$. By considering a reduction of the system to its transfer function representation, $G_p(s)$,

$$G_p(s) = c_p^\top (sI - A_p)^{-1} b_p = \frac{P(s)}{Q(s)} = \frac{p_0 + p_1 s + p_2 s^2 + \cdots + p_{n-1} s^{n-1}}{q_0 + q_1 s + q_2 s^2 + \cdots + q_{n-1} s^{n-1} s^n} \tag{3.2}$$

where $I \in \mathbb{R}^{n\times n}$ is an identity matrix, it becomes clear that even though $A_p, b_p, c_p$ of (3.1) contain $n^2 + 2n$ variables, a unique description of the plant requires only $2n$ parameters. In the case of (3.2) these $2n$ parameters are the coefficients of the transfer-function numerator and denominator, these parameters are directly related to the poles and zeros of the plant. In order to determine the full *state space* model from only input-output data some additional information is required in order to determine the remaining $n^2$ parameters, such as a common pre-defined representation.

This additional information is essential to estimate any internal states of a state space model. For example, we know the system of (2.29) is Jordan-normal form.

Without loss of generality, throughout this section we will assume that the system is initially described in observer-canonical form, with

$$A_p = \begin{bmatrix} & I_{n-1\times n-1} \\ -a_p & \\ & 0_{1\times n-1} \end{bmatrix} \quad c_p = \begin{bmatrix} 1 \\ 0 \\ \vdots \end{bmatrix} \tag{3.3}$$

where all unknown parameters of (3.1) are contained in the vectors $a_p, b_p \in \mathbb{R}^n$. An equivalent system can then be defined

$$\begin{aligned} \dot{x}(t) &= (F^{OC} + \theta_y c_p^\top)x(t) + b_p u(t) = F^{OC}x(t) + \theta_y y(t) + \theta_u u(t) \\ y(t) &= c_p^\top x(t) \end{aligned} \tag{3.4}$$

with $F^{OC} \in \mathbb{R}^{n\times n}$,

$$F^{OC} = \begin{bmatrix} & I_{n-1\times n-1} \\ -f & \\ & 0_{1\times n-1} \end{bmatrix} \tag{3.5}$$

chosen by the designer to obtain a stable, observable pair $(F^{OC}, c_p)$. All unknown parameters are now isolated into two vectors $\theta_u, \theta_y \in \mathbb{R}^n$ given by

$$\theta_u = b_p \;\; and \;\; \theta_y = f - a_p \tag{3.6}$$

Notice here that $\theta_u$ is independent of the filter choice $F^{OC}$ and $\theta_y$ is a linear combination of the plant and filter characteristic polynomial coefficients. Leveraging the property of superposition one can generate the output $y$ of (3.4) in an alternate form

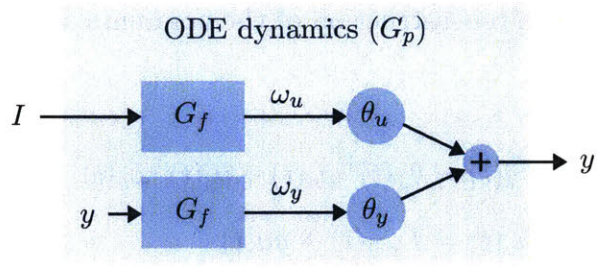


Figure 3-1: Equivalent system representation for the battery dynamics of the electrochemical model used.

using a nonminimal system in observer-canonical (OC) form

$$\begin{aligned} y(t) &= g^\top x_1(t) + g^\top x_2(t) \\ \dot{x}_1(t) &= F^{OC} x_1(t) + \theta_u u(t) \\ \dot{x}_2(t) &= F^{OC} x_2(t) + \theta_y y(t) \end{aligned} \tag{3.7}$$

with $g = c_p$. We perform one more transformation, generating the output $y(t)$ using control-canonical (CC) filters, $F = (F^{OC})^\top$, to obtain vector regressors $\omega_u, \omega_y$ as

$$\begin{aligned} y(t) &= \theta_u^\top \omega_u(t) + \theta_y^\top \omega_y(t) \\ \dot{\omega}_u(t) &= F\omega_u(t) + gu(t) \\ \dot{\omega}_y(t) &= F\omega_y(t) + gy(t) \end{aligned} \tag{3.8}$$

which follows from straight forward algebraic manipulation, and the suitable choice of initial conditions of $\omega_u$ and $\omega_y$. By transforming from a nonminimal system (3.7) in OC form to (3.8) in CC form we have manipulated the system such that all system unknowns are now in the output equation $y(t) = \theta_u^\top \omega_u(t) + \theta_y^\top \omega_y(t)$. The resulting figure is shown in Figure 3-1.

With the plant in (3.1) rewritten in the form of (3.8), one can construct an adaptive observer to generate the parameter estimates $\hat{\theta}_u$ and $\hat{\theta}_y$ [40]. The adaptive

observer is begins with the reconstruction of the nonminimal states and an estimate of the plant output,

$$\begin{aligned} \hat{y}(t) &= \hat{\theta}_u(t)^\top \hat{\omega}_u(t) + \hat{\theta}_y(t)^\top \hat{\omega}_y(t) \\ \dot{\hat{\omega}}_u(t) &= F\hat{\omega}_u(t) + gu(t) \\ \dot{\hat{\omega}}_y(t) &= F\hat{\omega}_y(t) + gy(t). \end{aligned} \tag{3.9}$$

We note from (3.8) and (3.9) that a corresponding error $e$ is obtained as

$$e(t) = \hat{y}(t) - y(t) \tag{3.10}$$

The estimates of the unknown plant parameters are identified using a gradient adaptive law [40]using the vector regressors $\hat{\omega}_u$ and $\hat{\omega}_y$ as

$$\begin{aligned} \dot{\hat{\theta}}_u(t) &= -\Gamma_u \hat{\omega}_u(t) e(t) \\ \dot{\hat{\theta}}_y(t) &= -\Gamma_y \hat{\omega}_y(t) e(t) \end{aligned} \tag{3.11}$$

where $\Gamma_u, \Gamma_y \in \mathbb{R}^{n\times n}$ are positive definite matrices free to be chosen in the adaptive observer design. We denote the adaptive observer defined by equations (3.9)-(3.11) as the vector regressor based adaptive observer (VR-AO). Before formally moving on to a rigorous proof of the observer's stability properties we define the nonminimal system state errors $\widetilde{\omega}_u = \hat{\omega}_u - \omega_u$ and $\widetilde{\omega}_y = \hat{\omega}_y - \omega_y$ which are described by

$$\begin{aligned} \dot{\widetilde{\omega}}_u &= F\hat{\omega}_u + g_u u - (F\omega_u + gu) \\ &= F\widetilde{\omega}_u \\ \dot{\widetilde{\omega}}_y &= F\hat{\omega}_y + g_u y - (F\omega_y + gy) \\ &= F\widetilde{\omega}_y \end{aligned} \tag{3.12}$$

which, since $F$ is Hurwitz, will decay exponentially to zero regardless of the parameter estimates. This is a result of our transformation of the nonminimal system from OC form of (3.7) to CC form in (3.8). With the vector-regressor based adaptive observer fully described, we now move on to prove stability of the VR-AO.

### 3.1.1 Stability of the VR-AO

For a nonminimal system (3.8), with an estimated system (3.9) and nonminimal state errors (3.12). We now analyze the stability of the nonminimal state errors at $\widetilde{\omega}_u = 0$ and $\widetilde{\omega}_y = 0$ and the parameter errors $\widetilde{\theta}_u = 0$ and $\widetilde{\theta}_y = 0$ assuming $u, y \in \mathcal{L}_\infty$. To ease the notation in what follows we combine nonminimal states $\omega_u$ and $\omega_y$ to create a single regressor $\omega$ and do the same for $\theta_u, \theta_y$, as well as their estimates, to obtain,

$$\omega = \begin{bmatrix} \omega_u \\ \omega_y \end{bmatrix}, \theta = \begin{bmatrix} \theta_u \\ \theta_y \end{bmatrix}, \hat{\omega} = \begin{bmatrix} \hat{\omega}_u \\ \hat{\omega}_y \end{bmatrix}, \hat{\theta} = \begin{bmatrix} \hat{\theta}_u \\ \hat{\theta}_y \end{bmatrix} \tag{3.13}$$

with errors defined as $\widetilde{\omega} = \hat{\omega} - \omega$ and $\widetilde{\theta} = \hat{\theta} - \theta$. Additionally we define $\overline{F}, \overline{g}$ such that $\dot{\omega} = \overline{F}\omega + \overline{g} \begin{bmatrix} u \\ y \end{bmatrix}$,

$$\overline{F} = \begin{bmatrix} F & \\ & F \end{bmatrix}, \overline{g} = \begin{bmatrix} g & \\ & g \end{bmatrix} \tag{3.14}$$

we update the parameters of the adaptive observer using a gradient descent adaptive law,

$$\dot{\hat{\theta}} = \dot{\widetilde{\theta}} = -\Gamma_\omega \hat{\omega} e \tag{3.15}$$

where we use a positive definite adaptive gain, $\Gamma_\omega \in \mathbb{R}^{2n\times 2n}$, and use the output error,

$$\begin{aligned} e &= \hat{y} - y \\ &= \hat{\omega}^\top \hat{\theta} - \omega^\top \theta = \hat{\omega}^\top \hat{\theta} - (\hat{\omega} + \tilde{\omega})^\top \theta \\ &= \underbrace{\hat{\omega}^\top \tilde{\theta}}_{e_\theta} + \underbrace{\tilde{\omega}^\top \theta}_{e_\omega} \end{aligned} \tag{3.16}$$

Notice from 3.16 that the error $e = e_\theta + e_\omega$ has been decomposed into two terms, $e_\theta$ and $e_\omega$ which are sensitive to the parameter error and the nonminimal state error respectively. To analyze the stability of the adaptive observer defined by (3.9),(3.13),(3.15) and (3.16) we define a radially unbounded Lyapunov function candidate

$$V = \frac{1}{2}\tilde{\theta}^\top \Gamma_v \tilde{\theta} + \tilde{\omega}^\top P \tilde{\omega} \tag{3.17}$$

with positive definite $\Gamma_v, P \in \mathbb{R}^{2n\times 2n}$. For which $P$ which satisfies the lyapunov equation,

$$\overline{F}^\top P + P\overline{F} + Q = 0 \tag{3.18}$$

for any positive definite $Q \in \mathbb{R}^{2n\times 2n}$, this $P$ will be positive definite and is guaranteed to exist for any Hurwitz $\overline{F}$. Using $\dot{\hat{\theta}}$ of (3.15) and $\dot{\tilde{\omega}}$ of (3.12) the time derivative of (3.17) is given by

$$\begin{aligned} \dot{V} &= \frac{1}{2}\left(\dot{\tilde{\theta}}^\top \Gamma_v \tilde{\theta} + \tilde{\theta}^\top \Gamma_v \dot{\tilde{\theta}}\right) + \dot{\tilde{\omega}}^\top P \tilde{\omega} + \tilde{\omega}^\top P \dot{\tilde{\omega}} \\ &= -\frac{1}{2}\left(e\hat{\omega}^\top \Gamma_\omega^\top \Gamma_v \tilde{\theta} + \tilde{\theta}^\top \Gamma_v \Gamma_\omega \hat{\omega} e\right) + \tilde{\omega}^\top \overline{F}^\top P \tilde{\omega} + \tilde{\omega}^\top P \overline{F} \tilde{\omega} \end{aligned} \tag{3.19}$$

Using $\epsilon$ from (3.16) and the lyapuov equation of (3.18) we can then rewrite (3.19) as

$$\begin{aligned}\dot{V} &= -\frac{1}{2}\left((\widetilde{\theta}^\top\hat{\omega}+\theta^\top\widetilde{\omega})\hat{\omega}^\top\Gamma_\omega^\top\Gamma_v\widetilde{\theta}+\widetilde{\theta}^\top\Gamma_v\Gamma_\omega\hat{\omega}(\hat{\omega}^\top\widetilde{\theta}+\widetilde{\omega}^\top\theta)\right)-\widetilde{\omega}^\top Q\widetilde{\omega}\\ &= -\frac{1}{2}\left(\widetilde{\theta}^\top\hat{\omega}\hat{\omega}^\top\Gamma_\omega^\top\Gamma_v\widetilde{\theta}+\widetilde{\theta}^\top\Gamma_v\Gamma_\omega\hat{\omega}\hat{\omega}^\top\widetilde{\theta}\right)-\widetilde{\omega}^\top Q\widetilde{\omega}-\frac{1}{2}\left(\theta^\top\widetilde{\omega}\hat{\omega}^\top\Gamma_\omega^\top\Gamma_v\widetilde{\theta}+\widetilde{\theta}^\top\Gamma_v\Gamma_\omega\hat{\omega}\widetilde{\omega}^\top\theta\right)\end{aligned} \tag{3.20}$$

Proceeding with $\Gamma_v=\Gamma_\omega^{-1}$, and using $e_\theta, e_\omega$ of (3.16), (3.20) simplifies to

$$\begin{aligned}\dot{V} &= -\frac{1}{2}\left(\widetilde{\theta}^\top\hat{\omega}\hat{\omega}^\top\widetilde{\theta}+\widetilde{\theta}^\top\hat{\omega}\hat{\omega}^\top\widetilde{\theta}\right)-\widetilde{\omega}^\top Q\widetilde{\omega}-\frac{1}{2}\left(\theta^\top\widetilde{\omega}\hat{\omega}^\top\widetilde{\theta}+\widetilde{\theta}^\top\hat{\omega}\widetilde{\omega}^\top\theta\right)\\ &= -\widetilde{\theta}^\top\hat{\omega}\hat{\omega}^\top\widetilde{\theta}-\widetilde{\omega}^\top Q\widetilde{\omega}-\theta^\top\widetilde{\omega}\hat{\omega}^\top\widetilde{\theta}\\ &\leq -e_\theta^2-\widetilde{\omega}^\top Q\widetilde{\omega}-e_\omega e_\theta\end{aligned} \tag{3.21}$$

Where the first term is a negative quadratic term in $e_\theta$ and the last is a sign indefinite term which is linear in $e_\theta$. We can explicitly write $e_\omega$ in terms of the initial condition of $\widetilde{\omega}$,

$$e_\omega = \theta^\top e^{\overline{F}(t)}\widetilde{\omega}(0) \tag{3.22}$$

From (3.21) we see that $\dot{V}\leq 0$ when $|e_\theta|\geq|e_\omega|$. This guarantees local stability outside of the compact set

$$S=\{\widetilde{\omega}\in\mathbb{R}^{2n},\widetilde{\theta}\in\mathbb{R}^{2n}:|\widetilde{\theta}^\top(\widetilde{\omega}+\omega)|<|\theta^\top\widetilde{\omega}|\} \tag{3.23}$$

Since $e_\omega=\theta^\top\widetilde{\omega}$ exponentially decreases independent of any inputs or adaptive parameters, $S$ exponentially decreases in size and we exponentially approach a globally stable system.

From here we consider two cases. For case 1, the input $u$ is bounded. With

$u \in \mathcal{L}_\infty$ it follows that since $F$ is Hurwitz and $G_p(s)$ is stable, $\omega, \hat{\omega}, \widetilde{\omega} \in \mathcal{L}_\infty$. Since $V$ is radially unbounded and $\dot{V} \leq 0$ outside the set $S$, $V(t) \leq \infty$ and therefore $V(t) \in \mathcal{L}_\infty$ which implies that $\hat{\theta}, \widetilde{\theta} \in \mathcal{L}_\infty$. We can then conclude that $e_\theta, e_\omega, \dot{\omega} \in \mathcal{L}_\infty$. With $\overline{F}$ Hurwitz we also have $e_\omega \in \mathcal{L}_2$. Furthermore, since $S$ exponentially decreases there will exist a time $t_1$ for which $t > t_1$ and $V(t) \leq V(t_1) \leq \infty$. With $\int_{t_1}^{t} \dot{V}(\tau)d\tau = V(t) - V(t_1)$ and since $V(t)$ is both positive definite and non-decreasing, we have $V(t_1) - V(t) \leq V(t_1)$ and therefore $-\int_{t_1}^{t} \dot{V}(\tau)d\tau \leq V(t_1)$ From (3.21) we have $\int_{t_1}^{t}(e_\theta^2 + e_\theta e_\omega + \widetilde{\omega}^\top Q\widetilde{\omega})d\tau \leq V(t_1)$, since we have $e_\omega \in \mathcal{L}_2$, $\int_{t_1}^{t}(e_\theta^2 + e_\theta e_\omega + \frac{1}{4}e_\omega^2 + \widetilde{\omega}^\top Q\widetilde{\omega})d\tau \leq V(t_1) + C_\omega$ where $\int_{t_1}^{\infty} e_\omega^2 d\tau = C_\omega$. This simplifies to $\int_{t_1}^{t}(e_\theta^2 + \frac{1}{2}e_\omega)^2 + \widetilde{\omega}^\top Q\widetilde{\omega})d\tau \leq V(t_1) + C_\omega$ and we find that $e_\theta, \widetilde{\theta} \in \mathcal{L}_2$. From this, we can conclude using Barbalat's Lemma [40]that $\lim_{t\to\infty} e_\theta(t) = 0$.

However, $e_\theta = 0$ does not imply $\widetilde{\theta} = 0$. Case 2 defines the necessary and sufficient conditions for $\lim_{t\to\infty} \widetilde{\theta}(t) = 0$. As we are guaranteed $\lim_{t\to\infty} \widetilde{\omega}(t) = 0$ and therefore $e_\omega \to 0$ we focus on the error $e_\theta$ alone. Recall that $e_\theta = \hat{\omega}^\top \widetilde{\theta}$, which in combination with our adaptive law $\dot{\widetilde{\theta}} = -\hat{\omega}\hat{\omega}^\top \widetilde{\theta}$ results in the so called error model 1 from [40]. Theorem 2.16 of [40]defines 4 equivalent conditions which assure the asymptotic stability of $\widetilde{\theta} = 0$. Here we utilize the $4^{th}$ which will be referred to as the persistence of excitation (PE) condition. *There exist positive constants* $t_0, T_0$ *and* $\epsilon_1$ *such that*

$$\begin{aligned} &\lambda_i[M(t)] \geq \epsilon_1, \quad i = 1, 2, ..., 2n, \quad \forall t \geq t_0, \\ &M(t) = \int_t^{t+T_0} \hat{\omega}\hat{\omega}^\top d\tau \end{aligned} \tag{3.24}$$

where $\lambda_i[A]$ denotes the $i$'th eigenvalue of matrix $A$. We denote condition (3.24) as $\hat{\omega} \in PE_{2n}$. This condition ensures that over any time span $T_0$, $e_\theta(t) = 0$, $\tau \leq t \leq \tau + T$ for any $\tau > t_0$ only if $\widetilde{\theta}(t) = 0$. Since we already showed the asymptotic stability of $e_\theta = 0$, if $\hat{\omega} \in PE_{2n}$ we are also guaranteed $lim_{t\to\infty}\widetilde{\theta}(t) = 0$. A more formal proof of this fact can be found in [40].

The slow nature of this convergence witnessed and commented on by previous authors such as [42] motivates the two approaches to improve this rate detailed in this Chapter. The first approach is by specific design of the observer filters.

### 3.1.2 Nonminimal equivalent system design

Although the vector regressor based adaptive observer first appeared more than 50 years ago, universal guidelines for the design of the filters, (3.5), which generate the nonminimal states are to the best of the author's knowledge absent in existing literature. The observer performance becomes particularly sensitive to filter design when the poles of the true plant, (3.1), are separated by more than an order of magnitude, as may be the case for the SPM of a lithium battery. In this section, we discuss how the filter parameters in $F$ and $g$ as well as the gains $\Gamma_u$ and $\Gamma_y$ can be chosen.

The sensitivity of the observer performance to the filters $(F, g)$ stems from the wide spread of $\lambda_i[M(t)]$ in (3.24) arrising from many choices of $(F, g)$. We propose a design procedure for choosing $F$ and $g$ such that the spread of $\lambda_i$ is small for an optimally exciting system input and therefore degree of PE, $\epsilon_1$, is optimized. For an unknown system, we require a signal with frequency content at at least $n$ distinct frequencies. However, to produce an unbiased fit of the system at all frequencies, a signal which is white is optimal. The easiest examples of white signals are the impulse signal or white noise, which can be represented as a sum of impulse signals. Furthermore, we must be careful when trying to maximize the degree of PE, $\epsilon_1$, as this could be accomplished by simply increasing the magnitude of the input $u$, or equivalently, increasing $g$. To account for this we search for the optimal filters with

two restrictions imposed. $|u(t)| \leq u_{max}$, $\forall t$ and $\|G_{fi}(s)\| \leq 1, \forall i$ with

$$G_f(s) = (F - sI)^{-1} g \tag{3.25}$$

the vector of transfer functions and $G_{f(i)}(s)$ the transfer function from input $u$ to nonminimal state $\omega_(i)$. These two conditions constrain optimization allowing a feasible solution.

We break the problem down into two steps. The first is placement of the filter poles based on a nominal estimate of the plant,

$$\begin{aligned} \dot{x}' &= A'x' + b'u \\ y' &= c'^{\top} x \end{aligned} \tag{3.26}$$

We use the Kalman filter design process to compute filters which will balance a preservation of signal strength in the bandwidth of the nominal plant and speed of the filter to ensure $\widetilde{\omega}$ decays reasonably fast. We emphasize that although the Kalman filter is designed to handle stochastic uncertainty of the plant input and output, we are not considering external noise in our problem statement. Instead, utilization of the steady-state kalman filter is justified by a property of the algebraic riccatti equation (ARE) of SISO systems for which $K$ is defined not by $Q$ and $R$ independently but by the ratio of $Q/R$. Therefore, allowing $K$ of (3.28) to be computed in the limit as $Q \to 0$, $R \to 0$. The quantity which remains $Q/R$ is a tuning parameter which qualitatively weights the speed of the filters with a similarity of the filters to the nominal plant.

The Kalman filter prescribes the optimal filter for a known plant with stochastic uncertainties on the input and output. Optimality is designated by the minimization of the expected output error squared. We assume the plant to be our nominal plant

from (3.26) with noise $w$, $v$ on the input and output respectively,

$$\begin{aligned} \dot{x} &= Ax + bu + bw \\ y &= c^\top x + v \end{aligned} \tag{3.27}$$

with the expected covariance of the noise $E[ww^\top] = Q \in \mathbb{R}$ and $E[vv^\top] = R \in \mathbb{R}$. The expected variance of the error $P$ is tracked as

$$\dot{P} = AP + PA^\top + Q + Pc^\top R^{-1} cP \tag{3.28}$$

with the subsequent Kalman gain then defined as

$$K = Pc^\top R^{-1} \tag{3.29}$$

The presence of $R^{-1}$ in both (3.28) and (3.29) presents an issue for setting $R = 0$. However, defining the noise ratio

$$\sigma = \frac{Q}{R} \tag{3.30}$$

we can rewrite the steady state (3.28) and (3.29),

$$\begin{aligned} A\overline{P} + \overline{P}A^\top + 1 - \overline{P}c^\top \sigma c\overline{P} &= 0 \\ K &= \overline{P}c^\top \sigma \end{aligned} \tag{3.31}$$

with $Q$, $R$ no longer appearing we compute our optimal filter for a system with no noise and instead a weighting between measurements and nominal plant, $\sigma$. The resulting kalman filter is then

$$\hat{x} = (A - Kc^\top)x + bu + Ky \tag{3.32}$$

With our nominal plant, (3.26) defined in observer canonical form, our kalman filter (3.32) will also be in observer canonical form. Noticing the similarity between (3.32) and (3.4), we can then define our nonminimal filter in observer canonical form as $F^{OC} = A - Kc^\top$.

The second step of the design process is to place the zeros for each filter input-state relationship. We begin with a control canonical filter $F_{f0} = (A - Kc^\top)^\top$ using $A, K, c$ from (3.32) and $g_0 = c$ from (3.26) with the corresponding filters

$$\begin{aligned} \dot{\omega}_{u0} &= F_{f0}\omega_{u0} + g_0 u \\ \dot{\omega}_{y0} &= F_{f0}\omega_{y0} + g_0 y \end{aligned} \tag{3.33}$$

We next determine $P_0$ as the solution to the Lyapunov equation

$$0 = F_{f0}P_0 + P_0 F_{f0}^\top + g_0 g_0^\top \tag{3.34}$$

which is decomposed as

$$VDV^\top = P_0 \tag{3.35}$$

where $D$ is a diagonal matrix containing the eigenvalues and $V$ contains the eigenvectors of $P_0$ respectively. A transformation matrix $T = D^{-1/2}V$ is then determined to find the final filter design

$$\begin{aligned} \dot{\omega}_{u1} &= F_{f1}\omega_{u1} + g_{u1} u \\ \dot{\omega}_{y1} &= F_{f1}\omega_{y1} + g_{y1} y \end{aligned} \tag{3.36}$$

with the filters defined as

$$F_{f1} = T_u F_{f0} T_u^{-1} \quad g_{u1} = T_u g_0 \quad g_{y1} = T_y g_0 \tag{3.37}$$

using the transformation matrices

$$\begin{aligned} T_u &= D^{-1/2}V \\ T_y &= pD^{-1/2}V \end{aligned} \tag{3.38}$$

where $p$ is a measure of the gain of the system, used here as a scaling parameter computed as

$$p = \left(c^\top P_p c\right)^{-1/2} \tag{3.39}$$

and $P_p$ is the solution to the Lyapunov equation

$$0 = AP_p + P_p A^\top + bb^\top \tag{3.40}$$

with $(A, b, c)$ are nominal values of the plant parameters of (3.26).

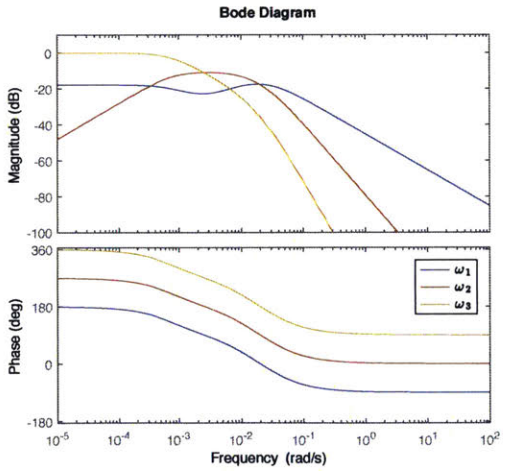


Figure 3-2: The transformations $T_u$ and $T_y$ locate the zeros of the transfer matrix to de-correlate the filter states assuming a input signal with a flat spectrum. Here the three transfer function Bode plots are shown for filters designed using a nominal SP model plant.

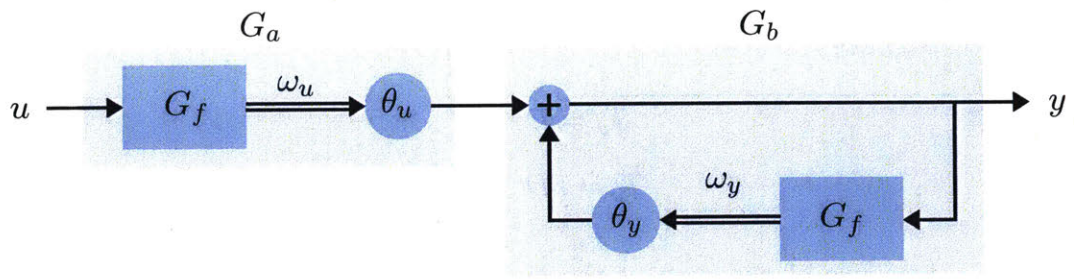


Figure 3-3: Equivalent system used to construct adaptive observers. The fact that $\theta_u$ is related exclusively to the zeros of the minimal system and that $\theta_y$ is related exclusively to the poles of the minimal system can be clearly seen via reduction of the block diagram to $G_a$ and $G_b$. The equivalent system poles, will appear in the denominator of $G_a$ and the numerator of $G_b$.

The reasoning behind the choice of the transformation $T_u$ and $T_y$ is to ensure the matrix $M(t)$ of (3.24), for large $t$, corresponding to the states in (3.36) is as close to identity as possible. It can be seen that $P_0$ in (3.34) coincides with $M(t)$ for a signal $u(t)$ with a uniform power spectrum, such as an impulse, and sufficiently large $T_0$. The reasoning for introducing $p$ is to accommodate the scaling between the 2-norm $\|u(t)\|_2$ and $\|y(t)\|_2$ when $u(t)$ is an impulse. Here we point out that although the tuned filters result in different $g_u$ and $g_y$ the poles of each filter remain the same, this matching of poles for the filters of the input and output respectively is a necessary condition for the observer. This can be seen algebraically when performing the pole-zero cancellations of the nonminimal system required to achieve the original plant. Alternatively, conceptually, the nonminimal system can be broken into two blocks, one with a feedback loop and one which is only feedforward. The filter of the output can be viewed as a system $G_f$ with full state feedback achieved using $\theta_y$ this full state feedback has the ability to place both the poles and zeros of this loop. Poles are placed to match the system poles and the resulting zeros will cancel the poles of signal from the input filter.

With the filter parameters chosen as in (3.36)-(3.37), we can set $\Gamma_y = \Gamma_u = \gamma \mathbf{I}$,

with the magnitude of $\gamma$ limited by the computational platform. With our transformation of the nonminimal system, a transformation of the original parameters $\theta_u$ and $\theta_y$ of (3.6) which correspond to the filters of (3.33) will be required. The new parameter set for the filters of (3.36) is

$$\begin{aligned} \theta_{u1} &= T_u^{-\top}\theta_u \\ \theta_{y1} &= T_y^{-\top}\theta_y \end{aligned} \tag{3.41}$$

which was derived by equating the output of the nonminimal systems (3.33) and (3.36) respectively,

$$\begin{aligned} y &= \theta_u^\top \omega_{u0} + \theta_y^\top \omega_{y0} \\ &= \theta_{u0}^\top T_u^{-1}\omega_{u1} + \theta_{y0}^\top T_y^{-1}\omega_{y1} \\ &= \theta_{u1}^\top \omega_{u1} + \theta_{y1}^\top \omega_{y1} \end{aligned} \tag{3.42}$$

### 3.1.3 Maintaining Parameter Constraints using Projection

On occasion one may have a-priori knowledge of the plant such as a known pole. In the case of the SPM we know that the plant will possess a free integrator, i.e. a pole at zero.

A projection operator in adaptive systems was rigorously described in [27] and proposed for parameter constraints in [21]. In the case of a known integrator, from our original system description (3.2) we know that $q_0 = 0$. Therefore the $n^{th}$ element of $\theta_y$ is known to be the corresponding element of the filter coefficients as is shown in (3.6). That is $\theta_{y(n)} = f_(n)$. If our adaptive observer was implemented using control canonical filters, it would be sufficient to simply set $\hat{\theta}_{y(n)}(0) = \theta_{y(n)}$ and $\dot{\hat{\theta}}_{y(n)} = 0$ to maintain this known constraint. However, in the previous section the system was transformed, the resulting constraint is now a hyperplane on which the parameter

$\hat{\theta}_{y1}$ must remain. Decomposing our transformation matrix

$$T_y = \begin{bmatrix} t_{t1} \, t_{y2} \, \cdots \, t_{yn} \end{bmatrix} \tag{3.43}$$

and using (3.41) in which $T_y^\top \theta_{y1} = \theta_y$ we can define the hyperplane constraint as the surface

$$\mathcal{S} = \{\theta_{y1} \in \mathbb{R}^n : f_{(n)} = t_{yn}^\top \theta_{y1}\} \tag{3.44}$$

With our original parameter update law of $\dot{\hat{\theta}}_1 = \omega_1 e$ with $\hat{\theta}_1 = [\hat{\theta}_{u1}^\top \; \hat{\theta}_{y1}^\top]^\top$ and $\hat{\omega}_1 = [\hat{\omega}_{u1}^\top \; \hat{\omega}_{y1}^\top]^\top$ we introduce a projection gain

$$\Gamma_c = I - \frac{t_c t_c^\top}{t_c^\top t_c} \tag{3.45}$$

where

$$t_c = \begin{bmatrix} 0 \\ t_{yn} \end{bmatrix} \in \mathbb{R}^{2n} \tag{3.46}$$

resulting in an a-posteriori update law projected onto the hyperplane $\mathcal{S}$

$$\dot{\hat{\theta}}_1 = -\Gamma_c \hat{\omega}_1 e \tag{3.47}$$

where this projection only maintains $\hat{\theta}_1$ on a hyperplane parallel to $\mathcal{S}$, therefore we must also have initialized $\hat{\theta}_1(0) \in \mathcal{S}$.

### 3.1.4 State Transformations

Up until this section we have presented algorithms which search for parameter estimates $\hat{\theta}_u, \hat{\theta}_y$ and compute nonminimal states $\hat{\omega}_u, \hat{\omega}_y$ in an arbitrary state space representation. Originally in control-canonical form, but after the previous section we have used a similarity transformation yielding a likely irrelevant system representation. Here we outline the options for obtaining parameter and state estimates in a desired form. We begin by adding superscripts to our nonminimal representations to idetify them from one another. First we have the states as implemented by the observer defined below.

$$\begin{aligned} \dot{\omega}_u^{AO} &= F^{AO}\omega_u^{AO} + g_u^{AO}u \\ \dot{\omega}_y^{AO} &= F^{AO}\omega_y^{AO} + g_y^{AO}y \\ y &= (\theta_u^{AO})^\top \omega_u^{AO} + (\theta_y^{AO})^\top \omega_y^{AO} \end{aligned} \tag{3.48}$$

Using the process of section 3.1.2 with ${}^{AO}T_u^{CC} = T_u$ and ${}^{AO}T_y^{CC} = T_y$ we have a relationship between control canonical (CC) nonminimal states and the adaptive observer's (AOs) nonminimal states

$$\begin{aligned} \omega_u^{AO} &= {}^{AO}T_u^{CC}\omega_u^{CC} \\ \omega_y^{AO} &= {}^{AO}T_y^{CC}\omega_y^{CC} \end{aligned} \tag{3.49}$$

and a similar relationship between the nonminimal system parameters of the CC and AO representations

$$\begin{aligned} \theta_u^{AO} &= ({}^{AO}T_u^{CC})^{-\top}\theta_u^{CC} \\ \theta_y^{AO} &= ({}^{AO}T_y^{CC})^{-\top}\theta_y^{CC} \end{aligned} \tag{3.50}$$

with $A^{-\top} = (A^{\top})^{-}1$. For reference we also define the CC nonminimal system

$$\begin{aligned} \dot{\omega}_u^{CC} &= F^{CC}\omega_u^{CC} + g^{CC}u \\ \dot{\omega}_y^{CC} &= F^{CC}\omega_y^{CC} + g^{CC}y \\ y &= (\theta_u^{CC})^{\top}\omega_u^{CC} + (\theta_y^{CC})^{\top}\omega_y^{CC} \end{aligned} \tag{3.51}$$

and from our original state space representation of prior sections we alter the notation for this section as

$$\begin{aligned} \dot{x}^{OC} = A^{OC}x^{OC} + b^{OC}u = (F^{OC} + \theta_y^{CC}(g^{CC})^{\top})x^{OC} + \theta_u^{CC}u \\ y = (g^{CC})^{\top}x^{CC} \end{aligned} \tag{3.52}$$

which can be broken apart by superposition into an observer canonical nonminimal system representation,

$$\begin{aligned} \dot{\omega}_u^{OC} &= F^{OC}\omega_u^{OC} + \theta_u^{CC}u \\ \dot{\omega}_y^{OC} &= F^{OC}\omega_y^{OC} + \theta_y^{CC}y \\ y &= (g^{CC})^{\top}\omega_u^{OC} + (g^{CC})^{\top}\omega_y^{OC} = (g^{CC})^{\top}(\omega_u^{OC} + \omega_y^{OC}) \end{aligned} \tag{3.53}$$

At this point we point out that the minimal system state of (3.52) in observer canonical form is the sum of our nonminimal states in OC form,

$$x^{OC} = \omega_u^{OC} + \omega_y^{OC} \tag{3.54}$$

however, it is important to note $x^{CC} \neq \omega_u^{CC} + \omega_y^{CC}$.

In general the process for determining states of a general state space form requires the ability to construct $A, b$ for this form strictly from the poles and zeros of the plant, or equivalently from the denominator and numerator polynomials of $G_p$. For example, Jordan normal form system representation only requires the poles, $\lambda_i$, of

the system

$$A^J = \begin{bmatrix} \lambda_1 & & & \\ & \lambda_2 & & \\ & & \ddots & \\ & & & \lambda_n \end{bmatrix} \quad b^J = \begin{bmatrix} 1 \\ 1 \\ \vdots \\ 1 \end{bmatrix} \tag{3.55}$$

when $\lambda_i \neq \lambda_j$, $\forall i \neq j$. In the context of our observer, we can estimate the jordan form matrices

$$\hat{A}^J = \begin{bmatrix} \hat{\lambda}_1 & & & \\ & \hat{\lambda}_2 & & \\ & & \ddots & \\ & & & \hat{\lambda}_n \end{bmatrix} \quad \hat{b}^J = b^J \tag{3.56}$$

where $\hat{\lambda}_i$ are estimated by computing the roots of the polynomial with coefficients $[1 \ (f^{CC} - \hat{\theta}_y^{CC})^\top]$ Transformation of a state $z$ in representation $i$ to $j$ is accomplished using a general transformation matrix ${}^jT_z^i$, where $z^j = {}^jT_z^i z^i$ with

$${}^jT_z^i = \mathcal{C}^j(\mathcal{C}^i)^{-1} \tag{3.57}$$

with $\mathcal{C}^i, \mathcal{C}^j$ being the controlability matrices for representation $i, j$ respectively. To obtain $x^J$ from $\omega_u^{AO}$ and $\omega_y^{AO}$ must first convert our nonminimal states to OC form before they can be summed to obtain our minimal state using

$$\begin{aligned} x^J &= {}^JT_x^{OC}\left(\omega_u^{OC} + \omega_y^{OC}\right) \\ x^J &= {}^JT_x^{OC}\left({}^{OC}T_{\omega_u}^{AO}\omega_u^{AO} + {}^{OC}T_{\omega_y}^{AO}\omega_y^{AO}\right) \end{aligned} \tag{3.58}$$

where

$$
\begin{aligned}
{}^{J}T_{x}^{OC} &= \mathcal{C}_{x}^{J}(\mathcal{C}_{x}^{OC})^{-1} \\
{}^{OC}T_{\omega_u}^{AO} &= \mathcal{C}_{\omega_u}^{OC}(\mathcal{C}_{\omega_u}^{AO})^{-1} \\
{}^{OC}T_{\omega_y}^{AO} &= \mathcal{C}_{\omega_y}^{OC}(\mathcal{C}_{\omega_y}^{AO})^{-1}
\end{aligned}
\tag{3.59}
$$

and our controllability matrices are computed as

$$
\begin{aligned}
\mathcal{C}_{x}^{J} &= \begin{bmatrix} b^J & A^J b^J & \cdots & (A^J)^{n-1} b^J \end{bmatrix} \\
\mathcal{C}_{x}^{OC} &= \begin{bmatrix} \theta_u^{CC} & (F^{OC} + \theta_y^{CC} g^{\top})\theta_u^{CC} & \cdots & (F^{OC} + \theta_y^{CC} g^{\top})^{n-1}\theta_u^{CC} \end{bmatrix} \\
\mathcal{C}_{\omega_u}^{OC} &= \begin{bmatrix} \theta_u & F^{OC}\theta_u & \cdots & (F^{OC})^{n-1}\theta_u \end{bmatrix} \\
\mathcal{C}_{\omega_u}^{AO} &= \begin{bmatrix} g_u & F^{AO} g_u & \cdots & (F^{AO})^{n-1} g_u \end{bmatrix} \\
\mathcal{C}_{\omega_y}^{OC} &= \begin{bmatrix} \theta_y & F^{OC}\theta_y & \cdots & (F^{OC})^{n-1}\theta_y \end{bmatrix} \\
\mathcal{C}_{\omega_y}^{AO} &= \begin{bmatrix} g_y & F^{AO} g_y & \cdots & (F^{AO})^{n-1} g_y \end{bmatrix}
\end{aligned}
\tag{3.60}
$$

similar to (3.58), jordan normal form state estimate can be computed as

$$
\hat{x}^{J} = {}^{J}\hat{T}_{x}^{OC}\left({}^{OC}\hat{T}_{\omega_u}^{AO}\hat{\omega}_{u}^{AO} + {}^{OC}\hat{T}_{\omega_y}^{AO}\hat{\omega}_{y}^{AO}\right) \tag{3.61}
$$

where

$$
\begin{aligned}
{}^{J}\hat{T}_{x}^{OC} &= \hat{\mathcal{C}}_{x}^{J}(\hat{\mathcal{C}}_{x}^{OC})^{-1} \\
{}^{OC}\hat{T}_{\omega_u}^{AO} &= \hat{\mathcal{C}}_{\omega_u}^{OC}(\mathcal{C}_{\omega_u}^{AO})^{-1} \\
{}^{OC}\hat{T}_{\omega_y}^{AO} &= \hat{\mathcal{C}}_{\omega_y}^{OC}(\mathcal{C}_{\omega_y}^{AO})^{-1}
\end{aligned}
\tag{3.62}
$$

Noting that $\mathcal{C}_{\omega_u}^{AO}$ and $\mathcal{C}_{\omega_y}^{AO}$ are completely known and no estimates are required.

The remaining controllability matrices are estimated as

$$\begin{aligned}
\hat{\mathcal{C}}_x^J &= \begin{bmatrix} b^J & \hat{A}^J b^J & \cdots & (\hat{A}^J)^{n-1} b^J \end{bmatrix} \\
\hat{\mathcal{C}}_x^{OC} &= \begin{bmatrix} \hat{\theta}_u^{CC} & (F^{OC} + \hat{\theta}_y^{CC} g^\top)\hat{\theta}_u^{CC} & \cdots & (F^{OC} + \hat{\theta}_y^{CC} g^\top)^{n-1}\hat{\theta}_u^{CC} \end{bmatrix} \\
\hat{\mathcal{C}}_{\omega_u}^{OC} &= \begin{bmatrix} \hat{\theta}_u^{CC} & F^{OC}\hat{\theta}_u^{CC} & \cdots & (F^{OC})^{n-1}\hat{\theta}_u^{CC} \end{bmatrix} \\
\hat{\mathcal{C}}_{\omega_y}^{OC} &= \begin{bmatrix} \hat{\theta}_y^{CC} & F^{OC}\hat{\theta}_y^{CC} & \cdots & (F^{OC})^{n-1}\hat{\theta}_y^{CC} \end{bmatrix}
\end{aligned} \tag{3.63}$$

Here, we have no guarantee that $\hat{\mathcal{C}}_x^{OC}$ will be non-singular, and we also are not guaranteed that $\mathcal{C}_{\omega_u}^{AO}$ and $\mathcal{C}_{\omega_y}^{AO}$ are not poorly conditioned subjecting the algorithm to amplification of numerical errors when implemented. Alternatively to (3.61) we can eliminate the need to invert $\mathcal{C}_{\omega_u}^{AO}$ and $\mathcal{C}_{\omega_y}^{AO}$ using an alternative method to estimate $\hat{x}^{OC}$ using an additional online estimate,

$$\dot{\hat{x}}^{OC} = F^{OC}\hat{x}^{OC} + \hat{\theta}_y^{CC} y + \hat{\theta}_u^{CC} u \tag{3.64}$$

for which we are then only required to compute ${}^J\hat{T}_x^{OC}$ of (3.62). The state estimate in jordan form is then

$$\hat{x}^J = {}^J\hat{T}_x^{OC}\hat{x}^{OC} \tag{3.65}$$

In general this second method using (3.64) and (3.65) will be used in the following chapters. Care should be taken if the parameter estimate is initialized at 0 as $\hat{\mathcal{C}}_x^{OC}$ will be initially singular.

## 3.2 Matrix-regressor (MR) Adaptive Observers

Asymptotic stability of parameter error estimates to zero can be shown for the vector regressor adaptive observer provided the input to the system is persistently exciting (PE). However, the rate of convergence is not only very difficult to compute, but also extremely slow. In order to generate adaptive observers with improved error convergence, matrix regressors have been explored in leiu of vector regressors [22,24, 25]. In this section be begin by introducing the notion of strong persistent excitation (SPE). We then present two matrix regressor based adaptive observers (MR-AOs). The first has been reported previously in [24,25,40], and is discussed in 3.2.2, while the second was introduced by the author in [22] and is a primary contribution of this research. This second MR-AO structure is discussed in 3.2.4

### 3.2.1 Strong Persistent Excitation

The drawback of the PE condition in (3.24) is that the degree of persistent excitation $\epsilon_1$ in (3.24) is not directly related to the convergence rate of $\widetilde{\theta}$ to zero in (3.15). More importantly, it has been observed in practice that the convergence rate, though guaranteed to be non-zero, is extremely slow. This motivates the notion of strong persistent excitation (SPE), for which we consider a matrix of regressors $\Omega \in \mathbb{R}^{n\times n}$ and the exponential stability of $\widetilde{\theta}(t) = 0$ of the differential equation

$$\dot{\widetilde{\theta}}(t) = -\Omega(t)\Omega^{\mathrm{T}}(t)\widetilde{\theta}(t) \tag{3.66}$$

**Theorem 1** (Strong Persistent Excitation 1). *If there exist positive constants $t_0$, $\epsilon_2$ and $\rho_2$ such that*

$$\rho_2 \geq \lambda_i \left[\Omega(t)\Omega^{\mathrm{T}}(t)\right] \geq \epsilon_2,\ i = 1, 2, ..., N,\ \forall t \geq t_0 \tag{3.67}$$

*then (i) $\Omega$ is said to satisfy strong PE, and (ii) the origin $\widetilde{\theta}(t) = 0$ is exponentially stable and satisfies the inequality*

$$e^{-\rho_2(t-t_0)} \leq \frac{||\widetilde{\theta}(t)||}{||\widetilde{\theta}(t_0)||} \leq e^{-\epsilon_2(t-t_0)}, \quad \forall t \geq t_0 \tag{3.68}$$

*for any initial condition $\widetilde{\theta}(t_0)$.*

The proof of Theorem 1 (as well as Theorem 2) is omitted as it follows directly from properties of linear time-varying systems. We denote condition (3.67) as $\Omega \in SPE_N$ and $\epsilon_2$ as the degree of SPE of $\Omega$.

A slightly weaker version can be formulated which allows for $\Omega(t)\Omega^\top(t)$ to be occasionally singular, and is stated in Theorem 2.

**Theorem 2** (Strong Persistent Excitation 2). *If there exist positive constants $T$, $t_0$, $\epsilon_3$ and $\rho_3$ such that $\forall t \geq t_0$*

$$T\rho_3 \geq \int_t^{t+T} \lambda_i \left[\Omega(\tau)\Omega^\top(\tau)\right] d\tau \geq T\epsilon_3, \; i = 1, 2, ..., N \tag{3.69}$$

*then (i) $\Omega$ is said to satisfy strong PE, and (ii) the origin $\widetilde{\theta}(t) = 0$ is exponentially stable and satisfies the inequality*

$$e^{-\rho_3(t-t_0)} \leq \frac{||\widetilde{\theta}(t)||}{||\widetilde{\theta}(t_0)||} \leq e^{-\epsilon_3(t-t_0)}, \quad \forall t \geq t_0 + T \tag{3.70}$$

*for any initial condition $\widetilde{\theta}(t_0)$.*

It should be noted that with the matrix regressor and the resulting differential equation in (3.66), if $\Omega$ satisfies either the SPE condition in (3.67) or the condition in (3.69), there is a direct relation between its degree of persistent excitation and the convergence rate of $\widetilde{\theta}(t)$ to zero in (3.66). This in turn implies that one can use the

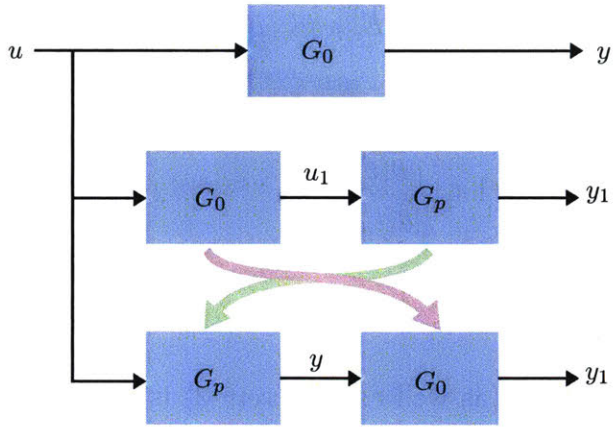


Figure 3-4: The equivalence of the relationship between $u, y$ and $u_i, y_i$ for MR-AO I is clear once initial condition errors decay.

degree of SPE as an on-line metric for evaluating parameter convergence in a given dynamic system.

It is easy to see that if $\Omega$ satisfies either (3.67) or (3.69), it will satisfy (3.24) for some positive constants $t_0, T_0$, and $\epsilon_1$.

We now discuss adaptive observers which use matrix regressors rather than vector regressors.

### 3.2.2 Matrix-Regressor (MR) Adaptive Observer (AO) I

The matrix regressor used in MR-AO I is composed of $2n$ vector regressors. To generate these multiple vector regressors, denoted $\omega_i$, instead of a single vector $\omega$ as in (3.9), we utilize additional filters of the regressors and system output $y(t)$. The base regressor is constructed as in (3.9)

$$\dot{\omega}_0 = \overline{F}\omega_0 + \overline{g}\begin{bmatrix} u \\ y \end{bmatrix}, \tag{3.71}$$

$$\overline{F} = \begin{bmatrix} F & 0 \\ 0 & F \end{bmatrix}, \quad \overline{g} = \begin{bmatrix} g & 0 \\ 0 & g \end{bmatrix}$$

where $F, g$ are defined as in (3.5). $2n-1$ additional regressors and output signals are created as

$$\omega_i = G_0^{(i)}(s)\omega_0, \quad y_i = G_0^{(i)}(s)y, \qquad i = 1, 2, ..., 2n-1 \tag{3.72}$$

where $y_0(t) = y(t)$, and $G_0^{(i)}(s) = \left(\frac{\beta}{s+\beta}\right)^i$, $\beta > 0$, and $s$ denotes the differential operator $\frac{d}{dt}$. Here $G_0(s)$ is a first order low pass filter, but in general any filter can be used, in the following chapter we will use a combination of high and low pass filters. With the total of $2n$ $\omega_i$, we generate the matrix regressor and vector output as

$$\Omega_I = [\omega_0, \omega_1, ..., \omega_{2n-1}], \qquad Y = \begin{bmatrix} y_0 \\ y_1 \\ \vdots \end{bmatrix} = \Omega_I^\top \theta \tag{3.73}$$

where Figure ?? depicts these signals in a block diagram form. For clarity it is helpful to point out that one can construct an equivalent set of regressors by sequentially filtering $u$ and $y$ as $u_i = (G_0(s))^{(i)}u$ and $y_i = (G_0(s))^{(i)}y$ and then compute filters as $\dot{\omega}_i = \overline{F}\omega_i + \overline{g}[u_i \; y_i]^\top$ for $i = 1, 2, \ldots, 2n-1$.

We now present the matrix regressor adaptive observer, denoted as MRAO-I

(see [24, 25] for details):

$$
\begin{aligned}
\dot{\hat{\omega}}_0 &= \overline{F}\hat{\omega}_0 + \overline{g}\begin{bmatrix} u \\ y \end{bmatrix} \\
\hat{\omega}_i &= G_0^{(i)}(s)\hat{\omega}_0, \quad i = 1, 2, \cdots, 2n-1 \\
\check{y}_i &= G_0^{(i)}(s)y, \quad i = 1, 2, \cdots, 2n-1 \\
\check{Y} &= \begin{bmatrix} y & \check{y}_1 & \cdots & \check{y}_{2n-1} \end{bmatrix}^\top \\
E &= \hat{\Omega}_I^\top \hat{\theta} - \check{Y} \\
\dot{\hat{\theta}} = \dot{\widetilde{\theta}} &= -\gamma \hat{\Omega}_I E \\
\hat{\Omega}_I &= \begin{bmatrix} \hat{\omega}_0, \hat{\omega}_1, \ldots, \hat{\omega}_{2n-1} \end{bmatrix}
\end{aligned}
\tag{3.74}
$$

where $\widetilde{\theta} = \hat{\theta} - \theta$ is the parameter error, $\hat{\omega}_i$ are estimates of the filter states $\omega_i$ of (3.71)-(3.72) implemented by the observer and $\gamma \in \mathbb{R}^+$ is a positive learning gain. Whether for the vector regressor adaptive observer in (3.9)-(3.11) or the MRAO in (3.71)-(3.74), a persistent excitation condition [40] must be satisfied for parameter errors $\tilde{\theta}(t)$ to converge to zero asymptotically. In the latter case, we previously defined the notion of Strong Persistent Excitation (SPE) and below a theorem that derives conditions under which parameter convergence takes place.

**Theorem 3.** *If the external input* $u(t) = \sum_{j=1}^{n} \sin v_j t$ *it can be shown that (i)* $\Omega_I \in SPE_{2n}$ *and (ii)* $\widetilde{\theta}(t) = 0$ *in* (3.73) *is exponentially stable and satisfies the inequality*

$$
\left\|\widetilde{\theta}(t)\right\| \leq \left\|\widetilde{\theta}(t_0)\right\| e^{-\gamma \epsilon_\Omega (t - t_0)}, \quad \forall t \geq t_0 \tag{3.75}
$$

*where* $\epsilon_\Omega$ *is the degree of SPE of* $\Omega_I$.

*Proof.* Using transformation matrices $J$ and $K$ the matrix regressor can be shown

to be

$$\Omega_I(t) = J[v_0(t), Kv_0(t), K^2v_0(t), ...K^{2n-1}v_0(t)] \tag{3.76}$$

where $v_0(t) = [\sin(v_1t), \cos(v_1t), ..., \sin(v_nt), \cos(v_nt)]^\top$, $J$ and $K$ are constructed as

$$\begin{aligned} J &= \begin{bmatrix} \mathbf{T} \\ \mathbf{T}\mathbf{R}_p \end{bmatrix} \mathbf{R}_1 \\ K &= \mathbf{R}_0 \end{aligned} \tag{3.77}$$

with the transformation matrices $\mathbf{T}$, $\mathbf{R}_p$, $\mathbf{R}_i \in \mathbb{R}^{n\times n}$,

$$\begin{aligned} \omega_{ui} &= \underbrace{\begin{bmatrix} \mathbf{T}_1 & \mathbf{T}_2 & \cdots \end{bmatrix}}_{\mathbf{T}} \underbrace{\begin{bmatrix} \mathbf{R}_{i1} & & \\ & \mathbf{R}_{i2} & \\ & & \ddots \end{bmatrix}}_{\mathbf{R}_i} \underbrace{\begin{bmatrix} \sin v_1t \\ \cos v_1t \\ \sin v_2t \\ \vdots \end{bmatrix}}_{\mathbf{S}} \\ \omega_{yi} &= \mathbf{T}\mathbf{R}_p\mathbf{R}_i\mathbf{S} \end{aligned} \tag{3.78}$$

and $\mathbf{R}_{ij} \in \mathbb{R}^{2\times 2}$ is a block of $\mathbf{R}_i$. $b_{ij}$ and $\phi_{ij} \in R$ are the gain and phase shift due to $G_i$ at frequency $v_j$ respectively.

$$\mathbf{R}_{ij} = b_{ij} \begin{bmatrix} \cos\phi_{ij} & \sin\phi_{ij} \\ -\sin\phi_{ij} & \cos\phi_{ij} \end{bmatrix} \tag{3.79}$$

$\mathbf{T}_j \in \mathbb{R}^{n\times 2}$ is another transformation matrix,

$$\mathbf{T}_j = \begin{bmatrix} 1 & 0 \\ 0 & v_j \\ -v_j^2 & 0 \\ 0 & -v_j^3 \\ \vdots & \vdots \end{bmatrix} \tag{3.80}$$

and $K$ is a block diagonal matrix whose $j$th block is given by

$$K_j = \begin{bmatrix} b_j \cos\phi_j & b_j \sin\phi_j \\ -b_j \sin\phi_j & b_j \cos\phi_j \end{bmatrix} \tag{3.81}$$

where $b_j$ and $\phi_j$ are the gain and phase of $G_0$ at frequency $v_j$. $v_0(t) \neq 0$ for all $t$ by construction.

It can be shown that $J$ is nonsingular [40]. We will now show that

$$\Psi = [v_0, Kv_0, K^2v_0, ...K^{2n-1}v_0] \tag{3.82}$$

is nonsingular.

The block diagonal structure of $K$ results in $q(s) = c^\top(sI - K)^{-1}b$ where $c$ and $b$ are arbitrary vectors in $\mathbb{R}^{2n}$. The structure of $K$ in (3.76) implies that $q(s)$ has $n$ pairs of complex conjugate poles and at most only one real zero for any $b$ and $c$ in $\mathbb{R}^{2n}$. This in turn implies that there are no pole-zero cancellations in the transfer function $q(s)$. Therefore the triple $\{c, K, b\}$ is controllable and observable which implies that $\Psi$ is nonsingular. This proves that $\Omega_I(t)$ is non-singular for all $t$ which proves (i). From Theorem 1 we conclude that there will exist an $\epsilon_\Omega > 0$ such that $\Omega_I\Omega_I^\top > \epsilon_\Omega \ \forall t \geq t_0$. This proves (ii) in Theorem 3. □

It should be noted, that as represented above, the adaptive observer in (3.74) will require $4n^2 + 4n - 2$ integrators. As a result, for a given set of frequencies in $u(t)$, the degree of SPE $\epsilon_\Omega$ may be rather small due to the filtering by a transfer function of order $4n$. This motivates the new MR-AO structure described in 3.2.4 which reduces this order to $2n^2$.

### 3.2.3 Stability of MR-AO I

For the nonminimal system (3.71) and subsequent filtered states and output of (3.72) we now analyze the stability of the matrix regressor error, $\widetilde{\Omega}_I = \hat{\Omega}_I - \Omega_I$, synthetic output error $\tilde{Y} = \check{Y} - Y$ and parameter error $\widetilde{\theta} = \hat{\theta} - \theta$. We begin by stacking the vector regressors which make up $\Omega_I \in \mathbb{R}^{2n\times 2n}$ into two vectors $W_u = [\omega_{u0}^\top\, \omega_{u1}^\top \cdots \omega_{u2n-1}]^\top]^\top \in \mathbb{R}^{2n^2}$ and $W_y = [\omega_{y0}^\top\, \omega_{y1}^\top \cdots \omega_{y2n-1}]^\top]^\top \in \mathbb{R}^{2n^2}$ which from (3.71) and (3.72) are constructed as

$$\begin{aligned} \dot{W}_u &= F_W W_u + g_W u \\ \dot{W}_y &= F_W W_y + g_W y \end{aligned} \tag{3.83}$$

with $F_W \in \mathbb{R}^{2n^2\times 2n^2}, g_W \in \mathbb{R}^{2n^2}$ defined as,

$$F_W = \begin{bmatrix} F & & & \\ \beta I_n & -\beta I_n & & \\ & \ddots & \ddots & \\ & & \beta I_n & -\beta I_n \end{bmatrix} \quad g_W = \begin{bmatrix} g \\ 0 \\ \vdots \\ 0 \end{bmatrix} \tag{3.84}$$

with $I_n \in \mathbb{R}^{n\times n}$ an identity matrix. The estimate $\hat{W}$ of $W$ is similarly

$$\begin{aligned}\dot{\hat{W}}_u &= F_W\hat{W}_u + g_W u \\ \dot{\hat{W}}_y &= F_W\hat{W}_y + g_W y\end{aligned} \tag{3.85}$$

resulting in error dynamics of the nonminimal states

$$\begin{aligned}\dot{\tilde{W}}_u &= F_W\tilde{W}_u \\ \dot{\tilde{W}}_y &= F_W\tilde{W}_y\end{aligned} \tag{3.86}$$

We additionally describe the construction of synthetic output vector $Y' = [y_1 \cdots y_{2n-1}]^\top$ and its implementation $\check{Y}'$ as,

$$\begin{aligned}\dot{Y}' &= F_Y Y' + g_Y y \\ \dot{\check{Y}}' &= F_Y \check{Y}' + g_Y y\end{aligned} \tag{3.87}$$

where $F_Y \in \mathbb{R}^{2n-1\times 2n-1}, g_Y \in \mathbb{R}^{2n-1}$ is constructed as

$$F_Y = \begin{bmatrix} -\beta & & & \\ \beta & -\beta & & \\ & \ddots & \ddots & \\ & & \beta & -\beta \end{bmatrix} \quad g_Y = \begin{bmatrix} \beta \\ 0 \\ \vdots \\ 0 \end{bmatrix} \tag{3.88}$$

resulting in a synthetic output error dynamics of

$$\dot{\tilde{Y}}' = F_y\tilde{Y}' \tag{3.89}$$

and the full output error of $\tilde{Y} \in \mathbb{R}^{2n} = [y\ (\tilde{Y}')^\top]^\top$. This error in the synthetic output vector is purely a result of initial condition mismatch due to our observer initializing

without a prior history of $y$.

We now expand the error $E$ of (3.74) for use in the analysis to follow,

$$\begin{aligned} E &= \hat{\Omega}_I^\top \hat{\theta} - \check{Y} \\ &= \hat{\Omega}_I^\top \hat{\theta} - \Omega_I^\top \theta - \tilde{Y} \\ &= \hat{\Omega}_I^\top \hat{\theta} - (\hat{\Omega}_I^\top - \widetilde{\Omega}_I^\top)\theta - \tilde{Y} \\ &= \underbrace{\hat{\Omega}_I^\top \widetilde{\theta}}_{E_\theta} + \underbrace{\widetilde{\Omega}_I^\top \theta}_{E_\Omega} - \tilde{Y} \end{aligned} \tag{3.90}$$

To analyze the stability of the MR adaptive observer in (3.74) we define a radially unbounded Lyapunov function candidate

$$V = \frac{1}{2}\widetilde{\theta}^\top \widetilde{\theta} + \tilde{W}^\top P_W \tilde{W} + (\tilde{Y}')^\top P_Y \tilde{Y}' \tag{3.91}$$

with positive definite $P_W \in \mathbb{R}^{2n^2 \times 2n^2}$ satisfying $F_W^\top P_W + P_W F_W + Q_W = 0$ for any positive definite $Q_W \in \mathbb{R}^{2n^2 \times 2n^2}$ and positive definite $P_Y \in \mathbb{R}^{2n-1 \times 2n-1}$ satisfying $F_Y^\top P_Y + P_Y F_Y + Q_Y = 0$ for any positive definite $Q_Y \in \mathbb{R}^{2n-1 \times 2n-1}$. Using $\dot{\hat{\theta}}$ of (3.74), $\dot{\tilde{W}}$ from (3.86) and $\dot{\tilde{Y}}'$ of (3.89) the time derivative of (3.91) is given by

$$\begin{aligned} \dot{V} &= \frac{1}{2}\left(\dot{\widetilde{\theta}}^\top \widetilde{\theta} + \widetilde{\theta}^\top \dot{\widetilde{\theta}}\right) + \dot{\tilde{W}}^\top P_W \tilde{W} + \tilde{W}^\top P_W \dot{\tilde{W}} + (\dot{\tilde{Y}}')^\top P_Y \tilde{Y}' + (\tilde{Y}')^\top P_Y \dot{\tilde{Y}}' \\ &= -\frac{1}{2}\left(E^\top \hat{\Omega}_I^\top \widetilde{\theta} + \widetilde{\theta}^\top \hat{\Omega}_I E\right) - \tilde{W}^\top Q_W \tilde{W} - (\tilde{Y}')^\top Q_W \tilde{Y}' \\ &= -\widetilde{\theta}^\top \hat{\Omega}(\hat{\Omega}_I^\top \widetilde{\theta} + \widetilde{\Omega}_I^\top \theta - \tilde{Y}) - \tilde{W}^\top Q_W \tilde{W} - (\tilde{Y}')^\top Q_W \tilde{Y}' \\ &= -\widetilde{\theta}^\top \hat{\Omega}\hat{\Omega}_I^\top \widetilde{\theta} - \widetilde{\theta}^\top \hat{\Omega}\widetilde{\Omega}_I^\top \theta + \widetilde{\theta}^\top \hat{\Omega}\tilde{Y}) - \tilde{W}^\top Q_W \tilde{W} - (\tilde{Y}')^\top Q_W \tilde{Y}' \\ &= -E_\theta^\top E_\theta - E_\theta^\top E_\Omega + E_\theta^\top \tilde{Y} - \tilde{W}^\top Q_W \tilde{W} - (\tilde{Y}')^\top Q_W \tilde{Y}' \end{aligned} \tag{3.92}$$

Where we see the fourth and fifth terms are negative definite while the first term is a negative quadratic term in $E_\theta$ and the second and third are linear in $E_\theta$. From

this we can conclude that $\dot{V} < 0$ outside of the compact set

$$\mathcal{S} = \left\{ \widetilde{\theta} \in \mathbb{R}^{2n}, \widetilde{\Omega} \in \mathbb{R}^{2n \times 2n}, \tilde{Y} \in \mathbb{R}^{2n} : \left\| \hat{\Omega}^{\top} \widetilde{\theta} \right\| > \left\| \widetilde{\Omega}^{\top} \theta + \tilde{Y} \right\| \right\} \tag{3.93}$$

From (3.86) and (3.89) we see that $\left\| \widetilde{\Omega}^{\top} \theta + \tilde{Y} \right\|$ exponentially decreases independent of excitation and other signals. And therefore $\mathcal{S}$ exponentially shrinks to the null set and we approach a globally stable system. Identical arguments to that of the VR-AO show that regardless of excitation $\lim_{t \to \infty} E_{\theta} = 0$ and with $\hat{\Omega} \in SPE_I$, $\widetilde{\theta}$ will exponentially decrease to 0.

Here it is important to note a caveat to claims of arbitrarily fast convergence of the observer. Clearly from the stability analysis our limiting factor to convergence is $\widetilde{\Omega}$ and $\tilde{Y}$ which determine the size of $\mathcal{S}$. In theory, the filters $F, g$ and $G_0(s)$ can be made arbitrarily fast and therefore $\mathcal{S}$ would shrink arbitrarily fast. However, in practice, numerical errors prevent using $F, g$ and $G_0(s)$ which are 'too fast' relative the original plant poles. Obviously, 'too fast' would be determined by the hardware available..

### 3.2.4 Matrix-Regressor Adaptive Observer II

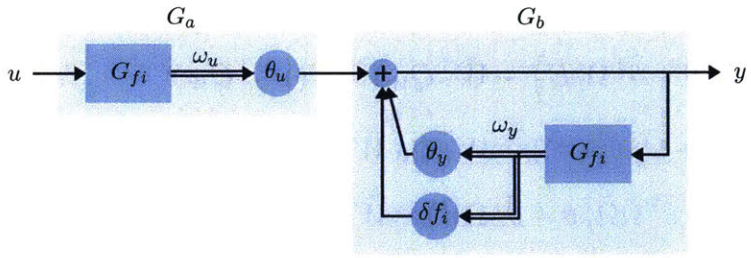


Figure 3-5: Equivalence of multiple independent nonminimal systems is achieved by an additional feedback term, $\delta f_i$ in the output filter $G_b$. Since this $\delta f_i$ is known, multiple nonminimal representations can be used simultaneously to construct a matrix of regressors.

In this section, we present a second matrix regressor adaptive observer with an inherently different method of generating the multiple regressor vectors. Recall that the adaptive observer is built upon a nonminimal equivalent system of (3.3)

$$\dot{x}(t) = (F_0^{OC} + \theta_y c_p^\top)x(t) + b_p u(t) = \begin{bmatrix} & I_{n-1\times n-1} \\ -f_0 & \\ & 0_{1\times n-1} \end{bmatrix} x(t) + \theta_y y(t) + \theta_u u(t)$$

$$y(t) = c_p^\top x(t) \tag{3.94}$$

and that of the true parameters,

$$\theta_u = b_p \;\; and \;\; \theta_y = f_0 - a_p \tag{3.95}$$

$\theta_u$ is independent of the filter $F^{OC}$ and $\theta_y$ is biased by the filter characteristic polynomial coefficients $f_0$. This allows the creation of additional nonminimal representations for the same system using the true parameters of (3.96)

$$\dot{x}(t) = \begin{bmatrix} & I_{n-1\times n-1} \\ -f_i & \\ & 0_{1\times n-1} \end{bmatrix} x(t) + \theta_y y(t) + \underbrace{(f_i - f_0)}_{\delta f_i} y(t) + \theta_u u(t)$$

$$y(t) = c_p^\top x(t) \tag{3.96}$$

The fundamental characteristic of matrix regressor adaptive observers is the generation of additional nonminimal state regressors which when excited will provide responses linearly independent of any other regressor. In the previous section and elsewhere in literature this was accomplished by creating virtual inputs and outputs,

$u_i$ and $y_i$ respectively, by filtering the true systems input, $u$ and output $y$. This new approach creates additional regressors instead through generation of an alternative equivalent system, something not seen before in the literature. The key enabling factor for this is that the same parameterization, $\theta_u, \theta_y$, is used for every equivalent system. With this understanding of the intracacies of equivalent systems, we present an alternative matrix regressor adaptive observer, designated here MR-AO-II.

We represent the plant using states $\omega_i$ that are generated as

$$\dot{\omega}_i = \overline{F}_i \omega_i + \overline{g} \begin{bmatrix} u \\ y \end{bmatrix}, \tag{3.97}$$

$$\overline{F}_i = \begin{bmatrix} F_i & 0 \\ 0 & F_i \end{bmatrix}, \quad \overline{g} = \begin{bmatrix} g & 0 \\ 0 & g \end{bmatrix}$$

$$F_i = \begin{bmatrix} & I_{n-1\times n-1} & \\ -f_i & & \\ & 0_{1\times n-1} & \end{bmatrix} \quad g = \begin{bmatrix} 1 \\ 0 \\ \vdots \end{bmatrix}$$

$$\Omega_{II} = \begin{bmatrix} \omega_0 & \omega_1 & \dots & \omega_{2n-1} \end{bmatrix}$$

where $f_i \neq f_j \ \forall i \neq j$. This leads to a total of $4n^2$ integrators that make up the matrix regressor $\Omega_{II}$.

With the above states, the plant output $y$ can be expressed as

$$Y = y \begin{bmatrix} 1 \\ 1 \\ \vdots \end{bmatrix} = \Omega_{II}^{\top}\theta + \sum_{i=1}^{2n-1} \mathbf{w}_i \omega_i^{\top} \delta\overline{f}_i \tag{3.98}$$

$$\delta\overline{f}_i = \begin{bmatrix} 0 \\ f_i - f_0 \end{bmatrix} \quad i = 1, 2, \cdots, 2n-1$$

where $\mathbf{w}_i$ is a unit vector directed in the $i$th dimension. It is the introduction of this offset to $\theta = -a_p + f_0$ which allows the construction of $2n$ error equations while only filtering the input by filters of order $2n$.

With the plant representation as in (3.98), we now generate errors

$$\begin{aligned} e_i &= (\hat{\theta} + \delta\overline{f}_i)^\top \hat{\omega}_i - y \\ E &= [e_0, e_1, ..., e_{2n-1}]^\top \end{aligned} \tag{3.99}$$

Since $f_i$ and $f_0$ are known for all $i$, the offset $\delta f_i$ is known. Therefore, $e_i(t)$ can be constructed at each instant of time using a single estimate of the parameter vector for which we can now choose an adaptive law similar to that in (3.74) as

$$\dot{\hat{\theta}} = \dot{\widetilde{\theta}} = -\gamma \hat{\Omega}_{II} E \tag{3.100}$$

where $\gamma \in \mathbb{R}^+$ and $\widetilde{\theta} = \hat{\theta} - \theta$ is the parameter error.

Note that the true unknown parameters will be different for each filter, but all related by known vector shifts $\delta\overline{f}_i$. Therefore only one vector parameter estimation $\hat{\theta}$ of $\theta$ is required. We now state the convergence result for MR-adaptive observer II, similar to Theorem 3.

**Theorem 4.** *Assume for all frequencies $v_j$ there exists a pair of filters $i, j$ such that $\sin(\phi_{ij} - \phi_{kj}) \neq 0$. If the external input $u(t) = \sum_{j=1}^{n} \sin v_j t$ it can be shown that (i) $\Omega_{II} \in SPE_{2n}$ and (ii) $\widetilde{\theta}(t) = 0$ is exponentially stable and $\exists T \geq 0$ such that $\left\|\widetilde{\theta}(t)\right\|$ satisfies the inequality*

$$\left\|\widetilde{\theta}(t)\right\| \leq \left\|\widetilde{\theta}(t_0)\right\| e^{-\gamma\epsilon_\Omega(t-t_0)}, \quad \forall t \geq t_0 + T \tag{3.101}$$

*where $\epsilon_\Omega$ is the degree of SPE of $\Omega_{II}$.*

*Proof.* Using transformation matrices $J$ and $K_i$ the matrix regressor can be shown to be

$$\Omega_{II}(t) = J[K_1 v_0(t), K_2 v_0(t), K_3 v_0(t), ...K_{2n} v_0(t)] \tag{3.102}$$

where $v_0(t) = [\sin(v_1 t), \cos(v_1 t), ..., \sin(v_n t), \cos(v_n t)]^\top$. As in Theorem 3, it follows that $v_0 \neq \mathbf{0}\ \forall t$. $J$ and $K$ are defined as

$$J = \begin{bmatrix} \mathbf{T} \\ \mathbf{T}\mathbf{R}_p \end{bmatrix} \tag{3.103}$$
$$K_i = \mathbf{R}_i$$

where the transformation matrices $\mathbf{T}$, $\mathbf{R}_p$, $\mathbf{R}_i \in \mathbb{R}^{n\times n}$ are

$$\omega_{ui} = \underbrace{\begin{bmatrix} \mathbf{T}_1 & \mathbf{T}_2 & \cdots \end{bmatrix}}_{\mathbf{T}} \underbrace{\begin{bmatrix} \mathbf{R}_{i1} & & \\ & \mathbf{R}_{i2} & \\ & & \ddots \end{bmatrix}}_{\mathbf{R}_i} \underbrace{\begin{bmatrix} \sin v_1 t \\ \cos v_1 t \\ \sin v_2 t \\ \vdots \end{bmatrix}}_{\mathbf{S}}$$

$$\omega_{yi} = \mathbf{T}\mathbf{R}_p\mathbf{R}_i\mathbf{S} \tag{3.104}$$

and $\mathbf{R}_{ij} \in \mathbb{R}^{2\times 2}$ is a block of $\mathbf{R}_i$. $b_{ij}$ and $\phi_{ij} \in R$ are the gain and phase shift due to $G_i$ at frequency $v_j$ respectively.

$$\mathbf{R}_{ij} = b_{ij} \begin{bmatrix} \cos\phi_{ij} & \sin\phi_{ij} \\ -\sin\phi_{ij} & \cos\phi_{ij} \end{bmatrix} \tag{3.105}$$

$\mathbf{T}_j \in \mathbb{R}^{n\times 2}$ is another transformation matrix,

$$\mathbf{T}_j = \begin{bmatrix} 1 & 0 \\ 0 & v_j \\ -v_j^2 & 0 \\ 0 & -v_j^3 \\ \vdots & \vdots \end{bmatrix} \tag{3.106}$$

and $K_i$ is a block diagonal matrix whose $j$th block is given by

$$K_{ij} = \begin{bmatrix} b_{ij}\cos\phi_{ij} & b_{ij}\sin\phi_{ij} \\ -b_{ij}\sin\phi_{ij} & b_{ij}\cos\phi_{ij} \end{bmatrix} \tag{3.107}$$

where $b_{ij}$ and $\phi_{ij}$ are the gain and phase of $G_i$ at frequency $v_j$.

It can be shown that $J$ is nonsingular [40]. We will now show that for all $t$, $\Psi = [K_1 v_0, K_2 v_0, K_3 v_0, ...K_{2n} v_0]$ is not singular.

The block diagonal structure of $K_i$ results in each block $K_{ij}$ multiplying only frequency $j$. Additionally by assumption $\exists i,k \quad s.t. \quad \sin(\phi_{ij} - \phi_{kj}) \neq 0$ and it follows that $\Psi_j = [K_{1j} v_0, K_{2j} v_0, \cdots, K_{2nj} v_0]$ is rank 2. Therefore, $\exists T, t_0$ such that $\int_t^{t+T} \lambda_m [\Psi]\, d\tau \geq 0 \;\; m = 1,2,...,2n \;\; \forall t \geq t_0$ which implies $\int_t^{t+T} \lambda_m [\Omega_{II}(t)]\, d\tau \geq 0 \;\; m = 1,2,...,2n \;\; \forall t \geq t_0$ and proves (i). From Theorem 2 we conclude that there will exist $t_0, T, \epsilon_\Omega > 0$ such that $\int_t^{t+T} \lambda_m \left[\Omega_{II}\Omega_{II}^\top\right] d\tau \geq \epsilon_\Omega \;\; m = 1,2,...,2n \;\forall t \geq t_0$. This proves (ii) in Theorem 4. □

Similar to MR adaptive observer I, as represented above, the adaptive observer in (3.100) will require $4n^2$ integrators. However, unlike MR adaptive observer I, no signal is filtered by a transfer function of order greater than $2n$, which has obvious advantages. Additionally, MR adaptive observer II is advantageous when the bandwidth of the plant is not well known. This is because, unlike MR adaptive observer I,

the filters of adaptive observer II can be distributed throughout the predicted range of the unknown plant's bandwidth.

To facilitate faster convergence, equation (3.74) should include positive definite gain matrix $\Gamma$. A similar proof to that of Theorem 3 can easily be derived for this case as well but was omitted here for ease of exposition.

### 3.2.5 Stability of MR-AO II

For the nonminimal systems (3.97) we now analyze the stability of the matrix regressor error, $\widetilde{\Omega}_{II} = \hat{\Omega}_{II} - \Omega_{II}$ and parameter error $\widetilde{\theta} = \hat{\theta} - \theta$.

We begin by expanding the error $E = [e_0\ e_1\ \cdots\ e_{2n-1}]^\top$ for use in the analysis to follow. First note that from (3.99)

$$e_i = (\hat{\theta} + \delta\overline{f}_i)^\top \hat{\omega}_i - y \tag{3.108}$$

$$= (\hat{\theta} + \delta\overline{f}_i)^\top \hat{\omega}_i - (\theta + \delta\overline{f}_i)^\top \omega_i \tag{3.109}$$

$$= (\hat{\theta} + \delta\overline{f}_i)^\top \hat{\omega}_i - (\theta + \delta\overline{f}_i)^\top (\hat{\omega}_i - \widetilde{\omega}_i) \tag{3.110}$$

$$= \widetilde{\theta}^\top \hat{\omega}_i + (\theta + \delta\overline{f}_i)^\top \widetilde{\omega}_i \tag{3.111}$$

$$\tag{3.112}$$

which can then be written in vector form as

$$E = \underbrace{\hat{\Omega}_{II}^\top \widetilde{\theta}}_{E_\theta} + E_\Omega \tag{3.113}$$

with

$$E_\Omega = \widetilde{\Omega}_{II}^\top \theta + \begin{bmatrix} 0 \\ \delta \overline{f}_1^\top \widetilde{\omega}_i \\ \vdots \\ \delta \overline{f}_{2n-1}^\top \widetilde{\omega}_i \end{bmatrix} \tag{3.114}$$

Additionally we compute the nonminimal state errors $\widetilde{\omega}_i = \hat{\omega}_i - \omega_i$,

$$\dot{\widetilde{\omega}}_i = F_i \widetilde{\omega}_i \tag{3.115}$$

To analyze the stability of the MR adaptive observer in (3.99) we define a radially unbounded Lyapunov function candidate

$$V = \frac{1}{2}\widetilde{\theta}^\top \widetilde{\theta} + \sum_{i=0}^{2n-1} \widetilde{\omega}_i^\top P_i \widetilde{\omega} \tag{3.116}$$

with positive definite $P_i \in \mathbb{R}^{2n \times 2n}$ satisfying $F_i^\top P_i + P_i F_i + Q_i = 0$ for any positive definite $Q_i \in \mathbb{R}^{2n \times 2n}$ for all $i \in \{0, 1, \ldots, 2n-1\}$. Using $\dot{\hat{\theta}}$ of (3.99), $\dot{\widetilde{\omega}}_i$ from (3.115) the time derivative of (3.116) is given by

$$\dot{V} = \frac{1}{2}\left(\dot{\widetilde{\theta}}^\top \widetilde{\theta} + \widetilde{\theta}^\top \dot{\widetilde{\theta}}\right) + \sum_{i=0}^{2n-1} (\dot{\widetilde{\omega}}_i^\top P_i \widetilde{\omega}_i + \widetilde{\omega}_i^\top P_i \dot{\widetilde{\omega}}_i) \tag{3.117}$$

$$= -\frac{1}{2}\left(E^\top \hat{\Omega}_{II}^\top \widetilde{\theta} + \widetilde{\theta}^\top \hat{\Omega}_{II} E\right) - \sum_{i=0}^{2n-1} \widetilde{\omega}_i^\top Q_i \widetilde{\omega}_i \tag{3.118}$$

$$= -\widetilde{\theta}^\top \hat{\Omega}_{II} \hat{\Omega}_{II}^\top \widetilde{\theta} - \widetilde{\theta}^\top \hat{\Omega}_{II} E_\Omega - \sum_{i=0}^{2n-1} \widetilde{\omega}_i^\top Q_i \widetilde{\omega}_i \tag{3.119}$$

$$= -E_\theta^\top E_\theta - E_\theta E_\Omega - \sum_{i=0}^{2n-1} \widetilde{\omega}_i^\top Q_i \widetilde{\omega}_i \tag{3.120}$$

$$\tag{3.121}$$

Where we see final summation term is negative definite while the first term is a negative quadratic term in $E_\theta$ and the second is linear in $E_\theta$. From this we can conclude that $\dot{V} < 0$ outside of the compact set

$$\mathcal{S} = \left\{ \widetilde{\theta} \in \mathbb{R}^{2n}, \widetilde{\Omega} \in \mathbb{R}^{2n \times 2n} : \left\| \hat{\Omega}^\top \widetilde{\theta} \right\| > \|E_\Omega\| \right\} \tag{3.122}$$

From (3.115) we see that $\|E_\Omega\|$ exponentially decreases independent of excitation and other signals. And therefore $\mathcal{S}$ exponentially shrinks to the null set and we approach a globally stable system. Identical arguments to that of the VR-AO show that regardless of excitation $\lim_{t\to\infty} E_\theta = 0$ and with $\hat{\Omega} \in SPE_{II}$, $\widetilde{\theta}$ will exponentially decrease to 0.

Once again, as with the MR-AO-I we can in theory achieve arbitrarily fast convergence of the parameter error with persistent excitation of the system implying SPE. However, we are still limited by the presence of $\mathcal{S}$.

A few comments are now in order to address differences between MR-AO I and II. First, in order to rapidly decrease the size of $\mathcal{S}$ of MR-AO-I we would need to increase the speed of the base filter. However, using a base filter which is very fast relative to the plant will result in poor SPE and poor learning in general. In MR-AO-II a number of filters can be used, with a range of speeds, from extremely fast relative to the system, to on the same order of the system. Introduction of scalar time varying gains for lerning from each regressor which start small but increase to unity at the same rate the error decreases allows poorly conditioned fast regressors when slower regressors contain error due to initial conditions, but using slower better conditioned filters once errors are expected to have decayed sufficiently. Secondly, the sequential filtering of regressors in MR-AO-I will significantly attenuate signal strength at higher frequencies, thereby potentially significantly reducing the degree of SPE if the input signal contains high frequency content. The MR-AO-II alternatively

only filters the original signal with its full strength. And third, as the order of the plant increases the number of regressors increases and when large would require a large number of filters to be assembled for MR-AO-II, as these filters must be spaced significantly apart in the frequency domain in order to maintain sufficient SPE it may become difficult for higher order plants. For these higher order plants, the best course of action would likely be a combination of multiple base regressors as constructed in MR-AO-II each sequentially filtered as in MR-AO-I in order to create at least $2n$ regressors. If resources permit, more than $2n$ regressors can increase the degree of SPE for a given input resulting in $\Omega \in \mathbb{R}^{2n \times m}$ with $m > 2n$.

THIS PAGE INTENTIONALLY LEFT BLANK

# Chapter 4

# Adaptive Observers for the modified SP model

## Contents



In the previous chapter we discussed adaptive observers for linear time invariant (LTI) strictly proper single-input, single-output (SISO) systems. For our battery management system (BMS) task, as can be seen from the model summarized in section 2.3.2, our system does not fit this description due to the presence of two static nonlinear functions, a nonlinearity at the output of the dynamic system and a nonlinear feedthrough, $f^1_{ocp}$ and $f^1_{over}$ respectively (Figure 5-1). In this chapter we assume that $f^1_{ocp}$ is known, but still present, and modify the adaptive observer to work in the cases of $f^1_{over}$ known and unknown.

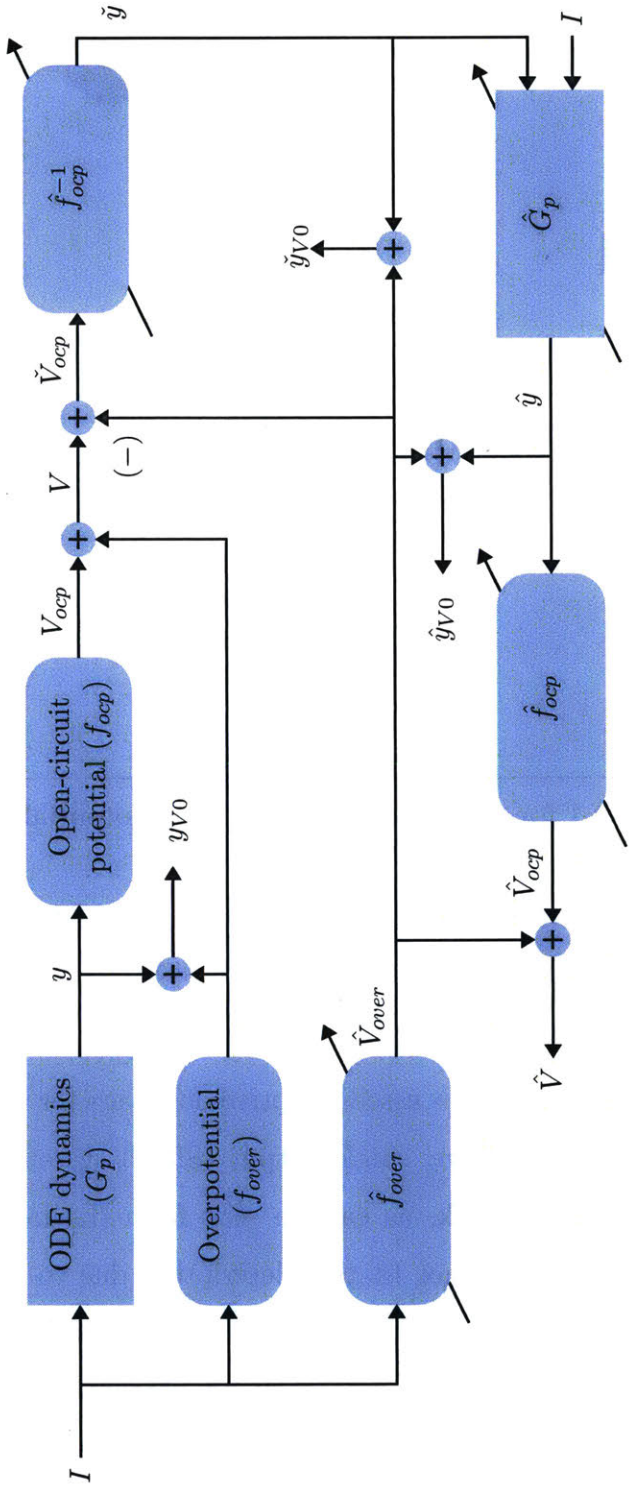


Figure 4-1: Schematic of true, predicted and estimated signals of the modified SP model for implementation of the MR-AO I.

## 4.1 MR-AO I for the modified SPM, overpotential known

For a physical cell the only measurements available are the input, $I$, and the potential across the cell terminals, $V$. For the nonminimal states of an adaptive observer to converge to their true states a measurement of the output of the dynamical system is required. We can compute an a-priori prediction of this signal, designated $\check{y}$ in figure 4-1, as

$$\begin{aligned} \check{V}_{ocp} &= V - \hat{f}^1_{over}(I) \\ \check{y} &= \left(\hat{f}^1_{ocp}\right)^{-1}(\check{V}_{ocp}) \end{aligned} \tag{4.1}$$

where $\check{V}_{ocp}$ is the predicted open circuit voltage after the estimated overpotential has been subtracted from the measured cell voltage and $\check{y}$ is the predicted dynamical system output. In the ideal case where $\hat{f}^1_{over} = f^1_{over}$ and $\hat{f}^1_{ocp} = f^1_{ocp}$, we have that $\check{V}_{ocp} = V_{ocp}$ and $\check{y} = y$. It is the synthesis of this signal, which will mimic the dynamical system output independent of its estimate that enables the use of an adaptive observer for this system despite the presence of nonlinearities on the output and feedthrough.

We first validate the performance of the adaptive observer described in Section 3.2. The problem is to identify the parameters the SP model defined by (2.34)-(2.39), using $I$ and the corresponding prediction of $y$, $\check{y}$, from measurements of $V$, first assuming both $f^1_{ocp}$ and $f^b_{over}$ are known.

To test the adaptive observer under realistic PE conditions a UDDS drive cycle [56] is used as the cell input and repeated for 3 hours. The UDDS signal is an urban dynamometer driving schedule used by the United States Environmental Protection Agency to test fuel economy representing city driving conditions. Examining the

frequency spectrum of this signal confirms that it is indeed persistently exciting. Figure 4-2 shows both the input profile as well as the cell voltage and internal state of charge. A total of 6 parameters are estimated by the adaptive observer, representing the 3 numerator coefficients and 3 denominator coefficients of the equivalent transfer function from $I$ to $y$. The filter $\hat{\Omega}_I$ was chosen as in (3.74), with $\hat{\omega}_0$ determined using $F_1, g_{u1}, g_{y1}$ as specified by (3.34)-(3.40) and $\hat{\omega}_i$ as in (3.72) with $G_0(s) = \frac{0.03}{s+0.03}$ and the scalar gain $\gamma = 3$. The MRAO-I described in (3.74) was evaluated with a 30% corruption in the six parameters what correspond to the 3rd order transfer function of the SPM.

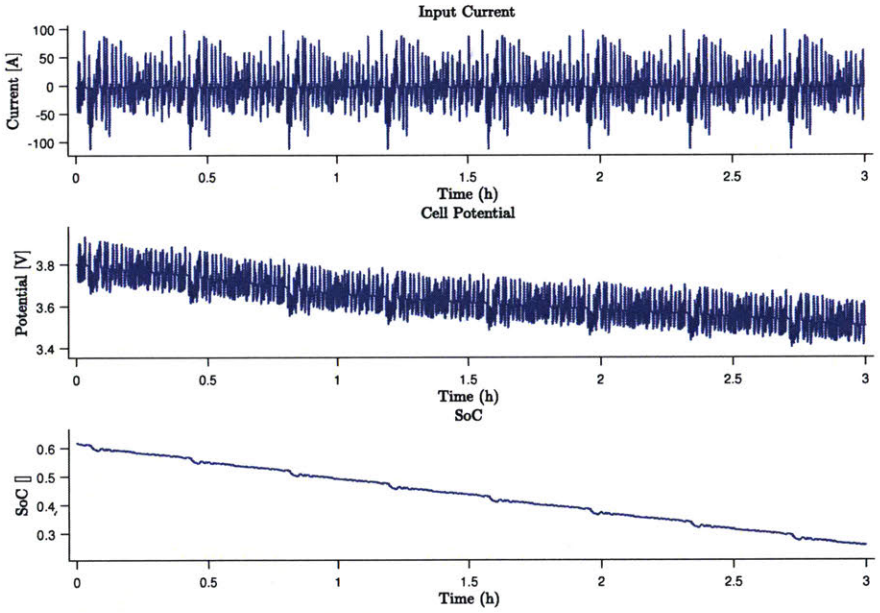


Figure 4-2: Input current, cell voltage and state of charge of the cell for all simulation results

Figure 4-3(a) shows the corresponding parameter estimates obtained using the predicted output $\check{y} = y$. Also shown in Figure 4-3(b) is the estimated output of the cell, which is a nonlinear transformation of the dynamical error used for the adaptive

learning. Figure 4-3(c) is the corresponding SOC estimate error, which corresponds to the estimation of the state variable $\overline{c}_s^-$ defined in (2.34). Given that a key goal of a BMS is an accurate estimation of SOC, Figure 4-3 clearly shows that assuming $f_{ocp}^1$ and $f_{over}^1$ are known a matrix regressor adaptive observer can successfully estimate internal states and correctly identify the underlying diffusion dynamics.

The results of Figure 4-3 are based on the assumption that $f_{over}$ and $f_{ocp}$ are fully known. We now relax this assumption and assess the need for estimating the nonlinear components of the SPM. We begin with a numerical evaluation of the system considered previously, and introduce a 50% reduction in $R_f^-$. From (4.1), it follows that this in turn leads to errors in $\check{y}$ where

$$y = \left(f_{ocp}^1\right)^{-1}\left(V - f_{over}^1(I)\right) \tag{4.2}$$

$$\check{y} = \left(f_{ocp}^1\right)^{-1}\left(V - \hat{f}_{over}^1(I)\right) \tag{4.3}$$

$$e_{\check{y}} = \check{y} - y = -k_t 0.5 R_f^- I \tag{4.4}$$

where $k_t \in \mathbb{R}^+$ is some time varying scalar gain. This therefore introduces errors in parameter estimation as well. Figure 4-6(a) shows the corresponding parameter estimates obtained using the corrupted output $\check{y}$ which clearly illustrate the lack of their convergence. Also shown in Figure 4-6(b) is the estimated output of the cell, which is a nonlinear transformation of the dynamical error used for the adaptive learning. Figure 4-6(c) is the corresponding SOC estimate error, which corresponds to the estimation of the state variable $\overline{c}_s^-$ defined in (2.34). Given that a key goal of a BMS is an accurate estimation of SOC, Figure 4-6 clearly shows that uncertainties in $f_{over}^1$ cannot be ignored. For this reason, estimation of the overpotential should be added to the adaptive observer and is addressed below.

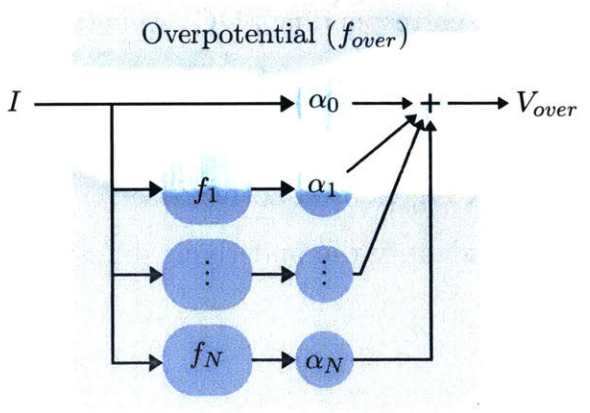


Figure 4-5: Overpotential basis function representation

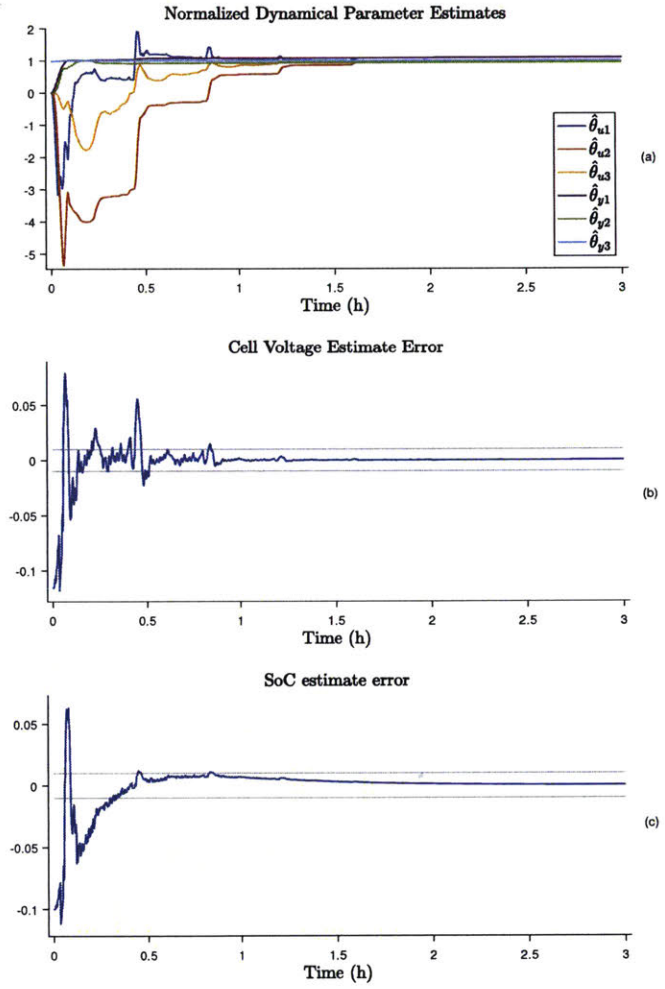


Figure 4-3: MR adaptive observer when $\hat{f}_{over} = f_{over}$ (a) normalized parameter estimates, $\frac{\hat{\theta}_i}{\theta_i}$, where $\theta_i$ is the $i$'th element of the true parameter (defined in (3.73)) (b) cell voltage estimate error (actual cell voltage can be seen in Figure 4-2) , (c) SoC estimation error

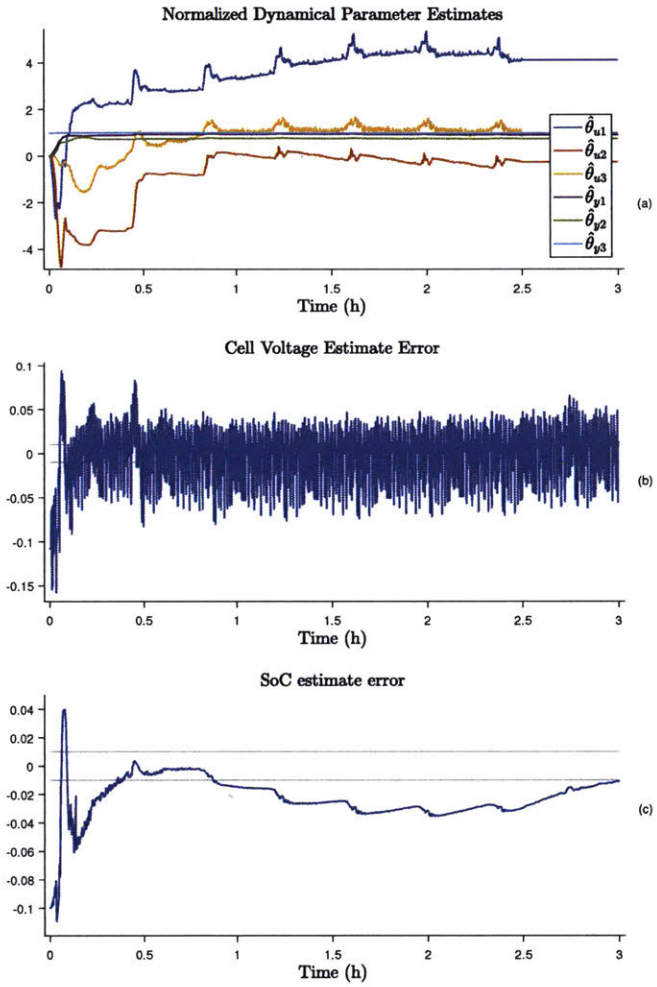


Figure 4-4: MR adaptive observer with corrupted $\hat{f}_{over}$ (a) normalized parameter estimates, $\frac{\hat{\theta}_i}{\theta_i}$, where $\theta_i$ is the $i$'th element of the true parameter (defined in (3.73)) (b) cell voltage estimate error (actual cell voltage can be seen in Figure 4-2) , (c) SoC estimation error

## 4.2 Augmented MR-AO I for the modified SPM, overpotential unknown

In the ideal case, when $f_{ocp}^{1}$ is perfectly known, it follows that a variable $y_{V0}$ can be synthesized as

$$y_{V0} = y + f_{over}(I) = y + \nu^{\top}\alpha \tag{4.5}$$

with

$$\nu = \begin{bmatrix} I \\ f_2(I) \\ \vdots \\ f_N(I) \end{bmatrix}, \quad \alpha = \begin{bmatrix} \alpha_1 \\ \alpha_2 \\ \vdots \\ \alpha_N \end{bmatrix} \tag{4.6}$$

This in turn leads to an underlying linear regression model of the form

$$y_{V0} = \mu_0^{\top}\theta \tag{4.7}$$

where

$$\mu_0 = \begin{bmatrix} \omega_u \\ \omega_y \\ \nu \end{bmatrix}, \theta = \begin{bmatrix} \theta_u \\ \theta_y \\ \alpha \end{bmatrix} \tag{4.8}$$

based on (3.71) and (2.32) The combined nonlinear MRAO observer is proposed as

$$\begin{aligned}
\hat{y}_{Vi} &= \hat{\mu}_i^\top \hat{\theta} \\
\dot{\hat{\omega}}_{u0} &= F\hat{\omega}_{u0} + g_u I \\
\dot{\hat{\omega}}_{y0} &= F\hat{\omega}_{y0} + g_y \check{y} \\
\hat{\mu}_i &= \begin{cases} \begin{bmatrix} \hat{\omega}_{u0}^\top & \hat{\omega}_{y0}^\top & \nu \end{bmatrix}^\top & i = 0 \\ G_0^{(i)}(s)\hat{\mu}_0 & 1 \le i < 2n \\ G_0^{(i-2n)}(s)G_b^{(i-2n+1)}(s)\hat{\mu}_0 & 2n \le i \le 2n+N-1 \end{cases}
\end{aligned} \tag{4.9}$$

where $n$ is the order of the dynamic system (2.29) and $N$ is the number of basis functions used for (2.32). $G_0^{(i)}(s) = \left(\frac{b}{s+b}\right)^i$, $b > 0$, is used to create the first $2n-1$ additional regressors and $G_b(s)$, a high pass filter, is introduced in the generation of the last $N$ filters required to assemble a full rank matrix of regressors. Recall from Section 3.2 that although a low pass filter, $G_0(s)$, was used, any filter can be used. Design of $F, g_u, g_y$ is given by Equations (3.33)-(3.40) described in Section 3.1.2. The reasoning behind the use of $G_b(s)$ will be described shortly.

In order to estimate the parameters, $\theta$, we need to generate an output error $e_i$ using $y_{V0}$ and $\hat{y}_{Vi}, i = 0, 1, \ldots, 2n+N$. However, as noted above, $y_{V0}$ is a synthetic variable only available when the nonlinearities are known. We therefore use variables $\check{y}(t)$ and $\check{V}_{ocp}(t)$ defined in (4.1) to generate the output errors as follows

$$\begin{aligned}
e_i &= \hat{y}_{Vi} - \check{y}_{Vi} \\
\check{y}_{Vi} &= \begin{cases} \check{y} + \nu^\top \hat{\alpha} & i = 0 \\ G_0^{(i)}(s)\check{y}_{V0} & 1 \le i < 2n \\ G_0^{(i-2n)}(s)G_b^{(i-2n+1)}(s)\check{y}_{V0} & 2n \le i \le 2n+N-1 \end{cases}
\end{aligned} \tag{4.10}$$

Using these output errors, the parameter estimate adaptive law is,

$$\begin{aligned}\dot{\hat{\theta}} &= -\Gamma_p \hat{\Omega}' E \\ \hat{\Omega}' &= \left[\begin{array}{c} \Gamma_0\hat{\mu}_0, \Gamma_1\hat{\mu}_1, \ldots, \Gamma_{2n+N}\hat{\mu}_{2n+N-1} \end{array}\right] \\ E &= \left[\begin{array}{c} e_0, e_1, \ldots, e_{2n+N-1} \end{array}\right]^\top \end{aligned} \tag{4.11}$$

where $\Gamma_p$ is a projection gain akin to the projection algorithm of [27] defined as

$$\begin{aligned}\Gamma_p &= I - \Gamma_a - \Gamma_b, \\ \Gamma_a &= \begin{cases} \frac{\nabla f_a (\nabla f_a)^\top}{(\nabla f_a)^\top \nabla f_a} f_a\Big|_{\hat{\theta}} & f_a(\hat{\theta}) > 0 \wedge (\nabla f_a(\hat{\theta}))^\top \hat{\Omega} E > 0 \\ 0 & otherwise \end{cases} \\ \Gamma_b &= \begin{cases} \frac{\nabla f_b (\nabla f_b)^\top}{(\nabla f_b)^\top \nabla f_b} f_b\Big|_{\hat{\theta}} & f_b(\hat{\theta}) > 0 \wedge (\nabla f_b(\hat{\theta}))^\top \hat{\Omega} E > 0 \\ 0 & otherwise \end{cases} \end{aligned} \tag{4.12}$$

where $f_a(\theta)$ and $f_a(\theta)$ are convex functions

$$\begin{aligned} f_a(\theta) &= \frac{\theta^\top Q_\theta \theta - \|\theta_{max}\|^2}{2\epsilon_p \|\theta_{max}\| + \epsilon_p^2}, \quad Q_\theta = \left[\begin{array}{ccc} T_u T_u^\top & & \\ & T_y T_y^\top & \\ & & 0^N \end{array}\right] \\ f_b(\theta) &= \frac{\theta^\top Q_\alpha \theta - \|\alpha_{max}\|^2}{2\epsilon_p \|\alpha_{max}\| + \epsilon_p^2}, \quad Q_\alpha = \left[\begin{array}{cc} 0^{2n} & \\ & I^N \end{array}\right], \end{aligned} \tag{4.13}$$

using $T_u, T_y$ of (3.38) and with $I^k \in \mathbb{R}^{k\times k}$, an identity matrix, and $0^k \in \mathbb{R}^{k\times k}$, a matrix of zeros. Use of the transformation matrices $T_u, T_y$ is required to maintain compatibility between this projection gain, $\Gamma_p$ and the constraint projection gain $\Gamma_c$ of (3.45). $\Gamma_p$ ensures the parameter estimate of the dynamic system $\hat{\theta}_{uy} = [\hat{\theta}_u^\top \hat{\theta}_y^\top]^\top$ remain within a convex set $\Theta_{uy} = \{\hat{\theta}_{uy} \in \mathbb{R}^{2n} : \left\|\hat{\theta}_{uy}\right\| \leq \overline{\theta}\}$ and the overpotential

parameter estimates, $\hat{\alpha}$, remain within a convex set $\Theta_\alpha = \{\hat{\alpha} \in \mathbb{R}^N : \|\hat{\alpha}\| \leq \overline{\alpha}\}$ where

$$\begin{aligned} \overline{\theta} &= \|\theta_{max}\| + \epsilon_p \\ \overline{\alpha} &= \|\alpha_{max}\| + \epsilon_p \end{aligned} \tag{4.14}$$

For this work conservative bounds $\theta_{max} = 10$, $\alpha_{max} = 1$ are chosen ensuring the true parameters, $\theta_{uy} \in \Theta_{uy}$ and $\alpha \in \Theta_\alpha$. $\epsilon_p = 0.1$ defines a finite region at the outer edges of $\Theta_{uy}$ and $\Theta_\alpha$ between which $\Gamma_p$ smoothly transitions from an identity matrix to what is known as a projection matrix. [60] Equation (4.11) can be rewritten in summation form as

$$\dot{\hat{\theta}} = -\Gamma_p \left( \sum_{i=0}^{2n-1} \Gamma_i \hat{\mu}_i e_i + \sum_{j=2n}^{2n+N-1} \Gamma_j \hat{\mu}_j e_j \right) \tag{4.15}$$

where $\hat{\mu}_j \in \mathbb{R}^{2n+N}$, $j \geq 2n$ are the regressors which have been high pass filtered. $\Gamma_i \in \mathbb{R}^{2n+N \times 2n+N}$ are diagonal tunable gains, which can be further broken down into two components

$$\Gamma_i = \begin{bmatrix} \gamma_{\omega_i} \mathbf{I}_{2n} & \\ & \gamma_{\nu_i} \mathbf{I}_N \end{bmatrix}, \quad i = 0, 1, \ldots, 2n + N - 1 \tag{4.16}$$

where $\gamma_{\omega_i} \in \mathbb{R}^+$ and $\gamma_{\nu_i} \in \mathbb{R}^+$. Since the nonlinear observer above used $\breve{y}$, defined in (4.1), rather than the true $y$, $\hat{\omega}_y$ in (4.9) can contain errors as $\hat{f}^1_{over}$ may not equal $f^1_{over}$. As these errors in $\hat{\omega}_y$ are due to incorrect estimation of $\hat{\alpha}$, we have introduced a high pass filter $G_b$ which can attenuate the effect of $\hat{\omega}_i$, but retain the component

of $\nu$ in $\hat{\mu}_i$, $i > 2n$. In particular, we choose $G_b(s)$ such that $\|G_b(s)\|_\infty \leq 1$ and

$$\begin{aligned} &\max_{i\in\mathcal{I},j\in\mathcal{J},\xi=u,y} \left\| G_b^{(i)}(s) G_o^{(i-1)}(s) \left[(sI-F)^{-1} g_\xi\right]_j \right\|_\infty \leq \epsilon_b \\ &\mathcal{J} = \{1, 2, \ldots, 2n+N\} \\ &\mathcal{I} = \{1, 2, \ldots, N\} \end{aligned} \tag{4.17}$$

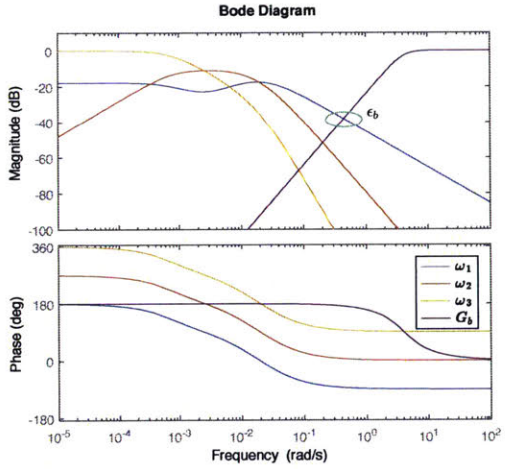


Figure 4-6: Bode diagram of the nonminimal system states and the high pass filter. All signals which pass through both of these filters will be attenuated by at least $\epsilon_b$, which here is $10^{-2}$.

where $[G(S)]_j$ denotes the $j^{th}$ element of a transfer vector $G(s)$. Additionally we define $\gamma_{\nu_i} = 1, \quad 2n \leq i \leq 2n+N$ and

$$\begin{aligned} &\gamma_{\nu_i} = \epsilon_b \left( \max_{j\in\mathcal{J},\xi=u,y} \left\| G_o^{(i-1)}(s) \left[(sI-F)^{-1} g_\xi\right]_j \right\|_\infty \right)^{-1} \\ &i \in \{0, 2, \ldots, 2n-1\} \end{aligned} \tag{4.18}$$

For the complete nonlinear battery model in (2.34)-(2.39), a nonlinear adaptive observer is now completely specified given by (4.1), (4.9)-(4.17). The following the-

orem summarizes the stability properties of the nonlinear observer.

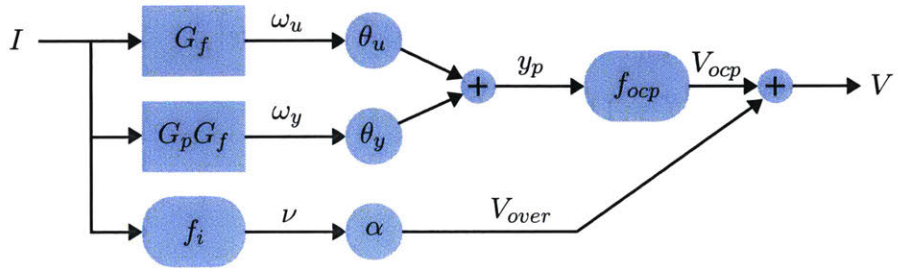


Figure 4-7: Nonminimal representation of the battery including overpotential nonlinearity, for this section we assume $f_{ocp}$ is known allowing it to be inverted and be transparent to the adaptive observer.

**Theorem 5.** *Let $\hat{\Omega} \in SPE$, the nonlinear observer in* (4.1), (4.9)-(4.17) *generates bounded parameter estimates $\hat{\theta}$ of the true parameter $\theta$ in* (4.8) *and bounded state estimates $\hat{\omega}_i$ of the nonminimal state $\omega_i$ in* (3.72) *with*

$$\left\|\hat{\theta}(t) - \theta\right\| + \sum_{i=0}^{2n+N-1} \|\hat{\omega}_i(t) - \omega_i(t)\| \leq \epsilon_t(t) \tag{4.19}$$

*where $\epsilon_t(t)$ is monotonically decreasing with $t$ to a value of $O(\epsilon_b)$.*

*Proof.* We begin with a state space description of the ideal plant (3.71)-(3.73) and its additional synthetic outputs required to create a matrix regressor.

$$\dot{W}_{i,\xi} = \underbrace{\begin{bmatrix} F_{zi} & 0 \\ gC_{zi} & F \end{bmatrix}}_{\overline{F}_i} W_{i,\xi} + \underbrace{\begin{bmatrix} g_{zi} \\ g_\xi \end{bmatrix}}_{\overline{g}_i} \xi \tag{4.20}$$

$$\omega_{\xi i} = \underbrace{\begin{bmatrix} 0 & 0 \\ 0 & I^{n\times n} \end{bmatrix}}_{\overline{C}_i} W_{i,\xi} \qquad \begin{array}{l} 0 \leq i < 2n+N \\ \xi = u, \text{ and } \xi = y \end{array}$$

with $F, g$ of (4.9), and $C_{zi}, F_{zi}, g_{zi}$ such that

$$C_{zi}\left(sI - F_{zi}\right)^{-1} g_{zi} = \begin{cases} G_0^{(i)}(s) & 0 \leq i < 2n \\ G_0^{(i-2n)}(s) G_b^{(i-2n+1)}(s) & 2n \leq i \leq 2n+N-1 \end{cases} \tag{4.21}$$

Equation (4.21) implies that $W_{i,\xi}, \overline{F}_i, \overline{g}_i, \overline{C}_i$ all have dimensions which vary with $i$, where $\overline{g}_i, \overline{C}_i^{\top}, W_{i,\xi} \in \mathbb{R}^m$, where $m = i + n$ when $0 \leq i < 2n$ and $m = i - n + n_b(i - 2n + 1)$ for $2n \leq i \leq 2n + N - 1$ with $n_b$ being the order of the high pass filter used. We can then construct the nonminimal state estimates,

$$\begin{aligned} \dot{\hat{W}}_{i,\xi} &= \overline{F}_i \hat{W}_{i,\xi} + \overline{g}_i \check{\xi} \\ \hat{\omega}_{\xi i} &= \overline{C}_i \hat{W}_{i,\xi} \qquad 0 \leq i < 2n+N, \\ &\qquad\qquad \check{\xi} = u, \text{ and } \check{\xi} = \check{y} \end{aligned} \tag{4.22}$$

To show the stability properties of the adaptive observer (4.8)-(4.16) we construct a Lyapunov function candidate

$$V_1 = \frac{1}{2}\widetilde{\theta}^{\top}\widetilde{\theta} + \sum_{\xi=u,y} \sum_{i=0}^{2n+N-1} \tilde{W}_{i,\xi}^{\top} P_i \tilde{W}_{i,\xi} \tag{4.23}$$

where $\widetilde{\theta} = \hat{\theta} - \theta$ is the parameter estimate error of $\theta$ defined as in (4.8), and the errors within the construction of the nonminimal states are, $\tilde{W}_{i,\xi} = \hat{W}_{i,\xi} - W_{i,\xi}$. To compute $\dot{V}_1$, we use (4.10), (4.11), (4.20), and (4.22) and note that the time-derivative

of (4.23) can be simplified as

$$\begin{aligned}\dot{V}_1 &= \tilde{\theta}^\top\dot{\tilde{\theta}} + \sum_{i=0}^{2n+N-1}\left(\tilde{W}_{i,u}^\top P_i\dot{\tilde{W}}_{i,u} + \dot{\tilde{W}}_{i,u}^\top P_i\tilde{W}_{i,u}\right) + \sum_{i=0}^{2n+N-1}\left(\tilde{W}_{i,y}^\top P_i\dot{\tilde{W}}_{i,y} + \dot{\tilde{W}}_{i,y}^\top P_i\tilde{W}_{i,y}\right)\\ &= -\tilde{\theta}^\top\Gamma_p\hat{\Omega}'E - \sum_{i=0}^{2n+N-1}\left(\tilde{W}_{i,u}^\top Q_i\tilde{W}_{i,u}\right)\\ &\quad + \sum_{i=0}^{2n+N-1}\left(\tilde{W}_{i,y}^\top P_i(\overline{F}_i\tilde{W}_{i,y} + \overline{g}_i(\check{y}-y)) + ((\check{y}-y)\overline{g}_i^\top + \tilde{W}_{i,y}^\top\overline{F}_i^\top)P_i\tilde{W}_{i,y}\right)\end{aligned} \tag{4.24}$$

where $Q_i > 0$ and $P_i$ solves $\overline{F}_i^\top P_i + P_i\overline{F}_i = -Q_i$ with $\overline{F}_i, \overline{g}_i$ of (4.20). Expanding $e_0$ of (4.11) we see that

$$\begin{aligned}e_0 &= y_{\hat{V}i} - y_{\check{V}i}\\ &= \hat{\omega}^\top\hat{\theta} + \nu^\top\hat{\alpha} - \left(\check{y} + \nu^\top\hat{\alpha}\right)\\ &= \hat{\omega}^\top\hat{\theta} - f_{ocp}^{-1}(\check{V}_{ocp})\\ &= \hat{\omega}^\top\hat{\theta} - f_{ocp}^{-1}(f_{ocp}(\omega^\top\theta) + \nu^\top\alpha - \nu^\top\hat{\alpha})\\ &= \hat{\omega}^\top\hat{\theta} - f_{ocp}^{-1}(f_{ocp}(\omega^\top\theta) + \nu^\top\tilde{\alpha})\end{aligned} \tag{4.25}$$

and due to the monotonicity of $f_{ocp}^1$ we have

$$\begin{aligned}e_0 &= \hat{\omega}^\top\hat{\theta} - \left(\omega^\top\theta - k_t\nu^\top\tilde{\alpha}\right)\\ &= \underbrace{\hat{\omega}^\top\tilde{\theta}}_{e_\theta} + k_t\underbrace{\nu^\top\tilde{\alpha}}_{e_\alpha}\end{aligned} \tag{4.26}$$

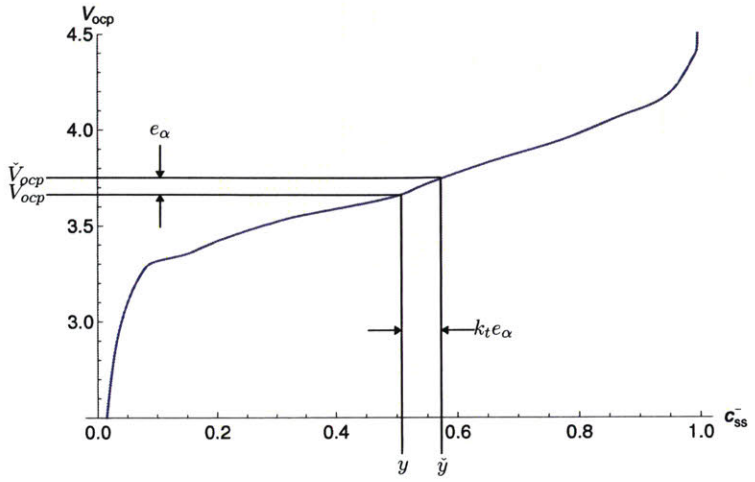


Figure 4-8: Due to the monotonicity of $f_{ocp}^1$ the error in the predicted open circuit potential $\check{V}_{ocp}$ will result in the same sign but scaled error in the predicted dynamical output $\check{y}$

where $k_t \in \mathbb{R}^+$, a bounded time-varying gain,

$$\frac{1}{\max_y \frac{\partial f_{ocp}^1(y)}{\partial y}} \leq k_t \leq \frac{1}{\min_y \frac{\partial f_{ocp}^1(y)}{\partial y}} \tag{4.27}$$

The error of the subsequently filtered regressors is

$$e_i = \begin{cases} G_0^{(i)}(s)e_0 & 1 \leq i < 2n \\ G_0^{(i-2n)}(s)G_b^{i-2n+1}(s)e_0 & 2n \leq i \leq 2n+N-1 \end{cases} \tag{4.28}$$

Additionally, the error in our a-priori prediction of $y$, $\check{y}$ is

$$\begin{aligned} \check{y} - y &= (\omega^\top \theta - k_t \nu^\top \tilde{\alpha}) - \omega^\top \theta \\ &= -k_t \underbrace{\nu^\top \tilde{\alpha}}_{e_\alpha} \end{aligned} \tag{4.29}$$

Using these errors in (4.24) we see that

$$\dot{V}_1 = -\sum_{i=0}^{2n+N-1} \widetilde{\theta}^\top \Gamma_p \Gamma_i \hat{\mu}_i \Gamma_t \hat{\mu}_i^\top \widetilde{\theta} - \sum_{i=0}^{2n+N-1} \left( \tilde{W}_{i,u}^\top Q_i \tilde{W}_{i,u} \right) - \sum_{i=0}^{2n+N-1} \left( \tilde{W}_{i,y}^\top Q_i \tilde{W}_{i,y} \right) - \sum_{i=0}^{2n+N-1} \left( \tilde{W}_{i,y}^\top P_i \overline{g}_i (k_{ti} e_{\alpha i}) + (k_{ti} e_{\alpha i}) \overline{g}_i^\top P_i \tilde{W}_{i,y} \right) + \sum_{i=0}^{2n+N-1} \widetilde{\theta}^\top \Gamma_p \Gamma_i \hat{\mu}_i \underbrace{\tilde{W}_i^\top \overline{C}_i^\top \theta}_{e_\omega} \tag{4.30}$$

$$\Gamma_t = \begin{bmatrix} I_{2n} & \\ & k_t' I_N \end{bmatrix} \tag{4.31}$$

Unfortunately, we are not assured that $e_\omega$ decays exponentially as we were with just a linear system due to our use of an a-priori estimate of the dynamical system output $\check{y}$ instead of the true $y$. With the construction of a second Lyapunov candidate we show that $e_\alpha$ and $e_\omega$ are of the order $\epsilon_b$ from (4.17). Let

$$V_2 = \tilde{\alpha}^\top \tilde{\alpha} \tag{4.32}$$

and recall from (4.15) that

$$\dot{\hat{\alpha}} = \dot{\tilde{\alpha}} = \Gamma_b' \sum_{i=0}^{2n+N-1} \gamma_{\nu_i} \nu_i e_i \tag{4.33}$$

where $\Gamma_b' \in \mathbb{R}^{N \times N}$ is the lower right block of $\Gamma_p$, the projection gain in (4.12), and $\gamma_{\nu_i}$ were defined in (4.18). Taking the derivative of (4.32) and expanding $e_i$ we arrive at

$$\dot{V}_2 = -\tilde{\alpha}^\top \Gamma_b' \left( \sum_{i=0}^{2n+N-1} \nu_i \nu_i^\top \gamma_{\nu i} \right) \tilde{\alpha} + \tilde{\alpha}^\top \Gamma_b' \left( \sum_{i=0}^{2n+N-1} \nu_i (\hat{\omega}_i^\top \widetilde{\theta} + \widetilde{\omega}_i^\top \theta) \gamma_{\nu_i} \right) \tag{4.34}$$

We now derive bounds on each term in the right hand side of (4.34). Due to our projection algorithm we have $\left\|\tilde{\theta}\right\| \leq \overline{\theta}$. From (4.17) and (4.18) we have $\gamma_{\nu_i} \left\|\tilde{\omega}_i(t)\right\| \leq \epsilon_b(2n+N)|\nu^\top \tilde{\alpha}| + \epsilon_b \left\|e^{Ft}\tilde{\omega}_i(0)\right\| \leq \epsilon_b(2n+N)u_{max}2|\overline{\alpha}| + \epsilon_b \left\|e^{Ft}\tilde{\omega}_i(0)\right\|$ as well as $\gamma_{\nu_i} \left\|\hat{\omega}_i\right\| \leq \epsilon_b z_{max}$ where $z_{max} = \max_t\{|u(t)|, |y(t)|\}$ resulting in

$$\begin{aligned} \dot{V}_2 \leq & -\tilde{\alpha}^\top \Gamma_b' \left( \sum_{i=0}^{2n+N-1} \nu_i \nu_i^\top \gamma_{\nu i} \right) \tilde{\alpha} \\ & + \epsilon_b \sum_{i=0}^{2n+N-1} \left|\tilde{\alpha}^\top \Gamma_b' \nu_i\right| \times \\ & (2\overline{\theta} z_{max} + (2n+N)u_{max}2\overline{\alpha} + e^{Ft}\tilde{\omega}(0)) \end{aligned} \tag{4.35}$$

The first term is quadratic in $\tilde{\alpha}$ and negative since $\hat{\Omega}$ and therefore $[\nu_1, \nu_2, \ldots, \nu_{2n+N-1}]$ is SPE. The second term is linear with $\tilde{\alpha}^\top \nu$ and a sum of bounded constants scaled by $\epsilon_b$ which can be made arbitrarily small via design of the filter $G_b$. Therefore $\tilde{\alpha}$ is asymptotically convergent to a set of size $\epsilon_b$. This in turn forces the third term of (4.24) to yet another small value proportional to $\epsilon_b$, resulting in asymptotic convergence of the remaining parameter and state errors to an arbitrarily small compact set on the order of $\epsilon_b$. □

To efficiently depict the effectiveness of this algorithm we turn to simulation, Figure 4-9 shows the normalized parameter estimates converging to 1 as expected and the state of charge estimation is once again to a level of less than 1%.

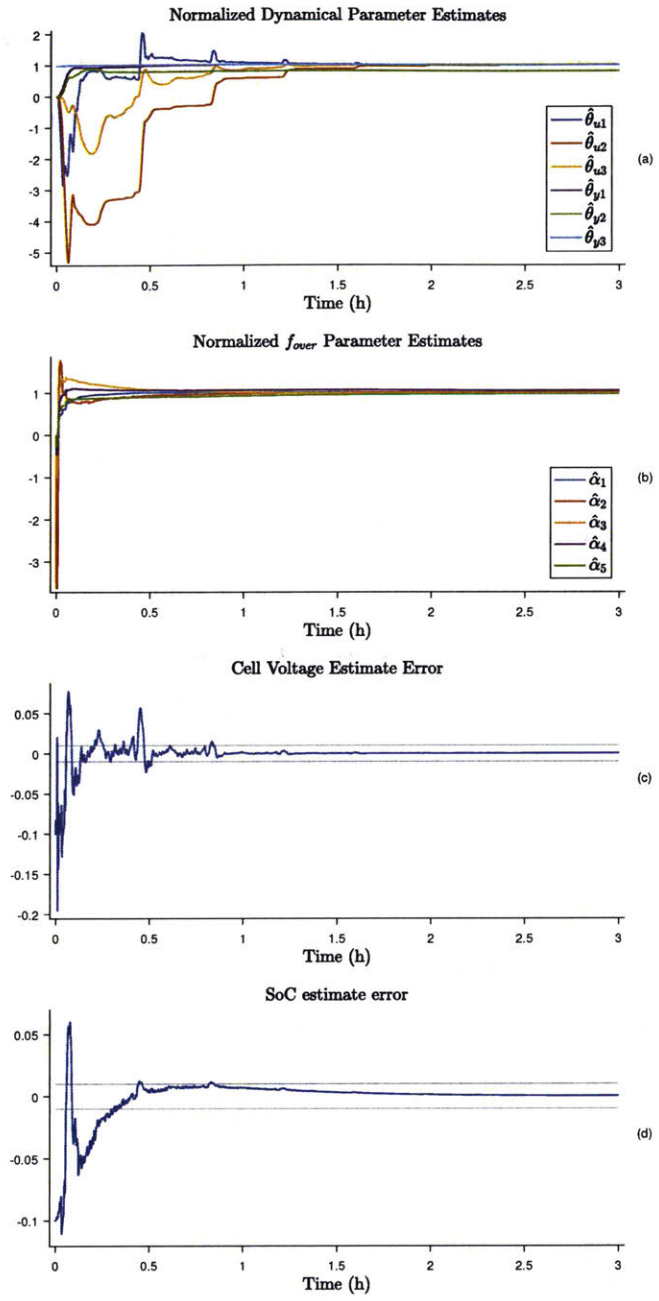


Figure 4-9: Full MR adaptive observer for both $\hat{G}_p$ and $\hat{f}_{over}$ (a) normalized dynamical parameter estimates, $\frac{\hat{\theta}_i}{\theta_i}$, where $\theta_i$ is the $i$'th element of the true parameter (defined in (3.73)) (b) normalized $\hat{f}_{over}$ parameter estimates, $\frac{\hat{\alpha}_i}{\alpha_i}$, where $\alpha_i$ is the $i$'th element of the true parameter (defined in (2.32)) (c) cell voltage estimate error (actual cell voltage can be seen in Figure 4-2) , (d) SoC estimation error

# Chapter 5

# Experimental Validation of Adaptive observers using Panasonic 18650 cells

In this chapter the augmented adaptive observer is experimentally validated using a commercially available 18650 cell. Before this can be accomplished, the final assumption of known $f^i_{ocp}$ must be satisfied and an experimental procedure for testing cells must be presented. We start with a procedure for estimating the parameters which define the resting open circuit potential, $f^i_{ocp}$. This algorithm is then validated using experimental data. This process is performed for each dataset collected in later sections to provide an accurate estimate of the state of charge throughout the experiment. Next, the experimental procedure and excitation signal are presented, followed by results of the augmented adaptive observer running using experimental data.

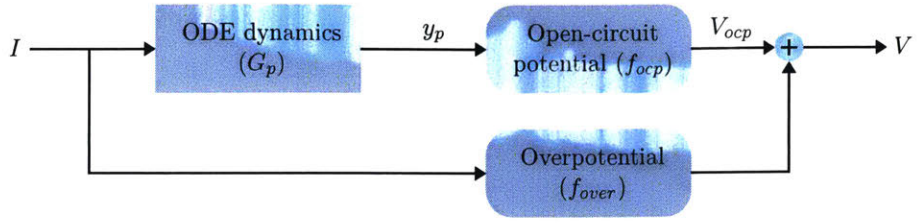


Figure 5-1: Block diagram of the electrochemical model used to represent a Lithium-Ion battery cell after simplifications are made for the observer.

## 5.1 Estimation of the Resting Open Circuit Potential

In this section the parameters required to determine either $f^1_{ocp}$ of (2.37) or $f^2_{ocp}$ of (2.44), from their underlying half-cell potentials are estimated. The structure of the SP model poses several challenges when it comes to on-line parameter estimation. The first is the presence of the nonlinearity $f_{ocp}$ which causes difficulty in determining the outputs of the linear dynamics on-line.

Previously, adaptive observers were developed for the system (2.34) for scenarios in which both $f^1_{over}$ and $f^1_{ocp}$ were known as well as when only $f^1_{ocp}$ was known. Here we now develop a procedure to estimate the model parameters required to obtain $f^1_{ocp}$ and $f^2_{ocp}$. Due to the nature of the open-circuit nonlinearity and the high sensitivity to parameters throughout the majority of a cell's operating voltage as well as the expectation that the parameters which define the resting OCP are very slowly varying, a offline approach is taken for its calibration. This could be extended to a recursive procedure. The algorithm of this chapter does not require states estimated by the adaptive observer, an important fact to establish stability and accuracy of the estimate. The only knowledge assumed of the system is a conservative estimate of the slowest pole in (2.34).

We begin with the generation of a signal, $\kappa$, the integral of the current

$$\kappa(t) = \int_{t_0}^{t} I(\tau)d\tau. \tag{5.1}$$

Using this signal, it directly follows that the state of (2.15) can be rewritten as

$$\overline{c}_s^{\pm}(t) = \alpha^{\pm}\kappa(t) + \beta^{\pm} \tag{5.2}$$

where $\alpha^{\pm}, \beta^{\pm} \in \mathbb{R}$ are parameters we wish to estimate, compactly assembled as

$$\theta_{ocp} = \begin{bmatrix} \alpha^{+} & \beta^{+} & \alpha^{-} & \beta^{-} \end{bmatrix}^{\top}. \tag{5.3}$$

With $\overline{c}_s^{\pm}$ parameterized as in (5.2) we can define the surface concentrations as

$$\overline{c}_{ss}^{\pm} = \alpha^{\pm}\kappa(t) + \beta^{\pm} + \overline{q}^{\pm}. \tag{5.4}$$

If we collect input-output data when $\overline{q}^{\pm} \approx 0$, then we will have an approximation of the surface concentrations as in (5.2) and hence the open circuit potential becomes

$$V_{ocp} \approx f'_{ocp}(\kappa, \theta_{ocp}) = \overline{\mathcal{U}}^{+}(\alpha^{+}\kappa + \beta^{+}) - \overline{\mathcal{U}}^{-}(\alpha^{-}\kappa + \beta^{-}) \tag{5.5}$$

In order to collect data that allows the simplification in (5.5), we determine an upper bound of $\overline{q}^{\pm}$ in (5.4) with a lower bound on the poles appearing in (2.18). With a conservative estimate of the slowest pole in (2.18) designated as $-a_{min}$ we then construct additional signals

$$\begin{aligned} &\dot{\rho}_j(t) = -a_j\rho_j(t) + a_j|I(t)| \\ &\forall a_j \in \{a_{min}, 10a_{min}, 10^2a_{min}, 10^3a_{min}, 10^4a_{min}\} \end{aligned} \tag{5.6}$$

and a composite of these which provides an upper bound on the relaxation of the cell,

$$\rho_c(t) = \max_j \rho_j(t). \tag{5.7}$$

Using this setup $\rho_c(t)$ can be used as a conservative estimate of the quantity $\overline{q}_s^{\pm}(t)$. If a sufficient quantity of base filters are used in (5.6)

$$\overline{q}_s^{\pm}(t) \leq \eta^{\pm}\rho_c(t) \tag{5.8}$$

where $\eta^{\pm}$ is an unknown constant. We therefore empirically choose a limit $\rho_{lim}$ such that when $I = 0$ and $\rho_c(t) \leq \rho_{lim}$, we can approximate the nonlinearity using (5.5) leading to $V_{ocp}(t) \approx f'_{ocp}(\kappa(t), \theta_{ocp})$.

### 5.1.1 Experimental Results

Data was collected using a custom battery cycler and two Panasonic NCR18650B lithium ion cells in a laboratory setting. Temperature of the ambient air is kept constant and the cell casing temperature only varies by $\pm 2\%$. The cycler's maximum sampling rate of $20Hz$ is used to obtain the most versatile data sets. Additional details of the battery cycler are proprietary and have been omitted. A number of experiments were run, in total cycling each cell close to 80 times. Each distinct experiment began with an input profile as seen in Figure 5-2. The resulting capacities computed at the start of each experiment are presented in Figure 5-5.

Unlike the later sections in which signals were all continuous, here we use discrete

measurements. For all discrete $t_i$ such that $T_0 < t_i < T_1$ and for which

$$\begin{aligned} |I(t_i)| &< I_{lim} = \frac{C}{10} \\ \rho_c(t_i) &< \rho_{lim} = 0.2 \end{aligned} \tag{5.9}$$

are satisfied, we computed discrete signals $\kappa_i = \kappa(t_i)$ defined in (5.1) and $\rho_i = \rho_c(t_i)$ defined in (5.7) as well as measured signals $V_i = V(t_i)$ and $I_i = I(t_i)$. These signals are accumulated into a set of sampled sequences of data $\vec{\Omega}^1_{ocp}$ as,

$$\vec{\Omega}^1_{ocp} \begin{cases} \vec{\kappa} &= \{\kappa_1, \kappa_2, ...\kappa_N\} \\ \vec{\rho} &= \{\rho_1, \rho_2, ...\rho_N\} \\ \vec{V} &= \{V_1, V_2, ...V_N\} \\ \vec{I} &= \{I_1, I_2, ...I_N\} \end{cases} \tag{5.10}$$

Using (5.5), and the sampled set (5.10), the estimate error $e_i$, a cost function $J_{ocp}$ and weights for each sample are defined as

$$\begin{aligned} e_i(\hat{\theta}_{ocp}) &= \left(V_i - f'_{ocp}(\kappa_i, \hat{\theta}_{ocp})\right) \\ J_{ocp}(\hat{\theta}_{ocp}) &= \sum_{i=1}^{N} \left(e_i(\hat{\theta}_{ocp})\right)^2 w_{fi}(\hat{\theta}_{ocp}) w_{\rho i} w_{Ii} \\ w_{fi}(\hat{\theta}_{ocp}) &= \left(\frac{1}{|\partial f_{ocp}/\partial \kappa|}\right)\Bigg|_{\kappa_i, \hat{\theta}_{ocp}} \\ w_{\rho i} &= \left(\frac{1}{\rho_i + \epsilon_\rho}\right) \\ w_{Ii} &= \left(\frac{1}{|I_i| + \epsilon_I}\right) \end{aligned} \tag{5.11}$$

The three weights are introduced in order to ensure that the data which corresponds to samples when the cell is closer to its equilibrium are used most heavily. Ideally $\vec{\Omega}^1_{ocp}$ in (5.10) would only contain measurements when $I = 0$ and $\rho = 0$, however, this may

never be the case in normal operation. By addition of the first two weights $w_{\rho i}$ and $w_{Ii}$, our data collection process is simplified greatly. The third weight corresponds to the inverse of the differential of the open circuit potential local to the current capacity measure $\kappa_i$. This ensures that the capacity error is also minimized when minimizing the voltage error $e_i$ and is essential to prevent over-weighting at extreme high and low capacities where the open circuit potential is extremely sensitive to lithium concentration. The resulting estimate of the parameter of (5.3) is

$$\hat{\theta}^*_{ocp} = \arg\min_{\hat{\theta}_{ocp}} J_{ocp}(\hat{\theta}_{ocp}) \tag{5.12}$$

where this minimization is performed using the interior point method in MATLAB.

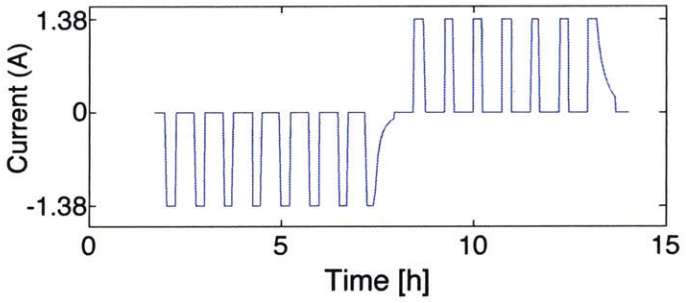


Figure 5-2: Tailored input current for estimation of (5.3), $\hat{\theta}_{ocp}$. Beginning with a fully charged cell, a series of 15 minute discharge pulses of $I(t) = -1.38A$ each followed by 30 minutes of $I(t) = 0$ are performed until a minimum voltage, $V = 2.5V$ is reached, held for 30 minutes at constant voltage, followed by 30 minutes of $I(t) = 0$. The discharge sequence is then reversed with pulses of $I(t) = 1.38A$ until a maximum voltage, $V = 4.2V$ is reached.

The resulting parameters in $\theta_{ocp}$ corresponds to those in (2.15) and (2.17) as

$$\hat{\alpha}^{\pm} = \frac{\pm 3}{R_p^{\pm} F a^{\pm} L^{\pm}} \qquad \hat{n}_{tot} = \frac{\hat{\beta}^+}{\hat{\alpha}^+} - \frac{\hat{\beta}^-}{\hat{\alpha}^-} \tag{5.13}$$

The fourth degree of freedom within $\hat{\theta}_{ocp}$ absorbs the unknown initial condition,

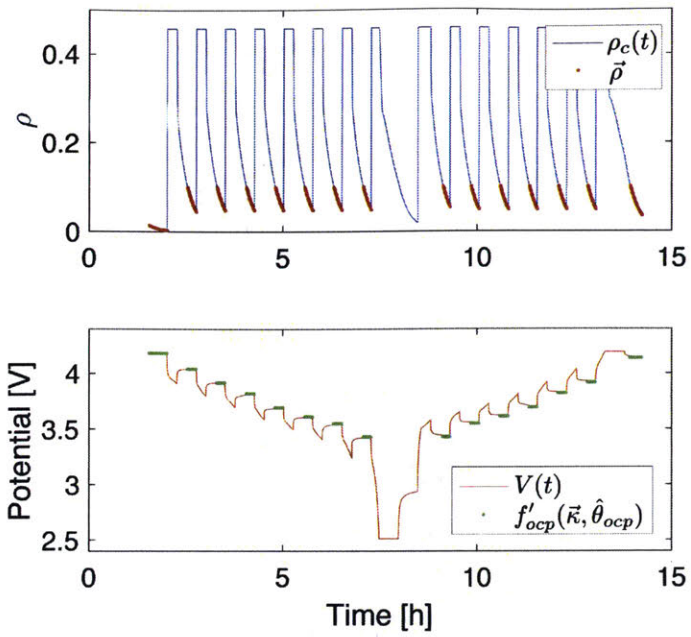


Figure 5-3: The top plot shows how the sampled sequence $\vec{\rho}$ were constructed from $\rho_c(t)$. The bottom plot shows the resulting optimal $f'_{ocp}(\vec{\kappa}, \hat{\theta}^*_{ocp})$ in green. For comparison, the corresponding voltage profile for the data shown above is also provided.

$\hat{\beta}^- = c_s^-(t_0)$.

The parameter estimates $\hat{\theta}^*_{ocp}$ were determined as in (5.12) using data collected from a number of experiments. For the two cells used, these estimated parameters from each experiment are distilled into a plot (Figure 5-5) of the decreasing capacity trend that would be expected under the cycling and excitation which the cells were subjected to.

The benefit of the algorithm presented above, in comparison to the general approach of using a slow charge/discharge cycle of the cell, is that the process of this section only requires points of relaxation spread over the operating voltage. This allows a cell to be pulsed, similar to what may be experienced when a vehicle is used for a series of trips with sufficient time between trips. The conventional method requires the battery be taken out of use and subjected to a 48+ hour calibration

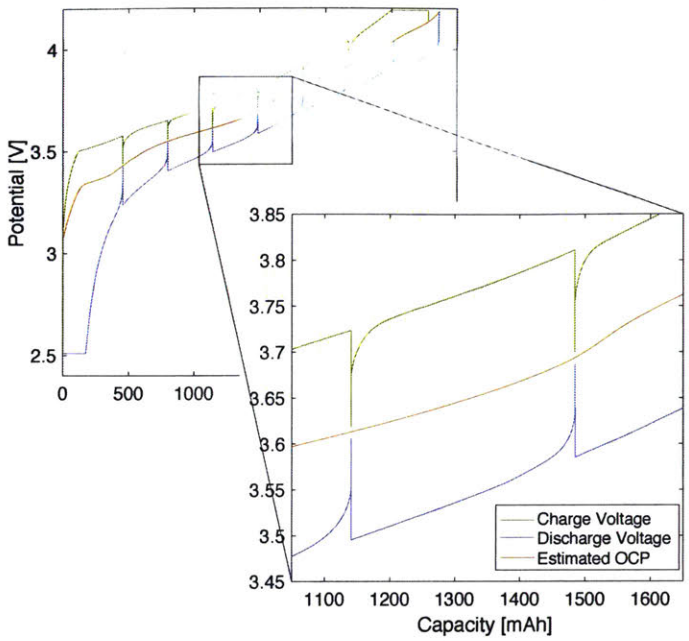


Figure 5-4: The relationship between the measured voltage from Figure 5-3 and the estimated equilibrium open circuit potential $f'_{ocp}(\kappa(t), \hat{\theta}_{ocp})$ from (5.5) and (5.12) with $Capacity(t) = \kappa(t) - \min_t \kappa(t)$ are shown in blue and red respectively.

test. In contrast, this method can be accomplished in under 8 hours, while being used.

It should be noted that one can replace the batch procedure for estimating the parameters of $f'_{ocp}$ in (5.11),(5.12) by a recursive procedure.

This algorithm was designed using experimental data hence the empirical choices for $I_{lim}$ and $\rho_{lim}$ in (5.9). Using the OCP calibration input profile of Chapter 5.2 and a values for limiting signals in (5.9) estimates $\hat{\theta}_{ocp}$ are consistent with the parameters resulting from routines used at Bosch for their model parameterization. The benefit of the algorithm presented above in comparison to the general approach of using a very slow charge/discharge cycle of the cell at a current of $C/25$ is that the process of this Chapter only requires points of relaxation spread over the operating voltage.

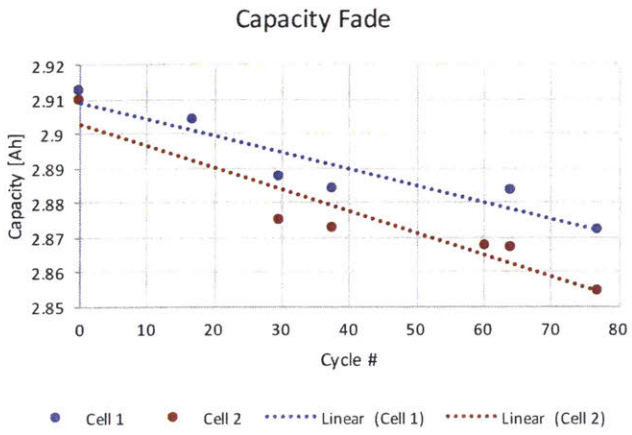


Figure 5-5: Cell capacities computed prior to each experiment performed. The number of cycles is computed as $Cycles(t) = \frac{1}{2C}\int_{t_0}^{t} |I(\tau)|\, d\tau$. A downward trend is observed and expected; inconsistent drops of capacity per cycle is expected due to differences between experiments.

This allows a cell to be pulsed, similar to what may be experienced when a vehicle is used for a series of trips with sufficient time between trips. The conventional method requires the battery be taken out of use and subjected to a 48+ hour calibration test. Whereas, this method can be accomplished in a few hours.

### 5.1.2 Recursive OCP Estimation

The above procedure would ideally provide a new estimate of the equilibrium OCP every time a sufficient amount of data is collected, for example, at $T_1$, $T_2$ etc in figure 5-6. Without loss of generality we assume there is an initial estimate $\hat{\theta}^*_{ocp} = \hat{\theta}^0_{ocp}$. This initial estimate could be generated by either using a set of calibration data collected before the cell is deployed or a manufacturer supplied estimation. Such a scenario would use $f'_{ocp}(\hat{\theta}^0_{ocp})$ for $T_0 \leq t < T_1$. During this time data would be accumulated into $\vec{\Omega}^1_{ocp}$ of (5.10). When sufficient data has been collected at $T_1$ a new estimate of the equilibrium OCP parameters would be computed $\hat{\theta}^*_{ocp} = \hat{\theta}^1_{ocp}$ and the

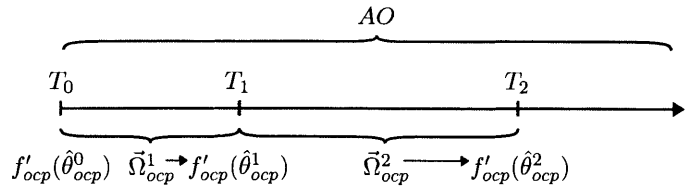


Figure 5-6: Schematic for implementation of Chapter 4 and Section 5.1 together. The adaptive observer will run continuously for all time. For $T_0 \leq t \leq T_1$ an initial estimate of $f_{ocp}$ designated $f'_{ocp}(\hat{\theta}^0_{ocp})$ is used. At $T_1$ data collected in $\vec{\Omega}^1_{ocp}$ is used to estimate $f'_{ocp}(\hat{\theta}^1_{ocp})$ which will then be used by the adaptive observer for $T_1 < t \leq T_2$. This process is repeated for the duration of use.

adaptive observer would then use $f'_{ocp}(\hat{\theta}^1_{ocp})$ for $T_1 \leq t < T_2$. Determination of when sufficient data has been collected within $\vec{\Omega}^i_{ocp}$ could be as simple as when there are data points within $\vec{V}$ in each of the five ranges,

$$\begin{aligned} V_i &\leq 3 \\ 3 < V_i &\leq 3.33 \\ 3.33 < V_i &\leq 3.67 \\ 3.67 < V_i &\leq 4 \\ 4 < V_i & \end{aligned} \tag{5.14}$$

at $T_2$ when sufficient data has been collected to generate an updated estimate $\hat{\theta}^*_{ocp} = \hat{\theta}^2_{ocp}$ and the adaptive observer would then use $f'_{ocp}(\hat{\theta}^2_{ocp})$ and the process would repeat.

Due to its highly nonlinear cost function the minimization of (5.12) requires a reasonable initial estimate of the true parameter. If the cost function of (5.11) is reformulated as a function of both the previous estimate $\hat{\theta}^{k-1}_{ocp}$ and a correction term $\delta\hat{\theta}^k_{ocp}$ as

$$J'_{ocp}(\hat{\theta}^{k-1}_{ocp}, \delta\hat{\theta}^k_{ocp}) = J_{ocp}(\hat{\theta}^{k-1}_{ocp} + \delta\hat{\theta}^k_{ocp}) \tag{5.15}$$

Then the initialization of $\delta\hat{\theta}^{k}_{ocp}$ within the minimization algorithm can be 0 and all information previously used is no longer discarded. At each $T_k$ the new correction term is then computed as

$$\delta\hat{\theta}^{k*}_{ocp} = \underset{\delta\hat{\theta}^{k}_{ocp}}{\arg\min}\, J'_{ocp}(\hat{\theta}^{k-1*}_{ocp}, \delta\hat{\theta}^{k}_{ocp}) \tag{5.16}$$

with

$$\hat{\theta}^{k*}_{ocp} = \hat{\theta}^{k-1*}_{ocp} + \delta\hat{\theta}^{k*}_{ocp} \tag{5.17}$$

to be used within $f'_{ocp}$ of (5.5).

## 5.2 Estimation of linear dynamics and overpotential

Having presented a matrix regressor based adaptive observer for the reduced SP model of (2.34)-(2.39), we now wish to validate this adaptive observer via experiments with a consumer 18650 lithium ion cell. These cells can be found in laptops, power-tools and electric cars. Experiments require additional considerations beyond those previously outlined, specifically the experiment design. Experiment design typically consists of selection of the signals which will be measured and excited, selection of the sampling rate of these measurements, the hardware to be used for both, as well as design of an excitation signal before implementation of the adaptive observer of Chapter 4.

Some of the decisions for the experiment design are constrained by the resources available and laboratory requirements. Without destruction of a cell, the only measurements available are the current, potential across the terminals and the temperature of the outer casing. Both the current and voltage are required by observer

algorithms, the temperature is assumed constant for these models and is recorded to ensure that this assumption is valid. In order to gather the most flexible data sets, the highest sampling rate possible is preferred. Internally the system samples at the kilohertz frequency, but due to data transmission limits, data can only be recorded at a frequency of $20Hz$. A potentially complex task of choosing which hardware would best suit the experiments to be performed was unnecessary as only one system was available which was capable of accomplishing the tasks required. The hardware used was a custom cell cycler designed for Bosch by PEC.

Design of the excitation signal was the largest task. An excitation signal can be characterized by two aspects, the shape of the signal (or waveform) and 2nd order properties such as the spectrum, $\Phi_u(\omega)$, where $\omega$ is frequency, not the regressor of previous chapters. Common excitation signals are sum of sinusoids, swept sines, filtered white noise, pseudo-random signals and binary signals [29]. System identification literature commonly refers to these signals as being informative if they are able to distinguish between any two models being considered by the experiment. This quality of "informative" is directly related to the condition of PE in (3.24). Similar to PE conditions previously mentioned, a input is informative for linear models of order $n$ when the signal spectrum is nonzero at at-least $n$ distinct frequencies.

The asymptotic properties of the estimate depend only on the input spectrum, not the actual waveform. As the optimal input design will depend on the system which is unknown, optimality of the input is difficult to achieve. Therefore in practice it is sufficient to choose a important frequency band and use a signal which has a flat spectrum across this band. [29] As our model contains a free integrator, slow poles as well as direct feedthrough, the frequency band of importance is across the full spectrum.

To guarantee a wide flat spectrum, of the previous list, filtered white noise or random binary signals are common. However, neither are ideal. Filtered white noise

possesses a very high (theoretically infinite) crest factor,

$$C_r = \sqrt{\frac{\max_t u^2(t)}{\lim_{N\to\infty} \frac{1}{2}\sum_{t=1}^{N} u^2(t)}} \tag{5.18}$$

The crest factor is a metric of the waveform of a signal. A good signal waveform is one that has a low crest factor [29]. Clearly from inspection of (5.18), $C_r \geq 1$, resulting in an optimal crest factor of 1. The physical interpretation of the optimization of the crest factor is the optimization of the signal to noise ratio when limits are imposed on the input, where noise in our case should encompass both signal noise as well as discretization errors. Binary signals possess the ideal $C_r = 1$, however, the nonlinearity in the SP model necessitates a signal which is not binary. Instead, a signal is generated using a sum of multiple random binary signals modified to result in a low crest factor.

In practice random binary signals can be deterministically synthesized using a pseudo random binary signal (PRBS). This signal maintains white noise like properties while being easily generated using a shift register.

$$\begin{aligned} \sigma_0^{k=11} &= \begin{bmatrix} 0 & 0 & 0 & 0 & 0 & 0 & 0 & 0 & 1 & 0 & 1 \end{bmatrix} \\ \sigma(i) &= \begin{bmatrix} \left( \mod_2\left((\sigma_0^k)^\top \sigma(i-1)\right)\right) & \sigma_{(1:k-1)}(i-1) \end{bmatrix} \\ u_1(i) &= \sigma_{(k)}(i) \end{aligned} \tag{5.19}$$

where $\mod_i$ is the modulo operator, and subscripts designate elements of a vector $\sigma_{(j:k)}$. $\sigma(i)$ is a shift register, where the new value entering on the left is the modulo 2 value of $\sigma_0^\top \sigma(i-1)$. Where $\sigma_0^k$ is the PRBS polynomial of length $k$. The length of the pseudo random sequence before repeating itself will be $2^k - 1$ with every permutation of binary vectors with length $k$ appearing with the exception of all 0's. A listing of polynomials for alternative length PRBS sequences can be found in [2, 33]

As previously mentioned a binary signal is not sufficient to identify a nonlinearity in the system. Therefore $N = 5$ PRBS signals are summed each with different initial shift register values,

$$u_N(i) = \sum_{j=1}^{N} u_1(i)|_{\sigma_{(j)}(0)=1} \tag{5.20}$$

with every other element of $\sigma(0) = 0$. The resulting signal maintains white like properties, however, the crest factor has grown to $C_r = \sqrt{5}$. As $N$ PRBS signals are summed the crest factor grows as $C_r = \sqrt{N}$ further decreasing the quality of the signal. Instead of $u_5$ the signal is modified using

$$u'_N(i) = \begin{cases} \frac{N+1-u_N(i)}{N} & u_N(i) > 0 \\ \frac{-(N+1)-u_N(i)}{N} & u_N(i) < 0 \end{cases} \tag{5.21}$$

resulting in a signal with $C_r = 1.16$ for $u'_5$. The above algorithm works for any odd $N$. The final remaining characteristics required to define the excitation signal are the base period and peak amplitude. For the experimental results shown in the following section, the base period is 10 seconds resulting in a roll-off of the flat frequency spectrum at $0.1Hz$. Resulting in a signal $I_{PRS}(t)$ generated from the sequence $u'_N(i)$ as

$$I_{PRS-N}(t) = k_I u'_N(i) + I_{bias}, iT_{PRS} \leq t < (i+1)T_{PRS} \tag{5.22}$$

where $k_I$ scales the pseudo random signal $u'_N$ which has a maximum amplitude of 1, the $I_{bias}$ term can induce a mean current to the signal resulting in a charging or discharging signal with the pseudo random signal as excitation on top of the bias current.

With the details of the experimental setup described and a excitation signal

defined with a low crest factor. The experiment is divided into two sections. In the first a full charge-discharge cycle are performed to estimate the equilibrium OCP parameters using the algorithm of Section 5.1. Second, the pseudo random signal $u_5'$ generated using (5.21) is used in two different scenarios. In the first scenario the cell is initialized to a voltage in the middle of one of bands in which the negative electrode is unobservable, $3.58V$ and the excitation signal $I_{PRS}$ of (5.22) is used with $I_{bias} = 0$. The second scenario adds a small bias current to the excitation signal to slowly sweep through the full range of SoC while exciting the cell. Results from this second scenario will be presented using the augmented MR-AO of Chapter 4.

Preliminary analysis was was performed using batch estimation tools to confirm that the model described in Chapter 2 is sufficient to capture the dominant response of the cell. Here, it was noticed that due to the limit imposed on the maximum current for the experiment the overpotential did not leave the nearly linear regime for low currents. This low current was chosen for two purposes, predominantly, to ensure the SP model assumption of low C-rate remains valid. As the cells used are energy cells, not power cells, we can expect $\pm 1C$ to be on the brink of model invalidity. Secondly, safety concerns in the laboratory led to conservative experiment design. The effect of this is that the overpotential does not need a full 4 basis function approximation, instead it is assumed to be linear to the input $I$ and only one parameter is augmented to the standard adaptive observers described in Chapter 3.

Using the adaptive observer of Chapter 4 implemented assuming the model structure of (2.41)-(2.46) and an excitation input $I_{PRS-5}(t)$ generated using (5.22) with $T_{PRS} = 20\text{sec}$, $k_I = 1.375A$ and $I_{bias} = -0.125A$ a NCR18650 Panasonic cell slowly discharged for 7 hours.

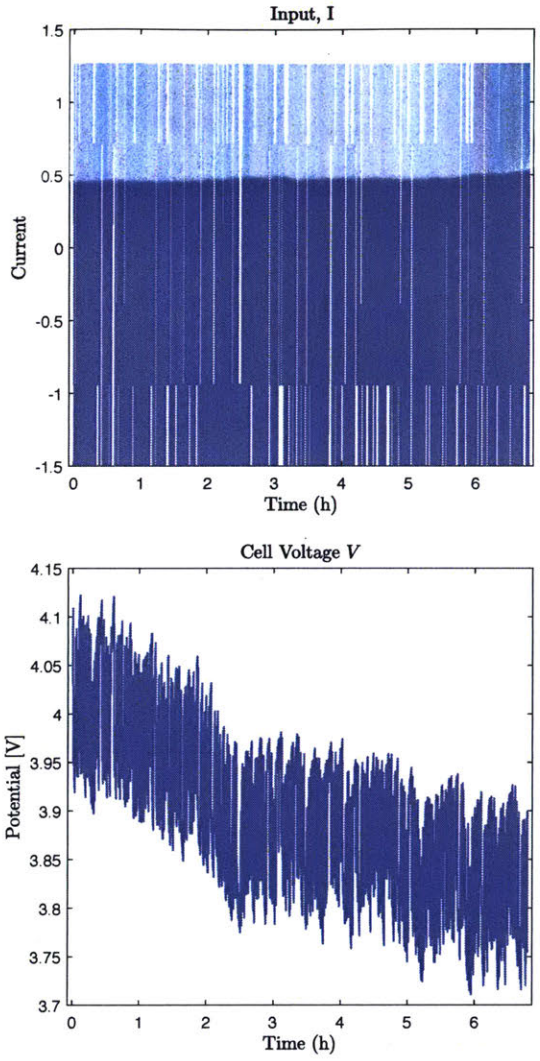


Figure 5-7: Excitation signal $I$ into the system and the resulting measured cell voltage. A small bias in the excitation signal results in a slow discharge of the cell while being excited.

Despite the differences between the true cell dynamics and the model (2.41)-(2.46) the dominant phenomena are correctly adapted to by the adaptive observer resulting in state of charge estimates within 1% of the true value. Where the true value is determined by $\overline{c}_s^-(t) = \hat{\alpha}^-\kappa(t) + \hat{\beta}^-$ using $\hat{\alpha}^-, \hat{\beta}^-$ from (5.12) and $\kappa(t)$ from (5.1).

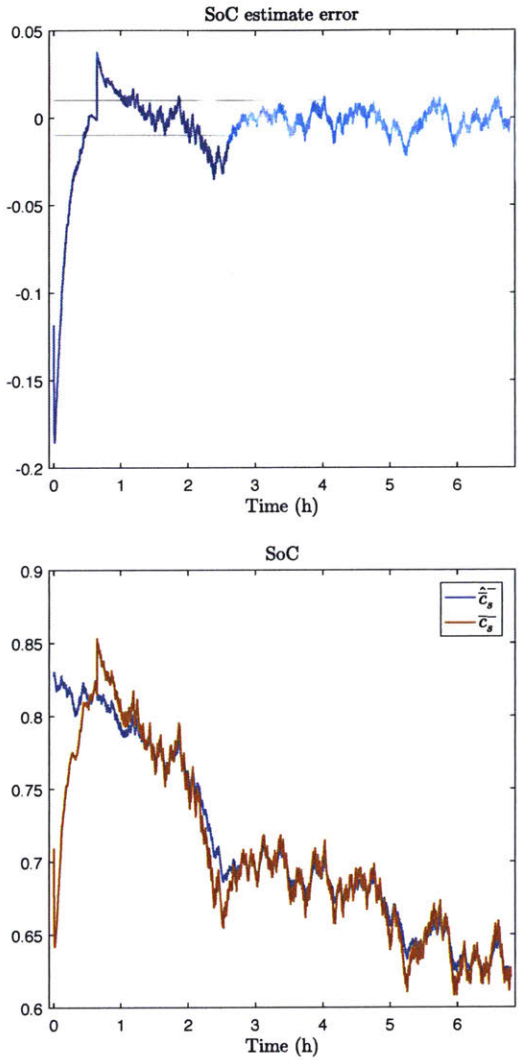


Figure 5-8: State of charge estimate and SoC estimate error.

The adaptive parameters converge to values which are appropriate for the cell, unfortunately, the true parameters cannot be determined.

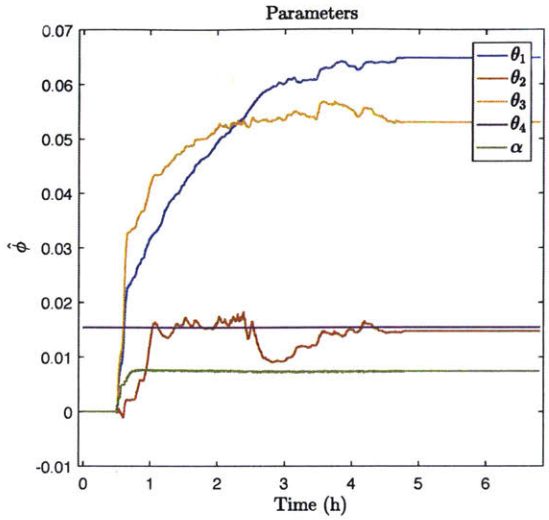


Figure 5-9: Resulting parameter estimates for the dynamical system and the over-potential approximation

The resulting estimated output voltage and its estimate are shown in Figure 5-10 where the error converges to within $\pm 10mV$ of the measured voltage.

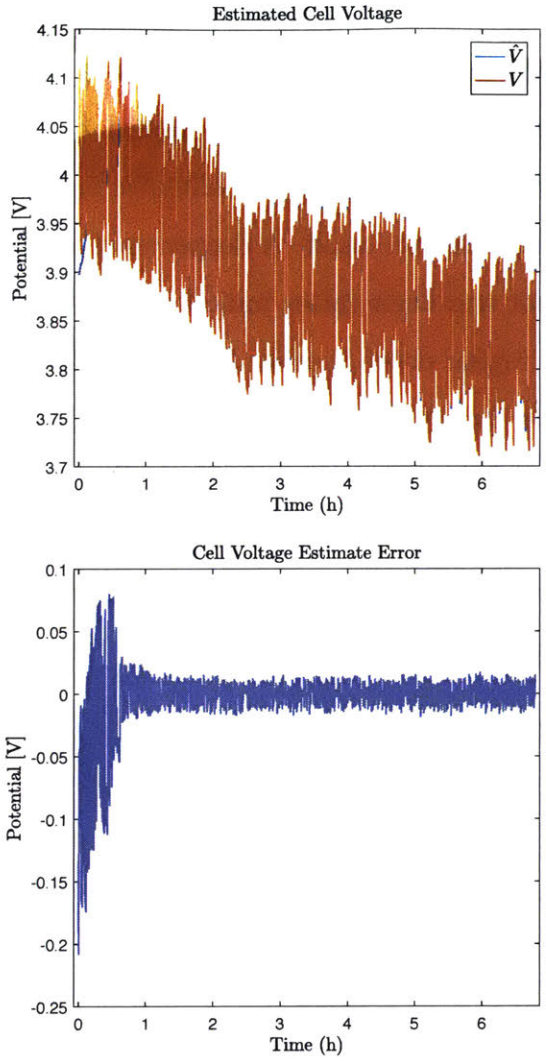


Figure 5-10: Estimated cell voltage and the corresponding error, zero mean error after 1 hour which does not decay further is the result of our approximation of the cell as our modified SP model.

## 5.3 Discussion

Although the true cell kinetic and dynamic properties are more complex than the modified SP model assumed, the matrix regressor adaptive observer provides accu-

rate output estimation as well as internal state estimates. Even through a projection algorithm is implemented to ensure stability of the overall system, the projection gain is never engaged and parameters estimates appear quite robust regardless of this projection. These well behaved parameter estimates may be partially due to the optimally exciting signal which were used. A deeper analysis of the frequency spectrums of the input, output and their ratios indicates that the diffusion may indeed by better represented by higher order transfer functions. If this is true, even signals which are SPE of the order $2n+N$ may not provide the optimal parameter estimates. Instead SPE of the order of the true system is ideal. Due to the modularity of the modified SP model higher order diffusion dynamical systems could be explored without significant changes required of the adaptive observer proposed, however, this is left to future work.

# Chapter 6

# Conclusions and Future Work

This thesis enumerated multiple developments in electrochemical modeling and adaptive observers in general. The first and fundamental component was a modification of the SP model with attractive features such as the encapsulation of lithium diffusion as a linear dynamical system independent of nonlinearities and decoupling of the nonlinear relationships defining the kinetic properties of lithium ion transfer and open circuit potential respectively. A second development defined a set of guidelines reducing the design parameters for adaptive observers from on the order of $n^2$ to a single tuning parameter. This enables rapid implementation and prototyping. Third, a new variant of adaptive observer, referred to here as matrix regressor adaptive observer II (MR-AO II), is derived for fast parameter convergence. This new observer uses multiple simultaneous equivalent system representations leveraging a linearity property between parameters equating the nonminimal system to that of the true system to allow tracking of a single set of parameters. A novel selection of both low pass and high pass filters used to generate additional regressors in the MR-AO I in addition to augmentation of the underlying equivalent system with nonlinear basis functions constitutes a fourth development extensively validated through numerical

simulation and theory. This adaptive observer combined with an independent offline algorithm to update effective electrode capacity and available lithium adapts every parameter of the modified SP model to account for aging or manufacturing differences. The offline equilibrium open circuit potential estimation algorithm is designed to operate using data collected from general use, eliminating the need for very slow capacity calibrations which could take days to run. Validation of this observer and ocp algorithm in hardware using commercially available Panasonic 18650 cells completes the goals originally set forth for this research.

The developments presented pave the way for fast, computationally efficient, advanced battery management systems with the potential to increase the effective capacity of a battery or alternatively reduce the size, and therefore cost, of batteries in various applications.

## 6.1 Future Work

There are a number of directions which could be explored as extensions to this work. Some of which are minor while others could require significant exploration.

### 6.1.1 Shaping of the full nonminimal system state

In the equivalent system design section, each filter $F, g$ were shaped independently. Alternatively shaping of the full regressor state $\omega = \begin{bmatrix} \omega_u^\top & \omega_y^\top \end{bmatrix}^\top$ could be explored. This would require use of the nominal plant model. Sensitivity of this resulting transformation to error in the nominal plant is unknown and could potentially yield a better performance when the nominal plant is close to the true plant, but worse performance when the nominal plant estimate is poor. For this reason, in addition to the complications imposed to estimate the minimal state representation states from

the resulting transformed regressors, this transformation was not explored here.

### 6.1.2 Higher order approximations of the model dynamics

There are a number of models which fall between the DFN and the modified SP model in complexity which still rely on ordinary differential equations to describe the diffusion dynamics. Less coarse discretizations in the $x$ domain would extend the accuracy of the model to higher currents, however, the resulting model will include algebraic relationships which can not be eliminated by inversion as was the case for the modified SP model. This would require the computation of multiple predicted outputs $\check{y}_i$ which would all contain errors until the system was identified. The effect of these errors is unclear, however, as they would be the result of solving an algebraic equation, the sum of all predicted output errors should be zero. This property may be able to be leveraged to show stability of an adaptive observer on this system. Alternatively, a higher order approximation to the diffusion dynamics of the SPM could also be made similar to [36, 46]. The solid particle diffusion dynamics can be shown to be more accurately represented by a transcendental transfer function of the form,

$$\frac{c_{ss}(s)}{I(s)} = \frac{-b_0 \sinh\left(\sqrt{s/\epsilon}\right)}{\left(\sqrt{s/\epsilon}\right)\cosh\left(\sqrt{s/\epsilon}\right) - \sinh\left(\sqrt{s/\epsilon}\right)} \tag{6.1}$$

This can be approximated using higher order transfer functions. Incorporation of this new diffusion dynamical model into the modular modified SP model would only require incorporation of additional constraints defining the relationship between the higher order transfer function coefficients.

### 6.1.3 Extension of the MR-AO II to discrete time observers

The original inspiration for MR-AO II was a question of the optimal sampling time when identifying discrete time systems. Clearly, the Nyquist frequency provides a upper bound on the sampling rate, however, in theory there is no lower limit. To generate a discrete time adaptive observer when the system dynamics are not well known, it would help performance to be able to use multiple discretizations simultaneously. Unfortunately, the relationship between parameters of different equivalent systems is not a simple shift of parameters.

# Bibliography


[1] Real-Time 3d Imaging Shows How Disposable Lithium Batteries Degrade.

[2] Linear-feedback shift register, January 2017. Page Version ID: 760893618.

[3] Brian D. O. Anderson, Robert R. Bitmead, C. Richard Johnson, Jr., Petar V. Kokotovic, Robert L. Kosut, Iven M.Y. Mareels, Laurent Praly, and Bradley D. Riedle. *Stability of Adaptive Systems: Passivity and Averaging Analysis.* MIT Press, Cambridge, MA, USA, 1986.

[4] P. Arora, B. N. Popov, and R. E. White. Electrochemical Investigations of Cobalt-Doped LiMn2 O 4 as Cathode Material for Lithium-Ion Batteries. *Journal of The Electrochemical Society*, 145(3):807–815, March 1998.

[5] Dimitri P. Bertsekas and John N. Tsitsiklis. *Introduction to Probability, 2nd Edition.* Athena Scientific, Belmont, Mass., 2nd edition edition, July 2008.

[6] I Bloom, B. W Cole, J. J Sohn, S. A Jones, E. G Polzin, V. S Battaglia, G. L Henriksen, C Motloch, R Richardson, T Unkelhaeuser, D Ingersoll, and H. L Case. An accelerated calendar and cycle life study of Li-ion cells. *Journal of Power Sources*, 101(2):238–247, October 2001.

[7] Robert L. Carroll and D. Lindorff. An adaptive observer for single-input single-output linear systems. *IEEE Transactions on Automatic Control*, 18(5):428–435, October 1973.

[8] C. C Chan, E. W. C Lo, and Shen Weixiang. The available capacity computation model based on artificial neural network for lead–acid batteries in electric vehicles. *Journal of Power Sources*, 87(1–2):201–204, April 2000.

[9] N. A. Chaturvedi, R. Klein, J. Christensen, J. Ahmed, and A. Kojic. Algorithms for Advanced Battery-Management Systems. *IEEE Control Systems Magazine*, 30(3):49–68, June 2010.

[10] N.A. Chaturvedi, R. Klein, J. Christensen, J. Ahmed, and A. Kojic. Modeling, estimation, and control challenges for lithium-ion batteries. In *American Control Conference (ACC)*, pages 1997–2002, June 2010.

[11] K. T. Chau, K. C. Wu, and C. C. Chan. A new battery capacity indicator for lithium-ion battery powered electric vehicles using adaptive neuro-fuzzy inference system. *Energy Conversion and Management*, 45(11–12):1681–1692, July 2004.

[12] Yi-Hsien Chiang and Wu-Yang Sean. Dynamical estimation of State-of-Health of batteries by using adaptive observer. In *2009 2nd International Conference on Power Electronics and Intelligent Transportation System (PEITS)*, volume 1, pages 110–115, December 2009.

[13] Yi-Hsien Chiang, Wu-Yang Sean, and Jia-Cheng Ke. Online estimation of internal resistance and open-circuit voltage of lithium-ion batteries in electric vehicles. *Journal of Power Sources*, 196(8):3921–3932, April 2011.

[14] Marc Doyle, Thomas F. Fuller, and John Newman. Modeling of Galvanostatic Charge and Discharge of the Lithium/Polymer/Insertion Cell. *Journal of The Electrochemical Society*, 140(6):1526–1533, June 1993.

[15] Wenbo Du, Amit Gupta, Xiangchun Zhang, Ann Marie Sastry, and Wei Shyy. Effect of cycling rate, particle size and transport properties on lithium-ion cathode performance. *International Journal of Heat and Mass Transfer*, 53(17–18):3552–3561, August 2010.

[16] Matthieu Dubarry, Cyril Truchot, and Bor Yann Liaw. Synthesize battery degradation modes via a diagnostic and prognostic model. *Journal of Power Sources*, 219:204–216, December 2012.

[17] Matthieu Dubarry, Cyril Truchot, Bor Yann Liaw, Kevin Gering, Sergiy Sazhin, David Jamison, and Christopher Michelbacher. Evaluation of commercial lithium-ion cells based on composite positive electrode for plug-in hybrid electric vehicle applications. Part II. Degradation mechanism under 2 C cycle aging. *Journal of Power Sources*, 196(23):10336–10343, December 2011.

[18] C. R. Gould, C. M. Bingham, D. A. Stone, and P. Bentley. Novel battery model of an all-electric personal rapid transit vehicle to determine state-of-health through subspace parameter estimation and a Kalman Estimator. In *Automation and Motion 2008 International Symposium on Power Electronics, Electrical Drives*, pages 1217–1222, June 2008.

[19] C. R. Gould, C. M. Bingham, D. A. Stone, and P. Bentley. New Battery Model and State-of-Health Determination Through Subspace Parameter Estimation and State-Observer Techniques. *IEEE Transactions on Vehicular Technology*, 58(8):3905–3916, October 2009.

[20] Meng Guo, Godfrey Sikha, and Ralph E. White. Single-Particle Model for a Lithium-Ion Cell: Thermal Behavior. *Journal of The Electrochemical Society*, 158(2):A122–A132, February 2011.

[21] Petros A. Ioannou and Jing Sun. *Robust Adaptive Control*. Courier Corporation, December 2012. Google-Books-ID: pXWFY_vbg1MC.

[22] B. Jenkins, A. M. Annaswamy, and A. Kojic. Matrix regressor adaptive observers for battery management systems. In *IEEE Multi-Conference on Systems and Control*, pages 707–714, September 2015.

[23] Joaquín Klee Barillas, Jiahao Li, Clemens Günther, and Michael A. Danzer. A comparative study and validation of state estimation algorithms for Li-ion batteries in battery management systems. *Applied Energy*, 155:455–462, October 2015.

[24] L.G. Kraft. Controllable form state variables obtained from an arbitrarily fast adaptive observer. In *1976 IEEE Conference on Decision and Control including the 15th Symposium on Adaptive Processes*, pages 1088–1094, December 1976.

[25] G. Kreisselmeier. Adaptive observers with exponential rate of convergence. *IEEE Transactions on Automatic Control*, 22(1):2–8, February 1977.

[26] Prabhakar Kudva and Kumpati S. Narendra. Synthesis of an adaptive observer using Lyapunov's direct method. *International Journal of Control*, 18(6):1201–1210, July 1973.

[27] Eugene Lavretsky and Travis E. Gibson. Projection Operator in Adaptive Systems. *arXiv:1112.4232 [cs, math, nlin]*, December 2011. arXiv: 1112.4232.

[28] P. M. Lion. Rapid identification of linear and nonlinear systems. *AIAA Journal*, 5(10):1835–1842, 1967.

[29] Lennart Ljung. *System Identification: Theory for the User*. Prentice Hall PTR, 1999. Google-Books-ID: nHFoQgAACAAJ.

[30] Languang Lu, Xuebing Han, Jianqiu Li, Jianfeng Hua, and Minggao Ouyang. A review on the key issues for lithium-ion battery management in electric vehicles. *Journal of Power Sources*, 226:272–288, March 2013.

[31] G. Luders and K.S. Narendra. An adaptive observer and identifier for a linear system. *IEEE Transactions on Automatic Control*, 18(5):496–499, October 1973.

[32] G. Luders and K.S. Narendra. Stable adaptive schemes for state estimation and identification of linear systems. *IEEE Transactions on Automatic Control*, 19(6):841–847, December 1974.

[33] Richard W Marsh. *Table of irreducible polynomials over GF (2) through degree 19.* Office of Technical Services, U.S. Dept. of Commerce, Washington, 1957. OCLC: 2688440.

[34] Toshio Matsushima. Deterioration estimation of lithium-ion cells in direct current power supply systems and characteristics of 400-Ah lithium-ion cells. *Journal of Power Sources*, 189(1):847–854, April 2009.

[35] Scott J. Moura, Federico Bribiesca Argomedo, Reinhardt Klein, Anahita Mirtabatabaei, and Miroslav Krstic. Battery State Estimation for a Single Particle Model with Electrolyte Dynamics. *eScholarship*, July 2015.

[36] Scott J. Moura, Miroslav Krstic, and Nalin A. Chaturvedi. Adaptive PDE Observer for Battery SOC/SOH Estimation. pages 101–110, October 2012.

[37] S.J. Moura, N.A. Chaturvedi, and M. Krstic. PDE estimation techniques for advanced battery management systems #x2014; Part I: SOC estimation. In *American Control Conference (ACC)*, pages 559–565, June 2012.

[38] S.J. Moura, N.A. Chaturvedi, and M. Krstic. PDE estimation techniques for advanced battery management systems #x2014; Part II: SOH identification. In *American Control Conference (ACC)*, pages 566–571, June 2012.

[39] Kumpati S. Narendra and Anuradha M. Annaswamy. *Stable adaptive systems.* Prentice-Hall information and system sciences series. Prentice Hall, Englewood Cliffs, N.J, 1989.

[40] Kumpati S. Narendra and Anuradha M. Annaswamy. *Stable Adaptive Systems.* Dover Publications, Mineola, N.Y, May 2005.

[41] John Newman. FORTRAN Programs for the Simulation of Electrochemical Systems, 2014.

[42] S. Nuyan and R.L. Carroll. An adaptive observer and identifier with an arbitrarily fast rate of convergence. In *1976 IEEE Conference on Decision and*

*Control including the 15th Symposium on Adaptive Processes*, pages 1081–1087, December 1976.

[43] Seyhan Nuyan and Robert L. Carroll. Minimal order arbitrarily fast adaptive observers and identifiers. *IEEE Transactions on Automatic Control*, 24(2):289–297, April 1979.

[44] Gregory L. Plett. Extended Kalman filtering for battery management systems of LiPB-based HEV battery packs: Part 1. Background. *Journal of Power Sources*, 134(2):252–261, August 2004.

[45] Gregory L. Plett. Extended Kalman filtering for battery management systems of LiPB-based HEV battery packs: Part 3. State and parameter estimation. *Journal of Power Sources*, 134(2):277–292, August 2004.

[46] Venkatasailanathan Ramadesigan, Vijayasekaran Boovaragavan, J. Carl Pirkle, and Venkat R. Subramanian. Efficient Reformulation of Solid-Phase Diffusion in Physics-Based Lithium-Ion Battery Models. *Journal of The Electrochemical Society*, 157(7):A854–A860, July 2010.

[47] Jürgen Remmlinger, Michael Buchholz, Markus Meiler, Peter Bernreuter, and Klaus Dietmayer. State-of-health monitoring of lithium-ion batteries in electric vehicles by on-board internal resistance estimation. *Journal of Power Sources*, 196(12):5357–5363, June 2011.

[48] M. Safari, M. Morcrette, A. Teyssot, and C. Delacourt. Life Prediction Methods for Lithium-Ion Batteries Derived from a Fatigue Approach II. Capacity-Loss Prediction of Batteries Subjected to Complex Current Profiles. *Journal of The Electrochemical Society*, 157(7):A892–A898, July 2010.

[49] Shriram Santhanagopalan, Qingzhi Guo, Premanand Ramadass, and Ralph E. White. Review of models for predicting the cycling performance of lithium ion batteries. *Journal of Power Sources*, 156(2):620–628, June 2006.

[50] Shankar Sastry and Marc Bodson. *Adaptive control: stability, convergence, and robustness.* Prentice Hall advanced reference series. Engineering. Prentice Hall, Englewood Cliffs, N.J, 1989.

[51] Alexander P. Schmidt, Matthias Bitzer, Árpád W. Imre, and Lino Guzzella. Experiment-driven electrochemical modeling and systematic parameterization for a lithium-ion battery cell. *Journal of Power Sources*, 195(15):5071–5080, August 2010.

[52] Pritpal Singh, Ramana Vinjamuri, Xiquan Wang, and David Reisner. Design and implementation of a fuzzy logic-based state-of-charge meter for Li-ion batteries used in portable defibrillators. *Journal of Power Sources*, 162(2):829–836, November 2006.

[53] R. Spotnitz. Simulation of capacity fade in lithium-ion batteries. *Journal of Power Sources*, 113(1):72–80, January 2003.

[54] Venkat R. Subramanian, James A. Ritter, and Ralph E. White. Approximate Solutions for Galvanostatic Discharge of Spherical Particles I. Constant Diffusion Coefficient. *Journal of The Electrochemical Society*, 148(11):E444–E449, November 2001.

[55] Karen E. Thomas, John Newman, and Robert M. Darling. Mathematical Modeling of Lithium Batteries. In Walter A. van Schalkwijk and Bruno Scrosati, editors, *Advances in Lithium-Ion Batteries*, pages 345–392. Springer US, 2002.

[56] OAR US EPA. Dynamometer Drive Schedules.

[57] Mark Verbrugge and Brian Koch. Generalized Recursive Algorithm for Adaptive Multiparameter Regression Application to Lead Acid, Nickel Metal Hydride, and Lithium-Ion Batteries. *Journal of The Electrochemical Society*, 153(1):A187–A201, January 2006.

[58] J. Wang, Z. Sun, and X. Wei. Performance and characteristic research in LiFePO4 battery for electric vehicle applications. In *2009 IEEE Vehicle Power and Propulsion Conference*, pages 1657–1661, September 2009.

[59] John Wang, Ping Liu, Jocelyn Hicks-Garner, Elena Sherman, Souren Soukiazian, Mark Verbrugge, Harshad Tataria, James Musser, and Peter Finamore. Cycle-life model for graphite-LiFePO4 cells. *Journal of Power Sources*, 196(8):3942–3948, April 2011.

[60] Eric W. Weisstein. Projection Matrix.

[61] Fangfang Yang, Yinjiao Xing, Dong Wang, and Kwok-Leung Tsui. A comparative study of three model-based algorithms for estimating state-of-charge of lithium-ion batteries under a new combined dynamic loading profile. *Applied Energy*, 164:387–399, February 2016.

[62] C. Zhang, L. Y. Wang, X. Li, W. Chen, G. G. Yin, and J. Jiang. Robust and Adaptive Estimation of State of Charge for Lithium-Ion Batteries. *IEEE Transactions on Industrial Electronics*, 62(8):4948–4957, August 2015.